Indian J Pure & Appl Phys, Vol 21 No. 5 pp 261-322
May 1983
CODEN : IJOPAU ISSN : 0019-5596
21(3) 261-322 (1983)

INDIAN JOURNAL OF PURE & APPLIED PHYSICS

Published by
PUBLICATIONS & INFORMATION DIRECTORATE, CSIR
NEW DELHI
in association with
THE INDIAN NATIONAL SCIENCE ACADEMY, NEW DELHI

CSIR SCIENTIFIC PERIODICALS

JOURNAL OF SCIENTIFIC & INDUSTRIAL RESEARCH (Monthly)

With a fine record of over 45 years service to the scientific community, this journal has grown into India's leading general science periodical. Intended to fulfil the responsibility of helping the research workers to keep themselves abreast of current developments in various fields of science and technology, the journal carries editorial features highlighting important scientific events in India and abroad, articles on science policy and management of science review articles on topics of current research interest, technical reports on international and national conferences; reviews of scientific and technical publications, and notes on major advances in various fields.

Annual subscription	Rs 100.00	£ 17.00	$ 38.00
Single copy	10.00	1.70	3.80

INDIAN JOURNAL OF CHEMISTRY (Monthly)

Section A: In the 20th year of publication, the journal is devoted to papers in Inorganic, Physical, Theoretical and Analytical Chemistry.

Annual subscription	Rs 125.00	£ 21.00	$ 47.00
Single copy	12.50	2.10	4.70

Section B: In the 19th year of publication, the journal is devoted to papers in Organic Chemistry including Medicinal Chemistry.

Annual subscription	Rs 125.00	£ 21.00	$ 47.00
Single copy	12.50	2.10	4.70

INDIAN JOURNAL OF PURE & APPLIED PHYSICS (Monthly)

This journal, which is running 20th year of its publication, is devoted to original research communications (full papers and short communications) in all conventional branches of physics (except radio and space physics).

Annual subscription	Rs 120.00	£ 20.00	$ 45.00
Single copy	12.00	2.00	4.50

INDIAN JOURNAL OF RADIO & SPACE PHYSICS (Bimonthly)

The journal, which is being published beginning from March 1972, is intended to serve as a medium for the publication of the growing research output in various areas of radio and space physics, such as ionospheric propagation, magnetosphere, radio and radar astronomy, physics and chemistry of the ionosphere; neutral atmosphere; airglow, winds and motion in the upper atmosphere; stratosphere-mesosphere coupling, ionosphere-magnetosphere coupling ; solar-terrestrial relationship, etc.

Annual subscription	Rs 90.00	£ 15.00	$ 34.00
Single copy	18.00	3.00	6.80

INDIAN JOURNAL OF TECHNOLOGY (INCLUDING ENGINEERING) (Monthly)

This journal publishes papers reporting results of original research of applied nature pertaining to unit operations, heat and mass transfer, products, processes, instruments and appliances, etc. The journal is of special interest to research workers in the departments of applied sciences in universities, institutes of higher technology, commodity research laboratories, industrial cooperative research institutes, and industrial research laboratories.

Annual subscription			
Single copy	Rs 90.00	£ 15.00	$ 34.00
	9.00	1.50	3.40

INDIAN JOURNAL OF EXPERIMENTAL BIOLOGY (Monthly)

This journal, devoted to the publication of research communications in the fields of experimental botany, zoology, microbiology, pharmacology, endocrinology, nutrition, etc., is the only one in India with such a wide coverage and scope.

Annual subscription	Rs 180.00	£ 30.00	$ 68.00
Single copy	18.00	3.00	6.80

INDIAN JOURNAL OF BIOCHEMISTRY & BIOPHYSICS (Bimonthly)

This journal, published in association with the Society of Biolog cal Chemists (India), Bangalore, is the only research journal in India devoted exclusively to original research communications in biochemistry and biophysics.

Annual subscription	Rs 60.00	£ 10.00	$ 23.00
Single copy	12.00	2.00	4.60

INDIAN JOURNAL OF MARINE SCIENCES (Quarterly)

Commencing publication from June 1972, this journal is devoted to research communications (full papers and short communications) pertaining to various facets of marine research, viz. biological, physical, geological and chemical oceanography.

Annual subscription	Rs 75.00	£ 13.00	$ 28.00
Single copy	22.00	4.00	8.40

RESEARCH AND INDUSTRY (Quarterly)

Intended to serve as a link between science and industry, this journal is addressed primarily to technologists, engineers, executives and others in industry and trade. It publishes informative original articles containing practical details of processes and products devoted in India, which show promise of ready utilization, and technical digests on new processes, products, instruments and testing methods which are of interest to industry. Developments in Indian industry are regularly reported.

Annual subscription	Rs 45.00	£ 8.00	$ 17.00
Single copy	13.00	2.50	5.00

INDIAN JOURNAL OF TEXTILE RESEARCH (Quarterly)

Commencing publication from March 1976, this journal is devoted to the publication of papers reporting results of fundamental and applied researches in the field of textiles.

Annual subscription	Rs 45.00	£ 8.00	$ 17.00
Single copy	13.00	2.50	5.00

MEDICINAL & AROMATIC PLANTS ABSTRACTS (Bimonthly)

Carries informative abstracts of scientific papers published in important Indian and foreign journals relating to different aspects of medicinal and aromatic plants. Each issue contains about 350 abstracts with a subject index.

Annual subscription	Rs 40.00	£ 7.00	$ 17.00
Single copy	7.50	1.50	3.00

INDUSTRIAL NEWS DIGEST (Monthly)

Provides technical and techno-economic information for industrialists, prospective entrepreneurs and experts in both government and private agencies dealing with the management and planning of industry. Each issue carries at least one profile on a particular industry.

Annual subscription	Rs 20.00	£ 4.00	$ 8.00
Single copy	2.00	0.50	1.00

CURRENT LITERATURE ON SCIENCE OF SCIENCE (Monthly)

Carries abstracts, digests, book reviews, news & notes and R & D statistics with emphasis on problems of S & T in developing countries, it also covers the areas of science policy, R & D planning and management, technology transfer, technology assessment and science and society.

Annual subscription	Rs 100.00	£ 12.00	$ 30.00

Please contact

Manager (Sales & Advertisment)
PUBLICATIONS & INFORMATION DIRECTORATE, CSIR
Hillside Road, New Delhi-110012

Indian Journal of Pure & Applied Physics

Published by the Publications & Information Directorate, CSIR, Hillside Road, New Delhi 110012
Editor-in-Chief : Y R Chadha

The Indian Journal of Pure & Applied Physics is issued monthly. The Directorate assumes no responsibility for the statements and opinions advanced by contributors. The editorial staff in its work of examining papers received for publication is assisted, in an honorary capacity, by a large number of distinguished scientists, working in various parts of India.

Communications regarding contributions for publication in the journal should be addressed to the Editor, Indian Journal of Pure & Applied Physics, Publications & Information Directorate, Hillside Road, New Delhi 110012.

Correspondence regarding subscriptions and advertisements should be addressed to the Sales & Distribution Officer, Publications & Information Directorate, New Delhi 110012.

Annual Subscription	**Single Copy**
Rs. 120.00 £20.00 $45.00	Rs. 12.00 £2.00 $4.50

50% Discount is admissible to research workers and students and 25% discount to non-research individuals, on annual subscription. Payments in respect of subscriptions and advertisements may be sent by cheque, bank draft, money order or postal order marked payable *only* to **Publications & Information Directorate, New Delhi 110012.** Claims for missing numbers of the journal will be allowed only if received within 3 months of the date of issue of the journal plus the time normally required for postal delivery of the journal and the claim.

Indian Journal of Pure & Applied Physics

VOLUME 21 NUMBER 5 MAY 1983

CONTENTS

Continued overleaf

CONTENTS

---

*The author to whom all correspondence is to be addressed is indicated by the (*) mark.

Indian Journal of Pure & Applied Physics
Vol 21, May 1983, pp 261-263

Estimation of Diffusion Coefficient of Lanthanum Ions from One-Dimensional Liesegang Formation

K V KURIEN†, V K VAIDYAN & M A ITTYACHEN*
Department of Physics, University of Kerala, Kariavattom, Trivandrum 695 581

Received 5 *July* 1982

Experimental conditions for obtaining Liesegang rings in the growth of lanthanum molybdate crystals in silica gel by single diffusion technique have been discussed. The time law, spacing law and the law relating diffusion depth and width are verified. Making use of Fick's law of diffusion, a method has been devised to estimate the diffusion coefficient of lanthanum ions in silica gel and the various parameters under which the coefficient varies are investigated.

1 Introduction

Diffusion is the spontaneous equalization of concentration of molecules, ions or colloidal particles in a system as a result of their thermal chaotic motion. The role of diffusion in crystal growth has been reviewed by several authors[1,2]. The work of Kirov[3] could elucidate the peculiarities of the diffusion and crystallization which help to control the growth of crystals by diffusion methods. Making use of a simple mathematical model, he could deal with the diffusion controlled crystal growth in a qualitative way and could calculate diffusion coefficient from the first and subsequent precipitates produced in the diffusion media due to counter-diffusion of two reacting substances. Malton and Packter[4] have shown that solprotection (by adsorption) and diffusion are important factors in rhythmic precipitation. Packter and Roy[5] have calculated the diffusion coefficient of alkaline earth metal ions in melt and found that the values are inversely proportional to their ionic radii. Diffusional characteristics of a wide number of inorganic ions in agar gel have been studied by Lee and Meeks[6]. Making use of the theory of one-dimensional Liesegang phenomena, Shinohara[7] could estimate diffusion coefficient of the diffusiong ions.

The authors have developed a method to estimate the effective diffusion coefficient of outer electrolyte in gel media, making use of the simple diffusion theory and nucleation conditions for the formation of one-dimensional Liesegang phenomena[8]. The present paper reports the Liesegang ring formation of lanthanum molybdate ($La_2(MoO_4)_3 . XH_2O$) crystals by single diffusion[9] technique and a method of estimating the diffusion coefficient of lanthanum ions.

†Department of Physics, Mar Thoma College, Tiruvalla

2 Experimental Details

Silica gels were prepared in test tubes using sodium silicate solution of specific gravity 1.03 with dilute HNO_3. A standard solution (1.0 *S*) was prepared using HNO_3, $(NH_4)_2NO_3$ and $(NH_4)_2MoO_4$ as follows. Two grammes each of $(NH_4)_2MoO_4$ and $(NH_4)_2NO_3$ were dissolved in distilled water and to this solution 6 ml of concentrated NHO_3 was slowly added and the whole system was kept cooled. Finally this solution was diluted with distilled water to make the total volume 100 ml.

The $(NH_4)_2MoO_4$ impregnated in the gel acted as the inner electrolyte. The acid content in the standard solution was utilized to adjust the *p*H of the gel medium. A set of test tubes with gelling mixtures of different *p*H values between 6 and 7.5 were prepared. After the gels were properly set, the outer electrolyte (lanthanum nitrate) solution of particular concentration was poured into the test tube. As soon as the outer electrolyte was poured a thick precipitate band was formed below the gel interface, below which Liesegang rings were formed. The distance between the successive bands was found to increase with the distance of the band from the interface and the concentration. The following rules:

$$X_n/t_n^{1/2} = \text{a constant (Ref. 10)} \quad \ldots(1)$$

$$X_{n+1}/X_n = \text{a constant (Ref. 11)} \quad \ldots(2)$$

and

$$X/\Delta X = \text{a constant (Ref. 12)} \quad \ldots(3)$$

were found to be obeyed, where X_n is the distance of the nth ring from the interface, t_n the corresponding time of formation of the ring, and ΔX is the distance between successive rings. Table 1 gives the parameters of Liesegang rings of a typical lanthanum molybdate system (Fig. 1).

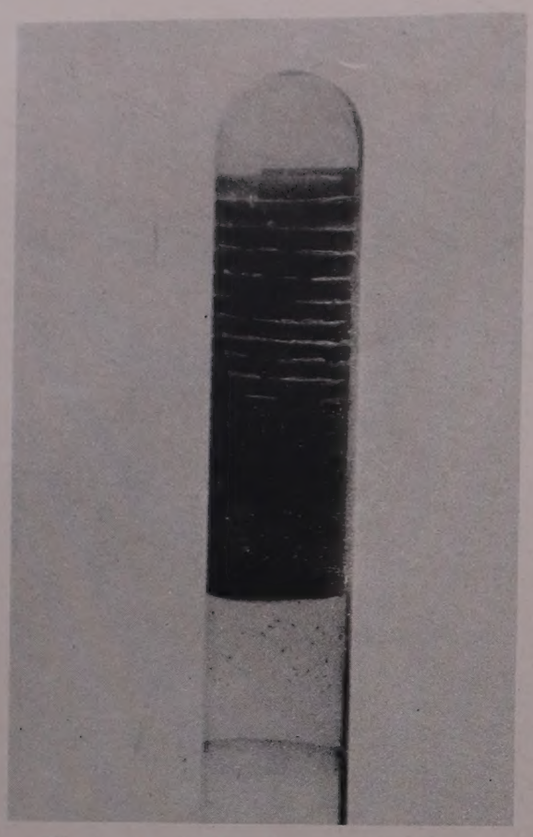

Fig. 1—A typical Liesegang ring system of $La_2(MoO_4)XH_2O$ in silica gel medium

Table 1—Parameters of Liesegang Rings of Lanthanum Molybdate Crystals

[Experimental details: Silica gel of density 1.03 g cm^{-3}; *p*H of gel: 6.5; Outer electrolyte: 0.5 *M* $La(NO_3)_3.6H_2O$; Age of gel: one day; Inner electrolyte: 0.25 *S* $(NH_4)_2MoO_4$; Working temperature range: 38-32 C]

Ring No. (*n*)	X cm	t hr	ΔX cm	X^2/t cm^{2}hr^{-1}	$X/\Delta X$	$\frac{X_{n+1}}{X_n}$	$\left[\frac{t_{n+1}}{t_n}\right]^{1/2}$
3	5.185	68	0.153	0.395	33.889	1.050	1.050
5	5.717	81	0.168	0.403	34.030	1.050	1.060
7	6.271	99	0.184	0.397	34.082	1.050	1.040
9	6.913	117	0.203	0.408	34.054	1.050	1.054

3 Estimation of Diffusion Coefficient

In order to determine the effective diffuison coefficient, it is assumed that C_A, the concentration of the outer electrolyte at distance X from the gel boundary, t seconds after the diffusion starts, is given by:

$$C_A = C_{0A} \exp(-X^2/4D_A t) \quad \ldots(4)$$

where C_{0A} is the concentration of the outer electrolyte at $t = 0$ and D_A is the effective diffusion coefficient of A ions (outer electrolyte) in the gel. Taking a large column of the outer electrolyte, we assume that C_{0A} is reasonably constant throughout the experiment. Thus a Liesegang ring forms at a distance X from the gel boundary when $C_A \cong C_B$ at that position, so that

$$C_B \cong C_{0A} \exp(-X^2/4D_A t) \quad \ldots(5)$$

Hence the effective diffusion coefficient of A ions, which is the result of the movement of both A and B ions in the medium, is

$$D_A = \frac{X^2/t}{4 \ln (C_{0A}/C_B)} \quad \ldots(6)$$

Thus by using Eq. (6), D_A is calculated.

In the actual experiment, three arbitrary values of inner electrolyte, viz. 0.25, 0.5 and 1.0 *S*, corresponding to C_B values 1.327, 2.666 and 5.310×10^{20} ions/cm^3, respectively, against the outer electrolyte concentration in the range 0.25-0.7 *M* were selected. The rate of movement of the advancing boundary X and time t were noted and the mean values of X^2/t (Table 2) were calculated and D_A values estimated. The uncertainty in the determination of D_A is of the order of 10%. Within this limit, the diffusion coefficient is estimated as $(0.73 \pm 0.07) \times 10^{-5}$ cm^{2}s^{-1}. For fixed value of C_B(0.25 *S*), values of D_A were estimated with C_{0A} being varied from 0.25 to 0.7 *M*. A small but observable diminution in the X^2/t and D_A values were observed due to C_B variation, for a fixed value of C_{0A}. The increase in inner electrolyte could cause a small retarding effect on the onward moving outer electrolyte.

Table 2—Estimation of Diffusion Coefficient of Lanthanum Ions in Silica Gel

[Experimental details: Silica gel of density 1.03 gcm^{-3}; *p*H of gel medium 6.5; Working temperature range 28-32 C]

Electrolyte		Conc. of A ions (C_{0A}) ($\times 10^{20}$cm^{-3})	Conc. of B ions (C_B) ($\times 10^{20}$cm^{-3})	X^2/t (cm^2.hr^{-1})	D_A ($\times 10^5$ cm^{2}s^{-1})
Outer	Inner				
0.5*M*	0.25*S*	57.250	1.327	0.400	0.738
0.5*M*	0.5 *S*	57.250	2.655	0.325	0.735
0.5*M*	1.0 *S*	57.250	5.310	0.245	0.717

Table 3—Effect of Gel Density (gcm^{-3}) and Ageing on X^2/t (cm^{2}hr^{-1}) and D_A ($\times 10^5$cm^{2}S^{-1}) Values

[$C_{0A} = 57.25 \times 10^{20}$ ions cm^{-3}; $C_B = 1.327 \times 10^{20}$ ions.cm^{-3}]

Gel Density

*p*H	1.025		1.030		1.035		1.040	
	X^2/t	D_A	X^2/t	D_A	X^2/t	D_A	X^2/t	D_A
6.0	0.390	0.730	0.400	0.738	0.402	0.745	0.404	0.750
6.5	0.392	0.728	0.394	0.727	0.396	0.742	0.398	0.745
7.0	0.389	0.720	0.391	0.722	0.393	0.737	0.395	0.742

Ageing

	One day		Two days		Three days	
6.0	0.410	0.756	0.404	0.745	0.400	0.738
6.5	0.400	0.738	0.396	0.730	0.390	0.720
7.0	0.390	0.720	0.385	0.710	0.380	0.700

As a result of mild interaction between gel and diffusing ions during the process of diffusion, the effective concentration of the outer electrolyte is controlled by the density of gel as derived by Malton and Packter[4]. In the present case, a slight increase in the density of the gel medium is found to act as a retarding medium for diffusion and retards the reaction of precipitation. Table 3 shows the change in D_A values with gel density variation. The age of gel is also found to affect a considerable decrease in the estimated values of D_A (Table 3). As the density increases, the cell wall of the gel thickens[9] and as the age increases, the gel gets shrunk, so that in both cases the pore size reduces[13], which in turn decreases the ionic diffusion. This explains the observed decrease in D_A with gel density and ageing.

4 Conclusion

The one-dimensional Liesegang phenomena can be utilized to estimate the effective diffusion coefficient of outer electrolyte. The diffusivity of the medium diminishes with increase in gel density and ageing.

References

1 Kroger F A, *Chemistry of imperfect crystals* (Inter Science, New York) 1964, 31.

2 Schroeder J B, Linares R C, *Progress in ceramic science* (Pergamon, London) 1966, 195.

3 Kirov G K, *J Cryst Growth (Netherlands)*, **15** (1972) 102.

4 Malton R & Packter A, *J Colloid Sci (USA)*, **10**(1) (1955) 46.

5 Packter A & Roy B J, *J Cryst Growth (Netherlands)*, **18** (1973) 88.

6 Robert E Lee (Jr) & Frank R Meeks, *J Colloid & Interface Sci (USA)*, **35** (1971) 584.

7 Shouji Shinohara, *J Phys Soc (Japan)*, **29** (1970) 1073.

8 Kurien K V, Vaidyan V K & Ittyachen M A, *Colloid & Polymer Sci (Germany)*, **260** (1982) 552.

9 Henish H K, *Crystal growth in gels* (University Park, Pennsylvania, USA) 1979.

10 Morce H W & Pierce G W, *Z Phys Chem (Germany)*, **45** (1903) 589.

11 Jablczynski K, *Bull Soc Chim (France)*, **33** (1923) 1592.

12 Mohanan Pillai K, Vaidyan V K & Ittyachen M A, *Colloid & Polymer Sci (Germany)*, **238** (1980) 831.

13 Liaw H W & Faust J W, *J Cryst Growth (Netherlands)*, **13/14** (1972) 471.

Indian Journal of Pure & Applied Physics
Vol 21, May 1983, pp 264-267

Effects of Quenching & γ-ray Irradiation on the Dielectric Properties of Calcite Single Crystals

N VEERAISH, H B GON & K V RAO*
Physics Department, Indian Institute of Technology, Kharagpur 721 302

Received 25 *September* 1982

Dielectric constant (K), loss ($\tan\delta$) and conductivity (σ) of calcite single crystals irradiated with γ-rays before and after quenching were measured as a function of frequency in the region 10^2-10^7 Hz and in the temperature range 30-400 °C with the electric field parallel to the optic axis of the crystal. Value of K at 30 °C (equal to 7.8 and frequency-independent) is unaffected by quenching and γ-ray irradiation, however, the values of $\tan\delta$, particularly at low frequencies, increase considerably on irradiation and quenching. Increase of K with temperature at different frequencies is more marked for γ-ray irradiated sample; the rate of increase of K at any frequency is maximum for the quenched and γ-ray irradiated sample. A similar behaviour is exhibited by $\tan\delta$ versus temperature graphs for these samples. The plots of $\log\sigma$ versus $1/T$ at different frequencies merge into a straight line beyond 300 °C; the activation energy values for conduction in this region are found to be 0.9, 0.73 and 0.71 eV respectively for the as-cleaved, γ-ray irradiated, and quenched and γ-ray irradiated samples. An attempt is made to explain these observation on the basis of space charge effects.

1 Introduction

Natural calcite is available in the form of large single crystals which are transparent in the near visible region. These crystals show an extraordinary long-period after-glow when irradiated with ionizing radiations like X-rays. As such, the optical properties of both pure and coloured calcite have been extensively studied[1-4]. Recently, possible models for colour centres responsible for absorption bands in X-ray irradiated calcite crystals have been suggested[5].

When X-ray irradiated calcite crystals exhibit phosphorescence or thermoluminescence resulting in release of charge carriers, itwas observed that the dielectric properties of the crystals were considerably affected. Such studies, carried out in this laboratory[6,7], gave useful information regarding the defect processes taking place in this solid.

γ-Ray irradiation is expected to produce considerable changes in the dielectric properties of calcite crystals—more so if the crystals are quenched from 800°C to room temperature. The aim of the present paper is to report the results of our investigations on the effect of γ-ray irradiation on the dielectric properties of natural calcite single crystals before and after quenching them. These properties are studied with electric field parallel to the optic axis ($E\|C$) of the crystals; the frequency region covered is 10^2-10^7 Hz and the temperature range is 30-400 °C. As far as is known to the authors, such a study has not been reported till now-though the dielectric properties of calcite crystals were investigated earlier[8].

2 Experimental Details

The present work was carried out on cleaved crystals of natural calcite of good optical quality. The samples were ground and polished and had, in their final form, the dimensions of $20 \times 20 \times 1$ mm^3. The orientation was checked by means of a polarizing microscope. The dielectric measurements were taken on a GR 716 type capacitance bridge[9] up to 10^5 Hz and on a Marconi circuit magnification metre type TF 329G in the range 10^6-10^7 Hz using the resonance curve principle[6]. Silver paint was applied on both sides of the crystals to serve as electrodes. The accuracy of the measurement of the dielectric constant K is 2% and the loss ($\tan\delta$) is to about 5%. Three samples of calcite crystals were studied and the agreement was within the limits mentioned. Flame photometric and chemical analysis of the calcite crystals showed that Sr is present to about 10 ppm and Mn to 4 ppm.

The samples were irradiated with γ-rays from a ^{60}Co source of 1000 Ci for 48 hr; the samples were kept practically touching the source. Quenching of the crystals to room temperature was done after heating them at 800 °C for 1 hr.

3 Results

The dielectric constant of calcite crystals at 30°C and 10^6 Hz with $E\|C$ is measured to be 7.8 and is frequency-independent, this value remaining unaffected by quenching and γ-ray irradiation; however, the dielectric loss is considerably increased (Fig. 1) due to γ-ray irradiation and quenching.

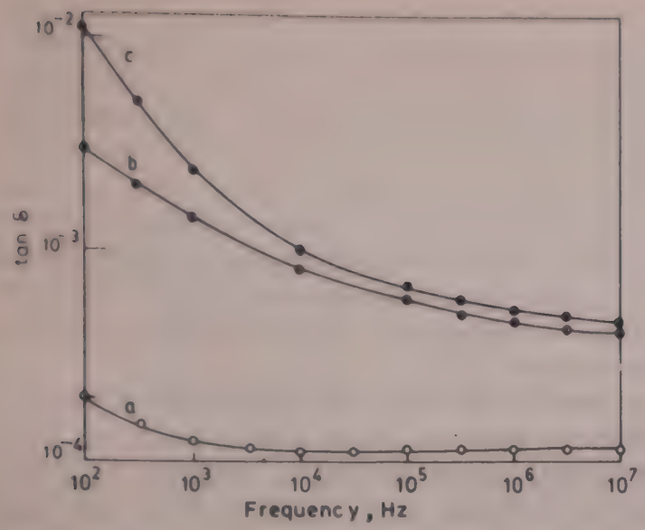

Fig. 1—Dielectric loss (tan δ) at 30°C as a function of frequency of calcite crystals under different conditions [(a), as-cleaved; (b), γ-ray irradiated; and (c), quenched and γ-ray irradiated]

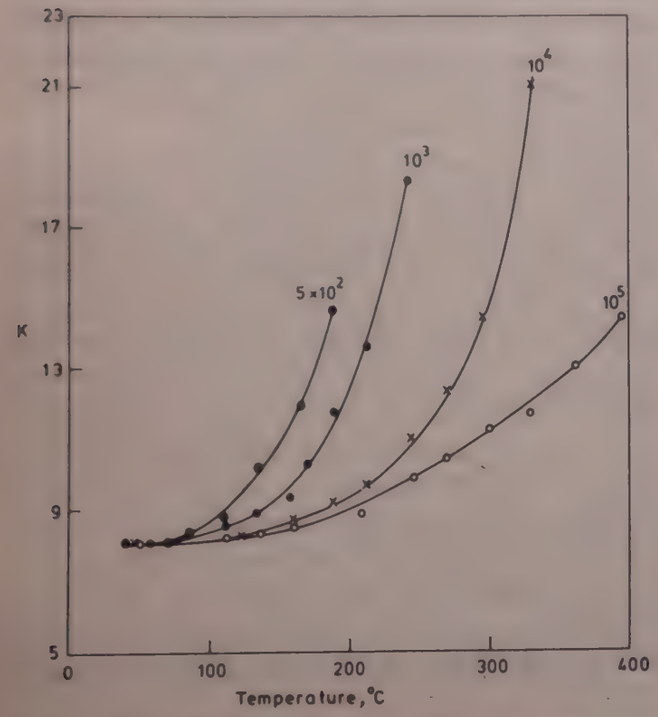

Fig. 2—Variation of dielectric constant (K) with temperature at different frequencies for γ-ray irradiated calcite crystals

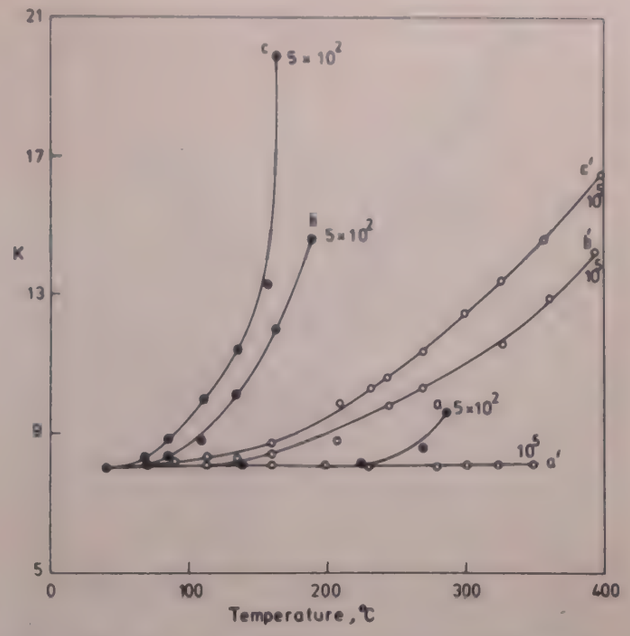

Fig. 3—Dielectric constant (K) as a function of temperature at 5 $\times 10^2$ and 10^5 Hz under different conditions for calcite crystals [(a) and (a'), as-cleaved; (b) and (b'), γ-ray irradiated and (c) and (c'), quenched and γ-ray irradiated]

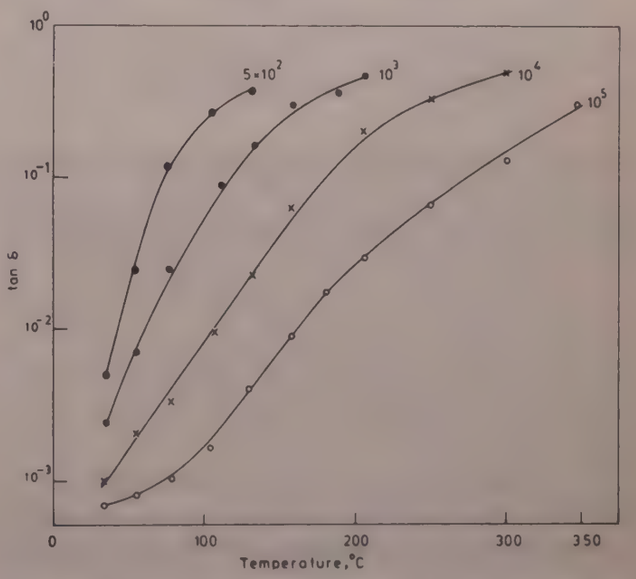

Fig. 4—Variation of dielectric loss (tan δ) with temperature at different frequencies for quenched and γ-ray irradiated calcite crystals

Fig. 2 presents the variation of K of γ-ray-irradiated calcite crystals with temperature at different frequencies. When compared with similar data on calcite, we find that the rate of increase of K with temperature at any frequency is considerably larger in γ-ray irradiated samples. The quenched and γ-ray irradiated sample exhibits the maximum rate of increase of K; in fact, the increase in K value at any temperature, particularly at a low frequency, is quite marked (Fig. 3). The rate of variation of tan δ with temperature at different frequencies (Fig. 4) is found to be also maximum for calcite crystals quenched and γ-ray irradiated.

Observations of the dielectric conductivity $\sigma = \omega K \tan\delta K_0$ (where K_0 is vacuum value of K) were made at different temperatures and the plots of $\log\sigma$ versus $1/T$ are shown in Fig. 5 for calcite crystals irradiated with γ-rays. The activation energy for conduction in the intrinsic region (high temperature, frequency-independent region) is calculated to be 0.73 eV. The pertinent data of the present investigations on calcite crystals are summarized in Table 1.

4 Discussion

Four types of polarizations contribute to dielectric

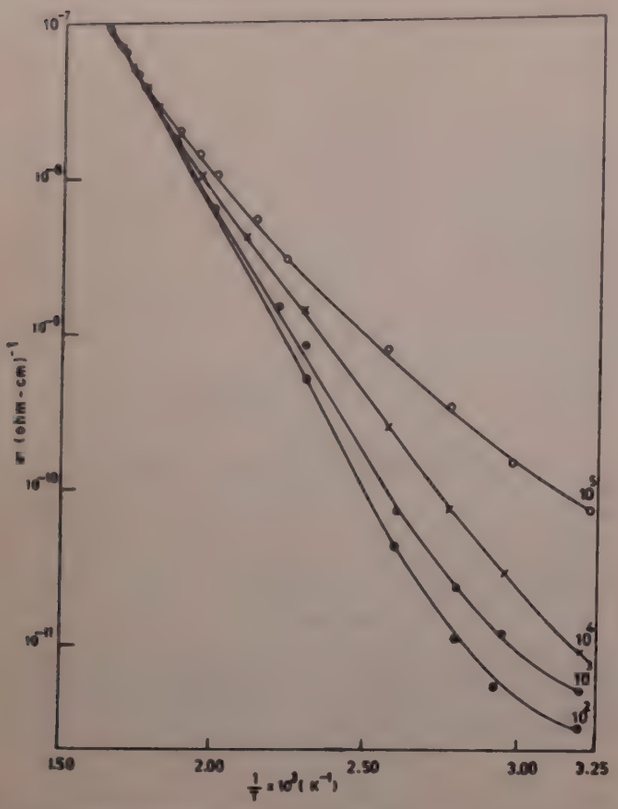

Fig. 5—Conductivity (σ) of γ-ray irradiated calcite crystals as a function of $1/T$ at different frequencies

constant of a material at low frequencies; electronic, ionic, dipolar and space charge. The nature of variation of K with frequency indicates which contributions are present. Space charge polarization depends on the purity and perfection of the crystals. Its influence is noticeable mainly in the low-frequency region. The dipole-orientational effect can be exhibited even up to 10^{10} Hz. The ionic and electronic polarizations always exist below 10^{13} Hz.

γ-Ray irradiation of a material is known to knock off ions from their positions in addition to producing electrons and holes[10]. The displaced ions may collect at the surface of the crystal and some of them may also occupy interstitial positions. As the carbonate bond in calcite is apparently weak, γ-ray irradiation of these crystals may knock off oxygen ions; additionally, some of the other ions of calcite lattice may also be removed from their positions. So the final effect on γ-ray irradiated calcite crystals seems to be the generation of a large number of charged defects like vacancies and interstitials. Quenching and γ-ray irradiation of the crystals are expected to enhance the concentration of these defects.

Reviewing our data, the considerable increase in dielectric loss at room temperature ($\simeq 30^{\circ}$C), particularly at low frequencies, exhibited by calcite crystals irradiated with γ-rays, before and after quenching, may be ascribed to space charge polarization due to the defects. However, the maximum value of $\tan\delta$ measured at 10^2 Hz in quenched and γ-ray irradiated calcite is only 0.01 which is still small enough not to affect the dielectric constant at that frequency. As such, the quenched and γ-ray irradiated samples did not show any increase in their K values at room temperature.

Temperature has a complicated influence on the dielectric constant. Increasing the temperature generally decreases the electronic polarization slightly. The increase in ionic polarization due to thermal expansion is also not very large. Even assuming the presence of a small number of dipoles and their contribution to dielectric constant, we know from Debye's theory that K is inversely proportional to temperature. As such, it is expected that the dielectric constant of calcite should not change considerably with increase in temperature. But we find large increase in K values with temperature in calcite crystals γ-ray irradiated before and after quenching. The crystal defects only can increase and also probably become more mobile with temperature making the space

Table 1—Summary of Data on Dielectric Properties of Calcite Single Crystals

Parameter	Freq.	As-cleaved						γ-ray irradiated						Quenched and γ-ray irradiated					
		10^2 Hz			10^6 Hz			10^2 Hz			10^6 Hz			10^2 z			10^6 Hz		
	Temp., C	30	150	300	30	150	300	30	150	300	30	150	300	30	150	300	30	150	300
K		7.8	8.0	9.1	7.8	7.9	8.5	7.8	13.0	—	7.8	8.2	9.8	7.8	14.5	—	7.8	8.8	11.0
$\tan\delta$		2.0×10^{-4}	2.5×10^{-4}	1.0×10^{-3}	1.1×10^{-4}	1.1×10^{-4}	1.4×10^{-4}	3.0×10^{-3}	8.0×10^{-1}		4.5×10^{-4}	1.8×10^{-3}	1.5×10^{-2}	1.0×10^{-2}	9.5×10^{-1}		5.1×10^{-4}	2.5×10^{-3}	4.0×10^{-2}
σ (ohm-cm)$^{-1}$		8.6×10^{-14}	1.1×10^{-13}	5.0×10^{-11}	4.7×10^{-10}	4.8×10^{-10}	6.6×10^{-9}	1.3×10^{-12}	5.7×10^{-10}	—	1.9×10^{-9}	8.2×10^{-9}	8.1×10^{-8}	4.3×10^{-12}	7.6×10^{-10}		2.2×10^{-9}	1.2×10^{-8}	2.4×10^{-7}

Activation energy (in eV) for conduction in the intrinsic region as-cleaved sample : 0.90; γ-ray irradiated sample : 0.73; quenched & irradiated : 0.71.

charge polarization dominant; hence K increases with temperature[11,12]. The changes in K with temperature in these samples are smaller at higher frequency as this type of polarization decreases considerably at such frequencies. Our results show that the rate of increase of K with temperature (at any frequency) is largest for the quenched and γ-ray irradiated sample, indicating a correspondingly largest concentration of defects in that sample. This conclusion seems to be supported by the fact that the activation energy for conduction in the intrinsic region in these samples is appreciably decreased[12] (Table 1).

References

1 Kolbe W F & Smakula A, *Phys Rev (USA)*, **124** (1961) 1754.

2 Meldin W L, *Phys Rev (USA)*, **135** (1964) 1770.

3 Visocekas R, Ceva T, Marti C, *et al.*, *Phys Status Solidi a (Germany)*, **35** (1976) 315.

4 Debendetti H, *Nuovo Cimento (Italy)*, **7** (1958) 251.

5 Veeraiah N, Gon H B & Rao K V, *Indian J Pure & Appl Phys*, **19** (1981) 1197.

6 Rao K V, *J Phys & Chem Solids (GB)*, **20** (1961) 193.

7 Rao K V & Sujata Roy, *Solid State Commun (USA)*, **20** (1976) 941.

8 Suryanarayana Rao K & Rao K V, *Z Phys (Germany)*, **216** (1968) 300.

9 Westphal W B, *Dielectric constant and loss measurements on high-temperature materials* (Lab for Ind Res MIT) Tech Rep, 182 (1963) 10.

10 Crawford J H(Jr) & Slifkin L M (editors), *Point defects in solids* (Plenum Press, New York) **1** (1972) 201.

11 Rao K V & Smakula A, *J Appl Phys (USA)*, **37** (1966) 319.

12 Govinda S & Rao K V, *Phys Status Solidi a (Germany)*, **27** (1975) 639.

Indian Journal of Pure & Applied Physics
Vol 21, May 1983, pp 268-270

Thermal Noise in an Insulator with Traps Lying above the Fermi Level in Non-constant Mobility Regime

R S AGRAWAL, Y K SHARMA* & S MOHAN
Department of Physics, R B S College, Agra 282003

Received 7 *July* 1982

Analytical expressions for the thermal noise in single injection solid state diodes with traps lying above the Fermi level have been evaluated by using regional approximation and salami methods. The mobility of the injected current carriers is proportional to the carrier density. The thermal noise is shown to be highly suppressed at high injection level of current.

1 Introduction

It is well known that the main origin of noise in space-charge-limited current flow through insulators is thermal noise[1-5] which is generated due to the scattering of injected current carriers with the lattice imperfections present in the device. The presence of traps in the insulator drastically affects the current-voltage characteristic. Therefore, the traps are influencing the thermal noise generated in the device. The noise calculations may be easily obtained by the salami method given by Van der Ziel[1,4]. In this method, the insulator is divided into small slabs which are having noise source present within them.

In a low mobility insulator, the mobility of the current carriers is proportional to carrier density. The results for space-charge-limited single injection current in low mobility insulators are obtained with the help of regional approximation method[6-8]. In this paper, the thermal noise is studied to show the effects of space charge, traps lying above the Fermi level and carrier density dependent mobility.

2 Regional Approximation Method

Let us consider a current injection in a low mobility insulator containing a significant density of a single set of traps lying above the Fermi level. The general equations governing the single injection current flow and Poisson's law in non-constant mobility regime are given by:

$$J = e\mu n E \qquad \ldots(1)$$

$$\left(\frac{\varepsilon}{e}\right)\frac{dE}{dx} = (n - n_0) + (n_t - n_{t,0}) \qquad \ldots(2)$$

where μ is the mobility of the current carrier, n and n_0 are the concentrations of free electrons and their thermal equilibrium value and n_t and $n_{t,0}$ are the concentrations of trapped carriers, and their thermal equilibrium value respectively.

Wintle[6] has shown that in a low mobility insulator containing trapping sites, there is no delay to the moving carriers due to the trapping effect, because the trapping states are permanently occupied by electrons. It gives rise to the mobility (μ) of the current carriers proportional to the carrier density:

$$\mu = hn(x) \qquad \ldots(3)$$

where h is the proportionality constant. These equations are subjected to a boundary condition for ohmic contact

$$E(0) = 0 \qquad \ldots(4)$$

At an appropriate injection level of current, the insulator is divided into four separate regions with the help of the regional approximation method[5,7,8]. These regions are well separated by three imaginary transition planes x_1, x_2 and x_3 which are shifted towards the anode with the increase of injection level of current. The three regions I-III are space-charge-limited and the region IV is ohmic. Agrawal *et al.*[8] have given the detailed description of the application of the regional approximation method to the present problem. The results for transition planes are given by[8]

$$x_1 = \frac{2\varepsilon J}{3e^2 h B^3 n_0^3} \qquad \ldots(5)$$

$$x_2 = \frac{\varepsilon J}{e^2 h B C^2 n_0^3} \qquad \ldots(6)$$

$$x_3 = \frac{2\theta\varepsilon J}{3e^2 h n_0^3} \qquad \ldots(7)$$

where $B = N_t/n_0$, $C = N/gn_0$ and $\theta = C/B$ $\qquad \ldots(8)$

here N_t is the total number of traps, g the statistical weight of traps and N has already been defined elsewhere[7]. It is obvious from Eqs (5)-(7) that the transition planes are proportional to the current density. Therefore, the planes are reaching towards the anode with increase of current.

The complete current-voltage characteristic is divided into four separate regimes by three critical currents defined as

$$x_3(J_{cr,1}) = L, \quad x_2(J_{cr,2}) = L, \quad x_1(J_{cr,3}) = L \qquad \ldots(9)$$

3 Thermal Noise Calculations

The scattering of the current carriers with the lattice imperfections of the insulator yields the current or voltage fluctuations which is the main source of noise in the space-charge-limited solid state diode. A very simple method of noise calculations in such a device is given by Van der Ziel[4]. In this method, the insulator is divided into slabs of small thickness by the planes perpendicular to the current flow. The noise is generated in each slab due to the presence of noise sources in them. The total noise voltage across the device is obtained by taking the sum of voltage drops across each slab.

According to Van der Ziel[4], the noise voltage in a frequency interval Δf in the open-circuited device may be represented as the mean square noise voltage given by:

$$\overline{\Delta v^2} = 4kT\,\Delta R\,\Delta f, \quad \Delta R = \frac{\Delta x}{e\mu nS} = \frac{E\Delta x}{JS} \qquad \ldots(10)$$

where ΔR is the small resistance of a small section Δx, S is the area of cross-section and Eq. (1) is used to obtain the last equality. Summing over all sections of the insulator, Eq. (10) yields

$$\overline{v^2} = 4kTR\,\Delta f, \quad R = \Sigma\,\Delta R = \frac{V}{JS} \qquad \ldots(11)$$

$$\text{where} \quad V = \int_0^L E(x)dx \qquad \ldots(12)$$

The thermal noise is generated in the complete range of current-voltage characteristic in the order of regimes as discussed below.

3.1 Ohmic Regime ($J < J_{cr,1}$), ($x_3 < L$)

Initially the injection level of current is very low so that the injected space-charge does not reach the anode. The current flow is carried by the thermally generated free-carriers. Therefore, Eqs (1) and (12) with $n = n_0$ give the current-voltage characteristic in ohmic regime as:

$$J = e\,h\,n_0^2\frac{V}{L} \qquad \ldots(13)$$

Eq (13) represents the Ohm's law ($J \propto V$). The ohmic resistance (R_Ω) and thermal noise ($\overline{v_\Omega^2}$) are derived from Eqs. (11) and (13) as:

$$R_\Omega = \frac{L}{ehn_0^2S}, \quad \overline{v_\Omega^2} = 4kTR_\Omega\Delta f \qquad \ldots(14)$$

The values of R_Ω and $\overline{v_\Omega^2}$ given by Eq. (14) are constants in nature. This regime will terminate at a critical current $J_{cr,1}$ when the plane x_3 lies on the anode.

3.2 Shallow Trap Regime ($J_{cr,1} < J < J_{cr,2}$)

The three regions I-III are present in the insulator. The transition planes x_1 and x_2 are very close to cathode. Therefore, the main contribution to thermal noise is obtained by the shallow trap region III. From the analysis[8], the onset values of shallow trap regime are given by:

$$J_{cr,1} = \frac{3e^2hn_0^3L}{2\theta\varepsilon} \qquad \ldots(15)$$

$$V_{cr,1} = \frac{9en_0L^2}{10\theta\varepsilon} \qquad \ldots(16)$$

where the critical voltage $V_{cr,1}$ is corresponding to the critical current $J_{cr,1}$. The critical noise resistance and thermal noise are derived from Eqs (11), (15) and (16) given by:

$$R_{cr,1} = \frac{V_{cr,1}}{J_{cr,1}S} = \frac{3L}{5ehn_0^2S} \qquad \ldots(17)$$

$$\overline{v_{cr,1}^2} = 4kTR_{cr,1}\Delta f \qquad \ldots(18)$$

This regime is terminated at the critical current $J_{cr,2}$.

3.3 Trap Filled Limit (TFL) Regime ($J_{cr,2} < J < J_{cr,3}$)

In this regime, the regions I and II are present inside the insulator as the transition plane x_2 leaves the insulator at the onset critical values given by[8]

$$J_{cr,2} = \frac{BC^2e^2hn_0^3L}{\varepsilon} \qquad \ldots(18)$$

$$V_{cr,2} = \frac{Ben_0L^2}{2\varepsilon} \qquad \ldots(19)$$

All the traps are gradually filled during the TFL regime. The critical noise resistance and thermal noise corresponding to Eqs (18) and (19) are evaluated as:

$$R_{cr,2} = \frac{V_{cr,2}}{J_{cr,2}S} = \frac{L}{2C^2ehn_0^2S} \qquad \ldots(20)$$

$$\overline{v_{cr,2}^2} = 4kTR_{cr,2}\Delta f \qquad \ldots(21)$$

where Eq. (11) is used.

All the traps are completely filled at the terminating current and voltage[8]

$$J_{cr,3} = \frac{3B^3Le^2hn_0^3}{2\varepsilon} \qquad \ldots(22)$$

$$V_{cr,3} = \frac{9en_0BL^2}{10\varepsilon} \qquad \ldots(23)$$

The corresponding critical noise resistance and thermal noise is derived from Eqs (11), (22) and (23)

$$R_{cr,3} = \frac{V_{cr,3}}{J_{cr,3}S} = \frac{3L}{5B^2ehn_0^2S} \qquad \ldots(24)$$

$$\overline{v_{cr,3}^2} = 4kTR_{cr,3}\Delta f \qquad \ldots(25)$$

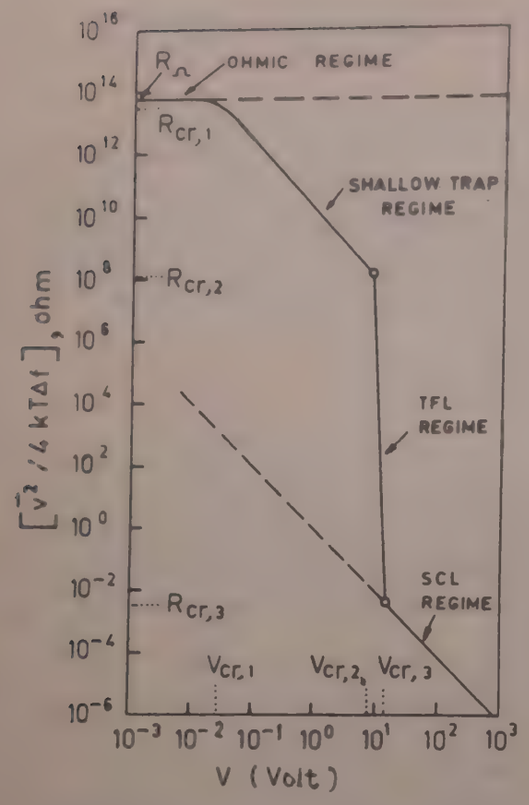

Fig. 1—Log-log plot of noise resistance ($\overline{v^2}/4kT\Delta f$) versus applied voltage.

3.4 Trap-Free Regime ($J > J_{cr,3}$)

The space-charge region I entirely fills the insulator in this regime. The current is controlled by space-charge conditions. Therefore, from Eqs (1)-(4) by neglecting n_0, n_t and $n_{t,0}$ in Poisson's Eq. (2), the current-voltage characteristic for trap free regime is given by:

$$J = 2.06 \frac{\varepsilon^2 h}{e} \frac{V^3}{L^5} \quad \ldots(26)$$

The noise resistance (R_s) and thermal noise ($\overline{i_s^2}$) for space-charge-limited trap-free regime are derived from Eqs (11) and (26):

$$R_s = \frac{V}{JS} = \frac{e L^5}{2.06 \varepsilon^2 h V^2 S} \quad \ldots(27)$$

$$\overline{i_s^2} = 4kT R_s \Delta f \quad \ldots(28)$$

Values of R_s and $\overline{i_s^2}$ given above show that the thermal noise is decreasing as the square of the applied voltage in the trap-free regime.

4 Discussion

Complete variation of noise resistance $[\overline{v^2}/4kT\Delta f]$ with applied voltage is shown in Fig. 1 on a log-log scale by using Eqs (13)-(28). The continuous curve is started from a miximum value R_Ω in the ohmic regime. The noise resistance in the shallow trap regime ($V_{cr,1} < V < V_{cr,2}$) is varied from $R_{cr,1}$ to $R_{cr,2}$ which are lower than the ohmic resistance. There is a steep fall from $R_{cr,2}$ to $R_{cr,3}$ during trap-filled-limit (TFL) regime ($V_{cr,2} < V < V_{cr,3}$). In the last space-charge-limited trap free regime ($V_{cr,3} < V$), the noise is decreasing with the increase in voltage. The following parameters and Eqs (13)-(28) are used to draw Fig. 1:

$B = 10^8$, $C = 500$, $h = 10^{-19}\ \mathrm{m^5 V^{-1} s^{-1}}$,

$L = 10^{-5}\ \mathrm{m}$,

$n_0 = 10^{12}\ \mathrm{m^{-3}}$, $\varepsilon = 10^{-10}\ \mathrm{F/m}$, $S = 10^{-5}\ \mathrm{m^2}$.

It may be pointed out from Fig. 1 and Eq. (27) that the noise resistance during shallow trap and SCL regimes are parallel to each other. Therefore, the thermal noise in shallow trap regime is also decreasing as the square of the applied voltage. In the complete range of current-voltage characteristic, the following inferences may be drawn:

(a) The space-charge highly suppresses the thermal noise from an initial high value.

(b) There is a large suppression in the thermal noise (over several orders of magnitude) during TFL regime for a restricted change in voltage. It is due to this fact that the traps are rapidly filled by electrons in this regime which reduces the fluctuation in current.

(c) Eq. (24) shows that the thermal noise is very much reduced for higher values of the parameter B.

References

1 Van der Ziel A, *Noise* (Prentice Hall, Engiewood Cliffs, New Jersey), 1954.

2 Van der Ziel A, *Solid-State Electron (GB)*, **9** (1966) 899.

3 Hsu S T, Van der Ziel A & Chenette E R, *Solid-State Electron (GB)*, **10** (1967) 129.

4 Van der Ziel A, *Proc IEEE (USA)*, **58** (1970) 1178.

5 Sharma Y K, *Phys Rev B (USA)*, **10** (1974) 3273.

6 Wintle H J, *J Appl Phys (USA)*, **43** (1972) 2927.

7 Sharma Y K, *J Appl Phys (USA)*, **53** (1982) 1241.

8 Agrawal R S, Sharma Y K & Gautam V K, unpublished work.

Indian Journal of Pure & Applied Physics
Vol 21, May 1983, pp 271-275

Successive Phase Transitions in Tetramethylammonium Tetrachlorozincate

V SRINIVASAN, C K SUBRAMANIAN & P S NARAYANAN*
Department of Physics, Indian Institute of Science, Bangalore 560012

Received 1 *February* 1983

Tetramethylammonium tetrachlorozincate ($TMAZnCl_4$) shows six successive phase transitions in the temperature range 80-300 K. Polarized Raman spectra of oriented single crystals of $TMAZnCl_4$ and the infrared spectra by the KBr pellet technique have been recorded from 298 K to 130 K, covering all the known phase transitions. An increase in the frequency of the Zn-Cl stretching vibration is found in Raman and infrared spectra as the temperature is lowered. Three bands are found in the Raman spectrum in the region where CH_3 frequencies usually occur and, in a similar way, three bands appear in the infrared spectrum at low temperature due to the deformation vibrations of the CH_3 group. The triggering mechanism of the phase transition at low temperature can be due to a coupling of the distortion of $(ZnCl_4)^{2-}$ groups and the CH_3 deformation, where the motion of relatively free methyl rotations is slowed down, favouring one equilibrium position below 161 K. The phase transition appears to be an order-disorder one with methyl rotational disorder in the high temperature paraelectric phase.

1 Introduction

Tetramethylammonium tetrachlorozincate abbreviated as $TMAZnCl_4$ belongs to the family of crystals of the type A_2BX (A = Rb, Cs, NH_4..., B = Zn, Co, Mn..., X = Cl, Br, I...) which shows an incommensurate phase in their phase transition sequence. $TMAZnCl_4$ undergoes six phase transitions in the temperature range 80-300 K. They are shown in Table 1. Dielectric and DTA[1], X-ray crystal structure[2,3], hydrostatic pressure[4] and neutron scattering studies[5] and ultrasound investigations[6] have been carried out on this crystal. The ferroelectric phase in this crystal goes through an incommensurate phase to the commensurate phase transition similar to the one found in ferroelectric K_2SeO_4 (Ref. 7). Raman scattering at the room temperature 293K has earlier been studied and the modes in the lattice region have been reported[8]. Takashigi *et al.* have studied Raman scattering of this crystal, in the ferroelectric phase 275K and could not find any softmode in this phase[9]. No detailed Raman and infrared studies have been reported to establish the nature of phase transition in the low temperature phases IV, V and VI. The present Raman and infrared studies have been undertaken to cover all the phase transitions and to look for, through spectra structure correlation, the possible triggering mechanism.

2 Experimental Details

Crystals of $[N(CH_3)_4]_2ZnCl_4$ were grown by a slow evaporation of an aqueous solution containing stoichiometric ratios of TMACl and $ZnCl_2$. The crystals were transparent and colourless. Crystal plates in the form of a parallelopiped were illuminated by an Ar^+ ion laser radiation (488 nm) of power 100-200 mW and the spectra were recorded with a SPEX Ramalog-6 spectrometer employing a photon counting system. The IR absorption spectra were recorded using a Perkin-Elmer 580 IR spectrophotometer and the KBr pellet technique. The spectral slit width in the Raman spectrometer was set to 1-2 cm^{-1} band pass. The temperature of the sample was varied using a simple continuous flow cryostat and the temperature stability was ± 1 K.

X-ray studies[2] show that the room temperature structure has the orthorhombic space group *Pnam* in the paraelectric phase, with four molecules per unit cell. The lattice constants are $a = 12.268$ Å, $b = 15.515$ Å, $c = 8.964$ Å. Between 293 K and 279 K $TMAZnCl_4$ has an incommensurate phase with a

Table 1 — Successive Phases in $TMAZnCl_4$

Transition temp., K:	Phase VI	161K	Phase V	181K	Phase IV	276K	Phase III	279K	Phase II	193K	Phase I
Phase	Ortho-rhombic $P2_12_12_1$		Monoclinic or triclinic $P2_1/C1$		Mono-clinic $P12_1n$		Ortho-rhombic $Pna2_1$		Incommen-surate		Ortho-rhombic *Pnam*

superstructure which is characterized by a wave vector $\mathbf{q}=(1-\delta)\mathbf{a}^*/3$ where δ depends on the temperature; $\delta = -0.34$ at $T_i=293$ K and $\delta=0$ at $T_c=279.2$ K. The crystal structure is similar to $CsZnCl_4$ where Cs^+ ions are replaced by $N(CH_3)_4^+$ ions[10]. There are two kinds of polyatomic radicals in the unit cell, one being the cation $N(CH_3)_4^+$,(8 per unit cell) and the other $(ZnCl_4)^{2-}$ (4 per unit cell). According to group theory, $TMAZnCl_4$ has 468 modes separated into 396 internal modes and 72 external modes (36 rotatory lattice modes and 36 translatory lattice modes of which 3 form the acoustic branches). The symmetry correlations for $[N(CH_3)_4]_2ZnCl_4$ in the paraelectric and ferroelectric phases are shown in Tables 2 and 3 respectively. The ions occupy only general positions in the other phases below 276 K.

3 Results

3.1 Raman and IR Spectra at Room Temperature (298 K)

Polarized Raman spectra of the single crystal of $TMAZnCl_4$ have been taken for six orientations in the range 50-3400 cm^{-1} at 298 K and the infrared spectrum of this compound was taken in the range 200-4000 cm^{-1}, using the KBr pellet technique at 298 K. The observed Raman and IR frequency shifts at 298 K and at low temperature and the assignments are shown in Table 4. The typical Raman spectra are shown in Fig. 1. The polarized Raman spectra of $TMAZnCl_4$ contains the lattice modes and $ZnCl_4^{2-}$ internal vibrations (50-350 cm^{-1}), the ammonium skeletal vibrations (350-1050 cm^{-1}) of the TMA^+ ions, the methyl bending and rocking vibrations (1050-1500 cm^{-1}) and the methyl stretching vibrations (2500-3200 cm^{-1}). In the lattice region, the Raman spectrum is generally weak in intensity excepting a sharp line at 277 cm^{-1} which is interpreted due to $ZnCl_4^{2-}$ internal vibrations. The C–N stretching frequencies at 757 cm^{-1} and 954 cm^{-1} are strong in intensity and are highly polarized. Both methyl symmetric deformation bands are weak but both methyl asymmetric deformation bands are strong.

Table 2—Symmetry Correlation for Paraelectric $[N(CH_3)_4]_2$ $ZnCl_4$ at Room Temperature (293 K)

Free ions		Sites	Crystal	Activity
$N(CH_3)_4^+$	T_d	C_s	D_{2h}	
$ZnCl_4^{2-}$				
A_1		A'	A_g	Raman
E			B_{1g}	Raman
F_1		A''	B_{2g}	Raman
			B_{3g}	Raman
F_2			A_u	Inactive
			B_{1u}	IR
			B_{2u}	IR
			B_{3u}	IR

Table 3—Symmetry Correlation for Ferroelectric $[N(CH_3)_4]_2$ $ZnCl_4$

Free ion	Sites	Crystal	Activity
T_d	C_1	C_{2v}	
A_1	A	A_1	Raman & IR
E		A_2	Raman
F_1		B_1	Raman & IR
F_2		B_2	Raman & IR

3.2 Low-Temperature IR and Raman Spectra

The Raman and IR spectra were taken at low temperatures covering all phase transitions listed in Table 1. The results are presented in Table 4. When the crystal is cooled to the ferroelectric phase, the $ZnCl_4^{2-}$ stretching frequency (ν_1) is increased from 277 to 279 cm^{-1}. In the infrared spectrum, this corresponding line is shifted from 270-277 cm^{-1}. The ν_2 symmetric deformation vibration of CH_3, which gives a weak band at 298 K, becomes sharper in the ferroelectric phase in the Raman spectra. The ν_1 symmetric stretching of CH_3 band 2987 cm^{-1} at 298 K is shifted to 2988 cm^{-1} which is reflected in IR spectra also. When the crystal is cooled to 133 K, covering the transition from phase V to VI, the ν_1 stretching band of $ZnCl_4^{2-}$ increases from 277 cm^{-1} to 282 cm^{-1} in Raman spectrum and from 270 to 285 cm^{-1} in IR spectrum. The ν_1 and ν_4 stretching vibrations of C–N increase from 757 to 760 cm^{-1} and 954 to 956 cm^{-1} respectively. The ν_4 asymmetric deformation of CH_3 increases in intensity while in the region of ν_2 symmetric deformation of CH_3, at 1420 cm^{-1}, three bands appear as 1408, 1414 and 1428 cm^{-1} respectively in the Raman spectra (Fig. 2). In the infrared spectra, the corresponding band shows maxima at 1409, 1419 and 1429 cm^{-1} respectively (Fig. 3). The ν_1 stretching frequency of CH_3 at 2987 cm^{-1} decreases in intensity, but leads to three bands at 2979 cm^{-1}, 2987 cm^{-1} and 2990 cm^{-1} respectively in Raman spectra (Fig. 2) while in the infrared spectrum, the ν_2 symmetric stretching of CH_3 gives rise to three bands at 1070 cm^{-1}, 1080 cm^{-1} and 1085 cm^{-1} respectively. Also the rocking mode of CH_3 in the infrared spectrum is split into two bands 1287 cm^{-1} and 1295 cm^{-1}. The width of ν_1 stretching band of

Table 4—Raman and Infrared Frequencies in $TMAZnCl_4$ in Various Phases

Assignment	298 K		278 K		263 K		173 K		133 K	
	Raman	IR	Raman	IR	Raman	IR	Raman	IR	Raman	IR
ν_L lattice	63	—	63	—	63	—	63	—	63	—
	70	—	70	—	70	—	70	—	70	—
$ZnCl_4^{2-}$ internal	132	—	125	—	126	—	131	—	132	—
vibrations	277	270	279	277	279	280	282	282	282	285
	370	—	370	—	371	—	372	—	372	—
Skeletal TMA	460	453	459	457	457	457	457	457	457	457
vibrations ν(C – N)	757	—	757	—	757	—	759	—	760	—
	954	948	954	950	954	950	956	912	956	912
								912		952
ν_2 symmetric stretching CH_3 (T_{2g})	1068	1070	1069	1080	1069	1080	1070	1070	1070	1070
								1080		1080
								1085		1085
ν_8-Rocking (E_g) CH_3	1174	1175	1175	1175	1175	1175	1175	1177	1176	1177
ν_8-Rocking CH_3 (T_{2g})	1284	1285	1285	1288	1286	1288	1286	1287	1286	1287
								1295		1295
ν_2 symmetric deformation CH_3 (T_{2g})	1420	1417	1420	1417	1420	1417	1408	1409	1408	1409
							1414	1419	1414	1419
							1428	1429	1428	1429
ν_4 asymmetric deformation (E_g) CH_3	1457	1450	1459	1450	1456	1450	1459	1447	1456	1447
Nonfundamental	1480	1485	1480	1482	1480	1482	1480	1470	1480	1470
								1480		1485
Nonfundamental	2930	—	2929	—	2930	—	2928	—	2928	—
	2960		2960		2928		2959		2960	
ν_1 symmetric stretching (A_{1g})	2987	2960	2988	2960	2987	2960	2979	2960	2979	2955
							2987		2987	
							2990		2990	
ν_3 asymmetric stretching (E_g or T_{2g})	3028	3020	3028	3020	3029	3020	3029	3020	3029	3025

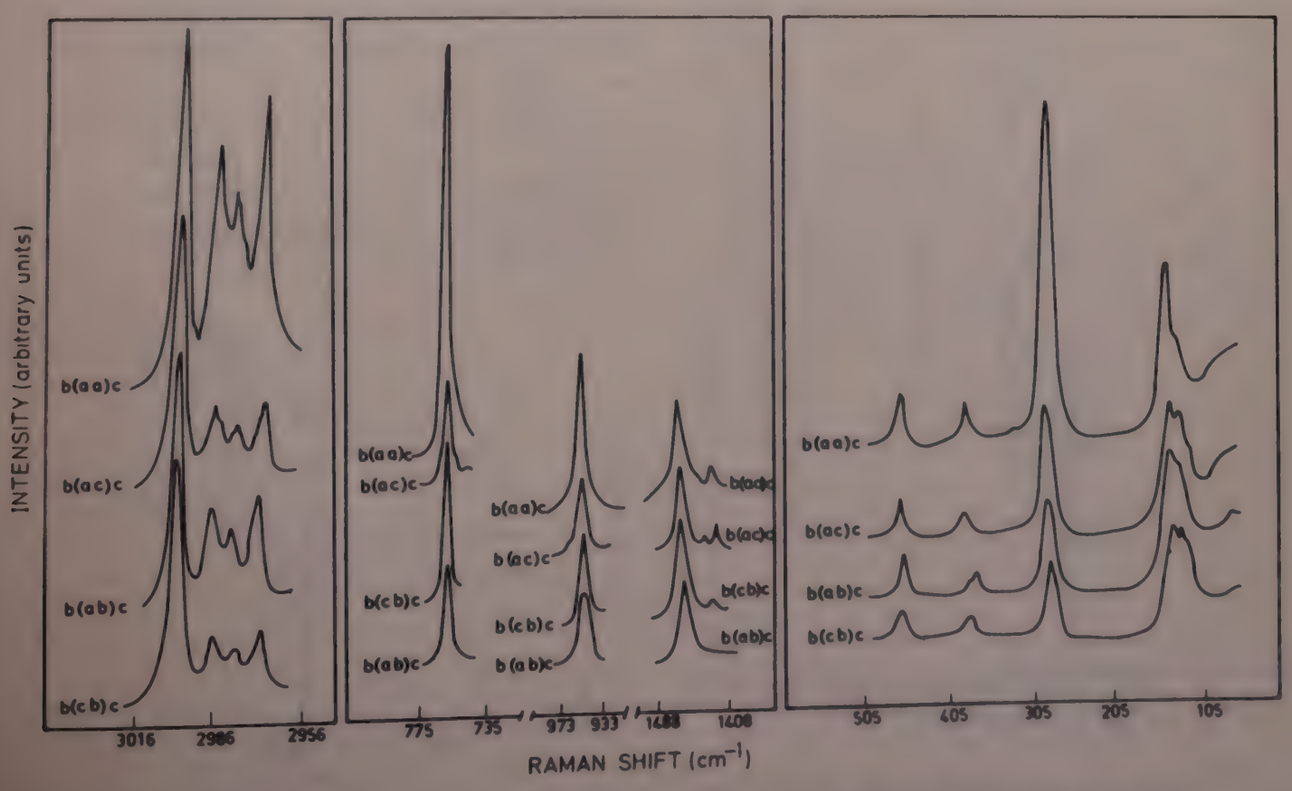

Fig. 1—Raman spectra of tetramethylammonium tetrachlorozincate at 298 K in the region 50-3000 cm^{-1}

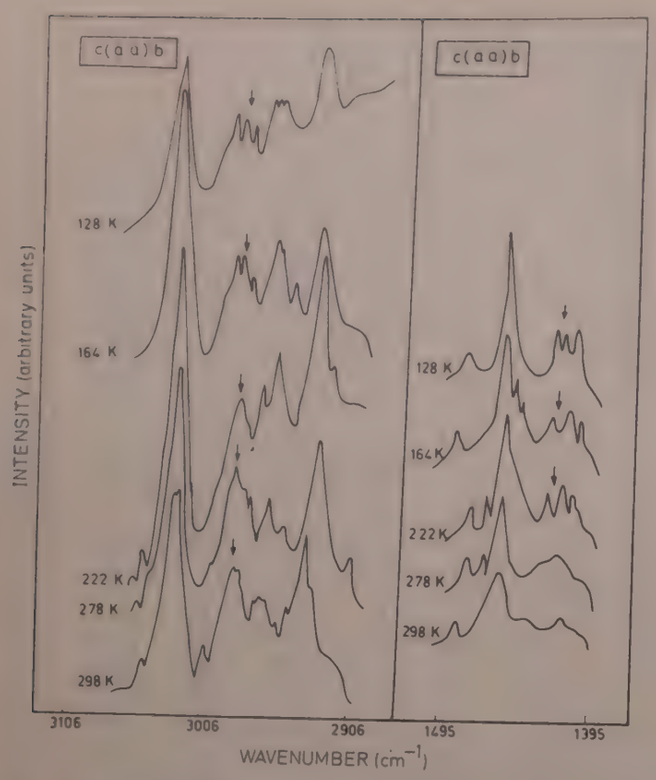

Fig. 2—Raman spectra of tetramethylammonium tetrachlorozincate at different temperatures

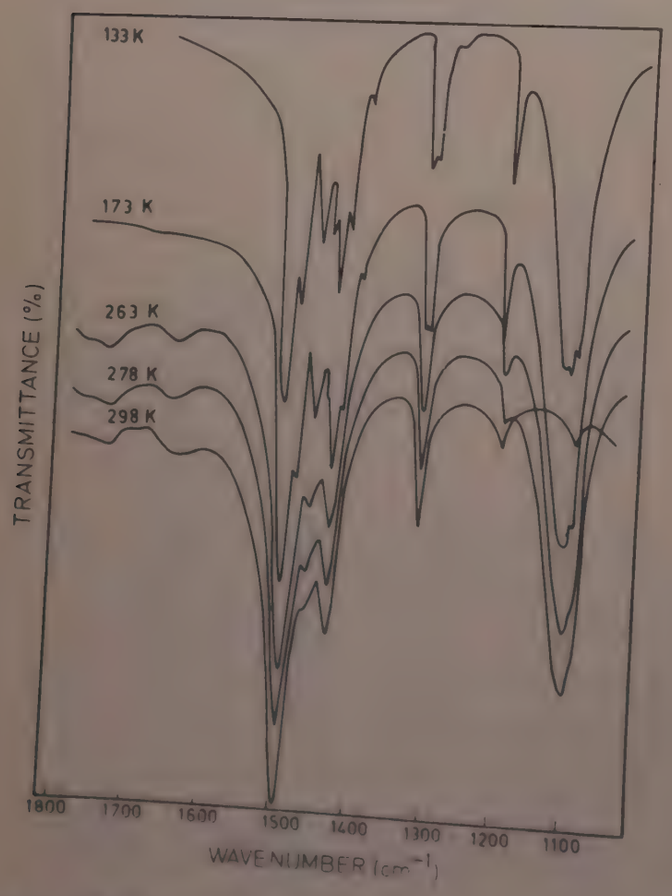

Fig. 3—Infrared spectra of tetramethylammonium tetrachlorozincate in the region 1100-1800 cm^{-1} at different temperatures

CH_3 increases at low temperatures. The single band at 952 at room temperature in the infrared spectra splits up into two bands and this could be due to nonequivalent C−N bonds in the low temperature. The variation of CH_3 stretching frequency with temperature in the IR spectra is shown in Fig. 4.

4 Discussion

The structure of $TMAZnCl_4$ is similar to $CsZnCl_4$. The $ZnCl_4$ units are not perfect tetrahedra but three of the $ZnCl_4$ bonds have lengths 2.274Å, 2.285Å and 2.285 Å whereas the fourth, Zn-Cl bond, is larger with a value of 2.303Å $ZnCl_4$ tetrahedra thus appear to be distorted in the form of flattened tetrahedra[3]. In the Raman and IR spectra, the observation of three frequencies, characteristic of the CH_3 stretching vibrations and three frequencies attributable to the deformation vibrations of the CH_3 groups in the infrared and Raman spectra of $TMAZnCl_4$ and the broadening of the line due to the CH_3 stretching vibrations at 133 K suggest that the motion of the deformed CH_3 groups play an important role in the transition from phase IV to VI. The decrease in intensity of ν_1 stretching vibrations of the CH_3 groups and the temperature sensitiveness of the band, indicated above, enable one to conclude that there is a strong coupling between the deformation of CH_3 groups and the distortion of the $(ZnCl_4)^{2-}$ in the low temperature phase and could be related to the ferroelectric behaviour in phase III.

The phase transitions at the low temperature can be viewed, therefore, as an order-disorder type with methyl rotation disorder in the high temperature paraelectric phase. The recent calorimetric studies reveal that methyl groups are ordered below 161 K whereas a large disorder is attained in the room temperature[11]. Blinc *et al.* have shown by NMR studies, that the methyl groups are ordered in the low temperature phase[12].

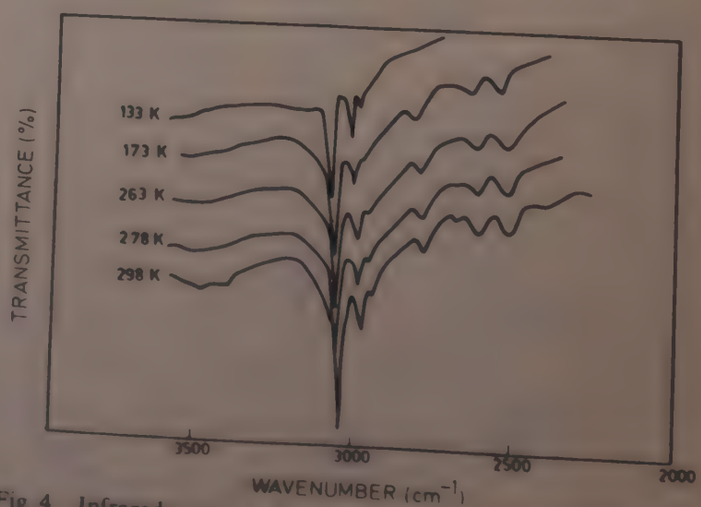

Fig. 4—Infrared spectra of tetramethylammonium tetrachlorozincate in the region 2000-3500 cm^{-1} at different temperatures

Acknowledgement

One of the authors (V. Srinivasan) wishes to express his thanks to Prof. R. Srinivasan, Chairman of Physics Department, for his keen interest in this work. He is also thankful to Prof. C.N.R. Rao, Chairman, Solid State and Structural Chemistry Unit, for getting the infrared absorption spectra of the sample. He is grateful to University Grants Commission, New Delhi for the award of teacher fellowship under the faculty improvement programme (FIP).

References

1 Sawada S, Shiroishi Y, Yamamoto A, *et al.*, *J Phys Soc Jpn* (*Japan*), **44** (1978) 687.

2 Morosin B & Lingaelter E O, *Acta Crystallogr*, (*Denmark*), **12** (1959) 611.

3 Weisner J R, Srivastava R C, Kennard C H L, *et al.*, *Acta Crystallogr* (*Denmark*), **23** (1967) 565.

4 Shimiza H, Oguri A, Abe N, *et al.*, *J Phys Soc Jpn* (*Japan*), **49** (1980) 223.

5 Gesi K & Izimi M, *J Phys Soc Jpn* (*Japan*), **48** (1980) 337.

6 Hashizaki H, Sawada A & Ishibashi Y, *J Phys Soc Jpn* (*Japan*), **47** (1979) 341.

7 Izumi M, Axe J D, Shirani G & Shimaoka K, *Phys Rev B* (*USA*), **15** (1977) 4392.

8 Bon A M, Almirac R, Massiri P, Benoit C & Ribet J L, *Phys Status Solidi b* (*Germany*) **101** (1980) K87.

9 Takashige M, Nakamura T & Sawada S, *Ferroelectrics* (*USA*), **24** (1980) 143.

10 Brchler B, *Z Kristallogr* (*Germany*), **68** (1957) 109.

11 Ruiz Lassea I, Lopez Echari A & Rellow M J, *J Phys C* (*GB*), **14** (1981) 3171.

12 Blinc R, Burger M, Slak J *et al.*, *Phys Status Solidi a* (*Germany*), **56** (1979) K65.

8 Bon A M, Almirac R, Massiri P, Benoit C & Ribet J L, *Phys Status Solidi* b (*Germany*), **101** (1980) K87.

Indian Journal of Pure & Applied Physics
Vol 21, May 1983, pp 276-279

Fundamental Absorption Edge of SnSe Crystal

A K GARG*†
Department of Physics, N A S College, Meerut 250001
A K JAIN
Electronics Commission, New Delhi 110016
&
O P AGNIHOTRI
Department of Physics, Indian Institute of Technology, New Delhi 110016

Received 11 *February* 1982; *accepted* 15 *February* 1983

Single crystals of *p*-type SnSe have been grown by simplified Bridgeman method. The crystals were analyzed by X-ray diffraction technique and the lattice parameter values obtained are: $a=4.3$ Å, $b=4.05$ Å and $c=11.62$ Å. The absorption spectrum of the crystal in the range 0.5-1.3 eV has been recorded for two light polarizations ($E \| a$ and $E \| b$). A detailed analysis of the absorption coefficient curve in the fundamental absorption edge region indicated the existence of indirect allowed transitions. The values of indirect energy gaps were 0.94 eV for $E \| a$ and 0.891 eV for $E \| b$. It was found that the phonon assisted transitions required the participation of a phonon with energy 0.022 eV for $E \| a$ and 0.009 eV for $E \| b$ at different energy thresholds.

1. Introduction

The binary IV-VI compounds with Ge, Sn and Pb as cations and S, Se and Te as anions form a very interesting class of semiconducting crystals. These can be divided into three groups according to crystal structure. The lead chalcogenides (PbS, PbSe and PbTe) crystallize in a cubic (NaCl) structure, are very easy to grow and have been thoroughly studied[1]. GeTe and SnTe have a rhombohedral structure at low temperatures, converting to cubic at T=0°C for SnTe and at $T=400$°C for GeTe. These compounds have also been extensively studied[2], though not as fully as lead compounds. The remaining four compounds, viz. GeS, GeSe, SnS and SnSe have an orthorhombic (space group D_{2h}^{16}) crystal structure[2] and are least studied of the three groups. These are in many ways intermediate between two-dimensional (layer) structures and three-dimensional crystals. SnSe is a fairly typical member of this interesting class of isomorphic materials.

The SnSe crystal is made up by tightly bound double layers of Sn and Se atoms stacked along the *C*-axis as shown in Fig. 1. This lattice structure[3] can be viewed as a severely distorted NaCl structure. Each atom has three strongly bonded neighbours within its own layer and three more distant weakly bonded neighbours one of which lies in an adjacent layer. The bonding between layers is weak, being of Van der Waal's type, and therefore, SnSe can be easily cleaved in the (001) plane. From this fact, one might expect SnSe to exhibit the typical anisotropy of a layer structure.

†Present address: Department of Physics, Institute of Advanced Studies, Meerut University, Meerut 250005

2. Experimental Details

Single crystals of SnSe were prepared by the Bridgeman technique. Fig. 2 shows the schematic diagram of the furnace used. A translucent silica tube of 5 cm diameter and 50 cm length was wound directly by using Kanthal A wire (1.78 Ω/m) covered with insulating beads. The muffle was kept in a central rectangular hole constructed from hot face good quality insulating bricks. The space between bricks and muffle was filled with alumina powder. The complete length of the silica tube was divided into two zones (20 and 30 cm respectively), each zone having its separate heating element, power supply and temperature controller. The temperature profile of the furnace used for growth is also shown in Fig. 2. A double walled quartz ampoule of 20 cm length and 2.2 cm diameter was half filled with stoichiometric amounts of powdered Sn and Se, evacuated and sealed properly. The tin and selenium used were of 99.999% purity supplied by Koch Light Ltd, England. The ampoule was vibrated for half an hour to ensure mixing of elements and held vertically in the upper zone for 2 days at a temperature above 900 C (the melting point of SnSe is 860°C). The ampoule was removed from the furnace, vibrated again for half an hour and put again in the furnace for 6 more hours in order to obtain complete reaction between the crystal components. Now, the ampoule was gradually lowered with a speed approximately 3 mm/hr using a gear box specially fabricated for this purpose. The melt of SnSe began to crystallize from the bottom of the inner ampoule. When the crystal reached the temperature of 650°C, it was annealed for 1 day to reduce crystal imperfections

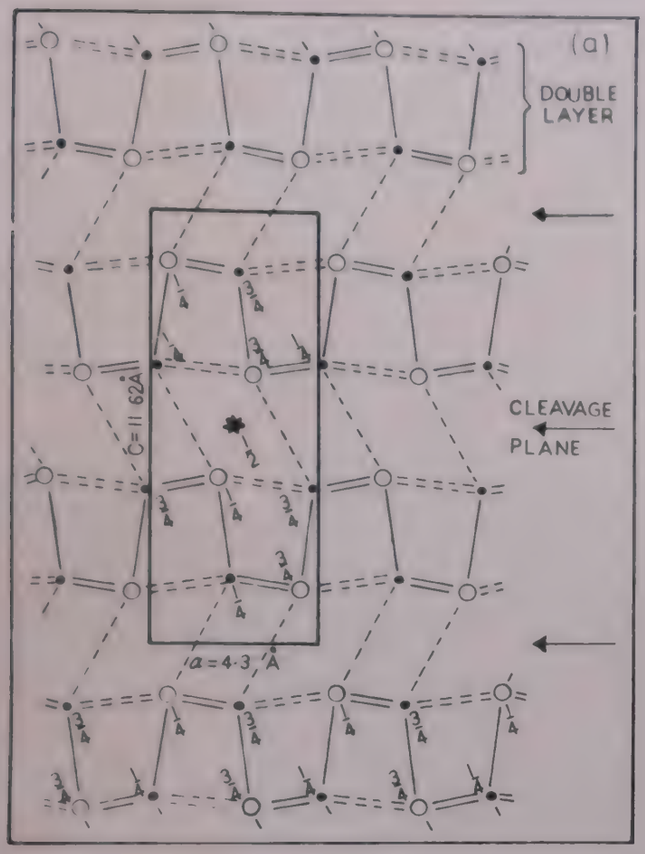

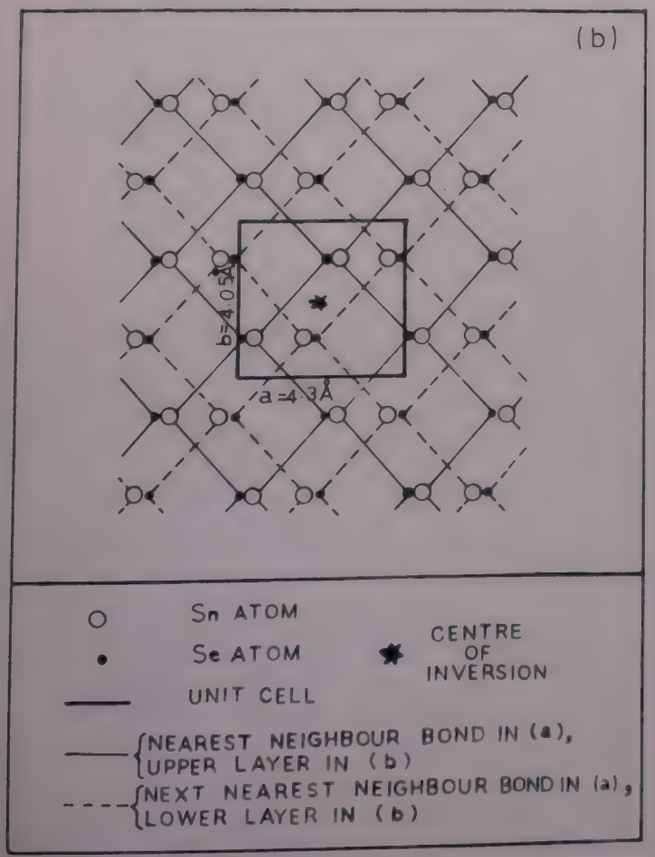

Fig. 1 SnSe structure [(a) Projection on (010) plane; (b) projection on (001) plane].

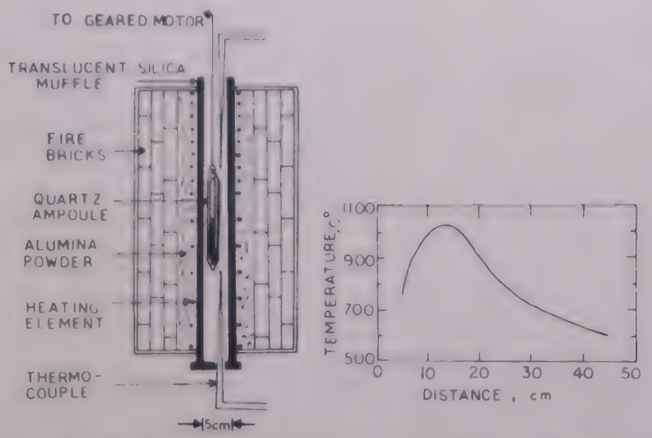

Fig. 2 Bridgeman furnace and its temperature profile

Fig. 3 Electron diffraction pattern of SnSe crystal

and then cooled down to room temperature at a rate of 20 C hr. The grown crystals were approximately 3 cm long and 1.5 cm in diameter. The electron diffraction photograph of the crystal (Fig. 3) showed that the material was a single crystal. From X-ray diffraction studies of the crystal powder, the values of lattice constants were found to be $a = 4.3$ Å, $b = 4.05$ Å and $c = 11.62$ Å. Subsequent electrical characterization measurements indicated that the specimens were of p-type with hole concentration in the range 10^{16}-10^{17} cm^{-3}.

Thin crystals (thickness 50-250 μm) for the absorption studies were obtained by cleavage, which was performed with the aid of cellophane tape. The a and b axes are contained in the cleavage plane of the specimens and were located using standard Laue diffraction technique. No measurements could be performed for $E \| c$ because the crystal was considerably soft and did not permit cutting and

polishing. The optical absorption data were obtained in the photon energy range 0.5-1.3 eV at room temperature (300 K). When the sample thickness was appropriate, interference fringes were observed in the transmitted beam for both directions of light polarization employed ($E \| a$, $E \| b$). The values of the optical parameters were determined following the method proposed by Hazelwood[4] using least squares refinement[5].

3 Results and Discussion

Fig. 4 shows the spectral variation of absorption coefficient and refractive index for two directions of polarization ($E \| a$, $E \| b$). The difference in the absorption coefficients for the two directions is greater in the vicinity of the absorption edge, converging to a single value as the wavelength increases. A detailed analysis[6] of the power dependence of the absorption curve in the fundamental absorption edge region revealed the existence of indirect allowed transitions. For indirect allowed transitions:

$$\alpha h\nu = A\{N_p(\hbar\nu - E_g + \hbar\omega_i)^2 + (1+N_p)(\hbar\nu - E_g - \hbar\omega_i)^2\} \quad \ldots (1)$$

where E_g is indirect band gap energy, $\hbar\omega_i$ is the energy of the phonon and N_p, the number of phonons is given by,

$$N_p = \{\exp(\hbar\omega_i/k_BT) - 1\}^{-1} \quad \ldots (2)$$

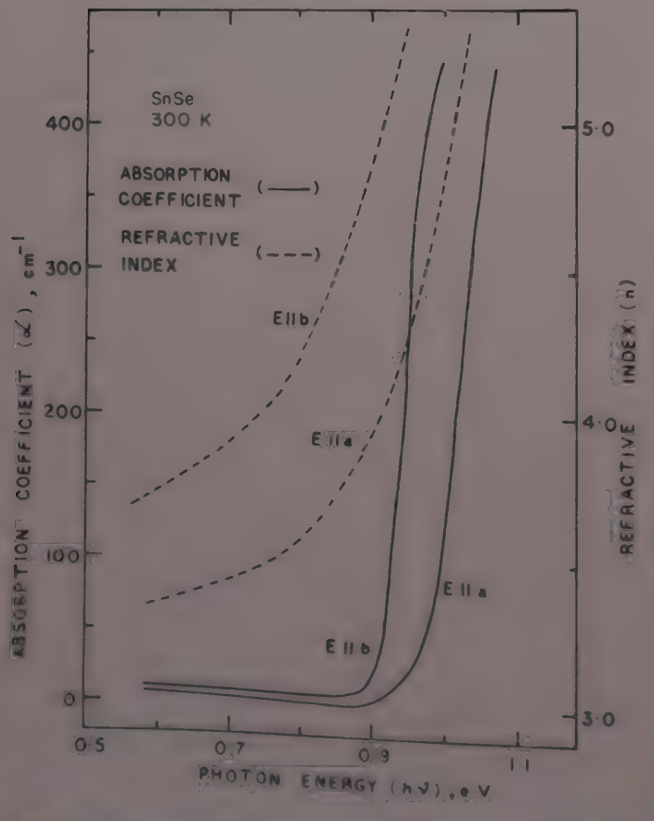

Fig. 4 Absorption coefficient and refractive index curves of SnSe

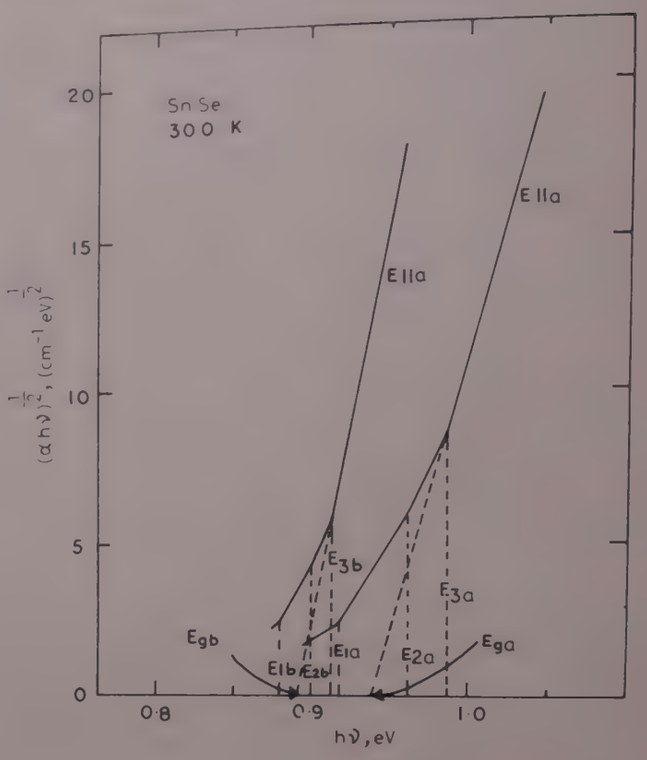

Fig. 5 The $[\alpha(h\nu)]^{1/2}$ versus $h\nu$ curves in SnSe for investigation for indirect interband transitions

The first term in Eq. (1) describes processes involving phonon absorption, while the second term describes phonon emission. Thus a plot of $[\alpha(h\nu)]^{1/2}$ vs $h\nu$ is expected to resolve into a straight line for each independent process. Such a plot for SnSe is presented in Fig. 5 from which multiphonon participation is evident. Since each curve shows three knees E_1, E_2 and E_3, it is safe to assume that two different phonons participate in the absorption process with the threshold energies spaced symmetrically about the energy gap value. As for the forbidden energy gap of pure crystal, E_g can be determined by extrapolating the high energy side of the absorption curve as shown in Fig. 5 to $\alpha = 0$. In this way, the analysis of the curve showed that E_g definitely corresponded to the midpoint between E_1 and E_2. The values of E_g obtained for $E \| a$ and $E \| b$ are $E_{ga} = 0.94$ eV and $E_{gb} = 0.891$ eV, respectively. The phonon energy $\frac{1}{2}(E_2 - E_1)$ is 0.022 eV for $E \| a$ and 0.009 eV for $E \| b$. Existence of a different phonon was indicated by the presence of a third knee at E_3 whose low energy side partner (the fourth knee) was not confirmed possibly because of the overlap of free carrier absorption. The estimated energy of the second phonon, $E_3 - E_g$, was found to be 0.047 eV for $E \| a$ and 0.022 eV for $E \| b$. The values of second phonon energy are roughly twice the values of first phonon energy. This may indicate a two-phonon-assisted phenomenon. The phonon frequencies[7] obtained by Raman and infrared measurements also support it.

References

1 Ravich Yu I, Efimova B A & Smirnov I A, *Semiconducting lead chalcogenides* (Plenum Press, New York) 1970.

2 Abrikosov N Kh, Bankina V F, Poretskaya L V, Shelimova L E & Skudnova E V, *Semiconducting* II-VI, IV-VI, *and* V-VI *compounds* (Plenum Press, New York) 1969.

3 Okazaki A & Ueda I, *J Phys Soc Jpn (Japan)*, **11** (1956) 470.

4 Hazelwood R A, *Thin Solid Films (Switzerland)*, **6** (1970) 329.

5 Lambros A P & Economou F A, *Sci Ann, Univ Thessaloniki (Greece)*, **13** (1973) 85.

6 Bardeen J, Blatt F J & Hall L H, *Photoconductivity – Proc Inc Conf, Atlanta city*, 1954 (John Wiley, New York) 1956.

7 Chandrasekhar H R, Humphreys R G, Zwick U & Cardona M, *Phys Rev B (USA)*, **15** (1977) 2177.

Indian Journal of Pure & Applied Physics
Vol 21, May 1983, pp 280-285

An Equation of State for Simple Fluids & Evaluation of Some Thermodynamic Properties

S K DATTA*
Department of Physics, Jalpaiguri Government Engineering College, Jalpaiguri 735 102

Received 21 *October* 1982

Two approximations, namely, the extended random phase approximation (ERPA) and the random phase approximation (RPA) have been employed to find the direct correlation function (DCF) in the long wave limit for the simple liquids characterized by Lennard-Jones and double Yukawa potential functions using the Weeks, Chandler and Andersen (WCA) prescription [*J Chem Phys (USA)*, **54** (1971) 5237] for the division of the pair potential. The ERPA results are found to be almost exactly identical with the RPA results, indicating that the ERPA does not constitute any significant improvement over the RPA at least for this particular long wave property. Using the compressibility sum rule and through the DCF in the long wave limit in the RPA, an equation of state has been formulated by neglecting the small density variation of the WCA diameters during integration of the compressibility relation with respect to density at constant temperature. Through this equation of state we derive the thermal expansion coefficient, isothermal compressibility, pressure variation of the bulk modulus, specific heat, sound velocity of the liquids and also their temperature variations. The agreement between theory and experiment in the evaluation of many of these properties shows that this approach forms a very important method in the formulation of equation of state.

1 Introduction

In a recent work, Evans and Sluckin[1] have used the random phase approximation (RPA) in their study of the long wave equilibrium behaviour of simple liquids characterized by a Lennard-Jones (LJ) potential. In the present work, the author intends to calculate the direct correlation function (DCF) in the long wave limit for the simple liquids modelled by a L-J potential using the extended random phase approximation (ERPA) of Evans[2] together with the Weeks, Chandler and Andersen (WCA) prescription[3] for the division of the pair potential. The author extends his calculations to include a double Yukawa (DY) potential with parameters adjusted to fit a L-J potential. Finally, the thermodynamic properties obtained from the RPA compressibility equation of state are calculated and compared with the experimental results.

2 Development of Theory

2.1 Inverse Compressibility in ERPA

First a WCA division of the pair potential is made. In the WCA prescription the pair potential $\varphi(r)$ is divided into two parts

$$\varphi(r) = \varphi_0(r) + \varphi_1(r) \qquad \ldots (1)$$

where $\varphi_0(r)$ is the reference part and $\varphi_1(r)$ the perturbation potential. $\varphi_0(r)$ includes all the rapidly varying repulsive forces and $\varphi_1(r)$ all the smoother attractive tail.

$\varphi_0(r)$ and $\varphi_1(r)$ are given by

$$\varphi_0(r) = \varphi(r) - \varphi(r_m) = \varphi(r) + \varepsilon \qquad r < r_m$$
$$= 0 \qquad r > r_m \qquad \ldots (2)$$

$$\varphi_1(r) = \varphi(r_m) = -\varepsilon \qquad r < r_m$$
$$= \varphi(r) \qquad r > r_m \qquad \ldots (3)$$

$-\varepsilon$ and r_m are the values of the potential minima and the separation distance at which $\varphi(r)$ is minimum, i.e.

$$\left.\frac{\partial \varphi(r)}{\partial r}\right|_{r=r_m} = 0, \qquad -\varepsilon = \varphi(r_m) \qquad \ldots (4)$$

The calculation of the isothermal compressibility which is a long wave property of simple liquids is based on ERPA for the direct correlation function $C(r)$. By treating DCF as a functional derivative of the free energy, Evans[2] showed that in the 'local density' approximation of the pairwise distribution function, DCF is given by

$$C(r) = C_0(r) - \beta\varphi_1(r) g_1(r) \qquad \ldots (5)$$

where $C_0(r)$ and $g_0(r)$ are the DCF and the pair distribution function respectively of the repulsive reference fluid of interaction potential $\varphi_0(r)$.

In order to calculate $C_0(r)$, following Jacobs and Andersen[4], the author approximates it by the sum of $C_{HS}(r)$, the DCF of the hard sphere (HS) fluid at the same temperature and density, and the Blip function $B(r)$ as

$$C_0(r) \simeq C_{HS}(r) + B(r) \qquad \ldots (6)$$

where

$$B(r) = Y_d(r)\{\exp[-\beta\varphi_0(r)] - \exp[-\beta\varphi_d(r)]\} \qquad \ldots (7)$$

$$Y_d(r) = g_d(r)\exp[\beta\varphi_d(r)] \qquad \ldots (8)$$

where $\beta = 1/(kT)$, k being the Boltzmann constant and

T the absolute temperature. The subscript 'd' refers to hard sphere quantities where the hard sphere diameter is d. It is determined at each temperature and density by the WCA requirement,

$$\int B(r)\,d^3r = 0 \qquad \ldots (9)$$

The compressibility equation of state is then given by

$$1-\rho\tilde{C}(0) = 1-4\pi\rho\int_0^d r^2 C_{HS}(r)\,dr + 4\pi\rho\beta\int_d^\infty r^2\varphi_1(r)g_0(r)\,dr \qquad \ldots (10)$$

where ρ is the number density, $\tilde{C}(0)$ the long wave limit of the Fourier transform of $C(r)$. The first two terms on the R.H.S. of Eq. (10) is just the inverse isothermal compressibility of the HS system. Using Carnahan and Starling[5] equation of state for HS, it is given by

$$1-4\pi\rho\int_0^d r^2 C_{HS}(r)\,dr = \frac{(1+2\eta)^2+\eta^3(\eta-4)}{(1-\eta)^4} \qquad \ldots (11)$$

where $\eta(=\pi\rho d^3/6)$ is the packing fraction.

In the WCA theory[3], the reference system radial distribution function is given by

$$g_0(r) \approx Y_d(r)\exp[-\beta\varphi_0(r)] \qquad \ldots (12)$$

Using Eqs (9), (12) and the fact that $Y_d(r) = g_d(r)$ for $r > d$, the last integral in Eq. (10) reduces to[6]

$$I = 4\pi\rho\beta\int_d^\infty \varphi_1(r)\,g_d(r)r^2\,dr \qquad \ldots (13)$$

For a Lennard-Jones fluid in the Percus-Yevick (PY) approximation[7], this integral has been shown to be given by[8]

$$I = 96\eta_w\beta\varepsilon\left[\frac{I_1^{12}-I_2^{12}}{d_w^{12}} - \frac{I_1^6-I_2^6}{d_w^6} - \frac{I_2^0}{4}\right] \qquad \ldots (14)$$

$$\text{where } \eta_w = \eta - \frac{\eta^2}{16},\ \mathrm{d}_w = \mathrm{d}\left(\frac{\eta_w}{\eta}\right)^{1/3} \qquad \ldots (15)$$

The integrals I_1^n and I_2^n are given in Ref. 8 and need not be reproduced again.

It is interesting to note that one can obtain the value of I_2^0 directly from the work of Thiele[9]

$$I_2^0 = \int_{d_w}^{r_m} g_d^{PY}\left(\frac{r}{d_w},\eta_w\right)r^2\,dr = \left[\frac{(\eta_w-4)(\eta_w^2+2)}{24(1+2\eta_w)^2} + \frac{1}{3}x_m^3\right] \qquad \ldots (16)$$

where $x_m = r_m/d_w$

Although this is an approximate result, it gives excellent results at high densities.

2.2 Compressibility for a Double Yukawa Fluid

Recently, Foiles and Aschroft[10] have shown that a double Yukawa (DY) potential provides a good physical representation for pair potentials in molecular fluids. They have shown that by judicious selection of parameters this potential can have very nearly the same form as Lennard-Jones potentials in the physically important range of separations and can therefore lead to essentially the same associated thermodynamic properties. The DY potential is given by

$$\varphi_{DY}(r) = \frac{E}{x}\{\exp[-a(x-1)] - \exp[-b(x-1)]\} \qquad \ldots (17)$$

where $x = r/s$

Foiles and Aschroft found that the set of parameters $E = 2.0199\varepsilon$, $s = \sigma$, $a = 14.735$ and $b = 2.6793$ may be a good choice for the matching of the DY and LJ potentials. Recently[11], the author has derived closed analytical expressions for the free energy and the virial compressibility factor of a DY fluid using the WCA perturbation theory[3]. He now calculates the isothermal compressibility of this system in the ERPA simply by finding the integral I for the DY case.

In the PY approximation, I is given by[11]

$$I = -(I_1 - I_2 + I_3) \qquad \ldots (18)$$

where

$$I_1 = 24\eta_w\beta\varepsilon I_2^0 \qquad \ldots (19)$$

$$I_2 = \frac{24\eta_w\beta E}{c_w}[e^a G(ac_w) - e^b G(bc_w)] \qquad \ldots (20)$$

$$I_3 = \frac{24\eta_w\beta E}{c_w}[F(a) - F(b)] \qquad \ldots (21)$$

$$c_w = d_w/\sigma$$

The integrals I_n are given explicitly as:

$$I_1 = 4\pi\rho\beta\varepsilon\int_{d_w}^{r_m} g_d^{PY}\left(\frac{r}{d_w},\eta_w\right)r^2 dr$$

$$I_2 = 4\pi\rho\beta E\int_{d_w}^{\infty}\left[\frac{\exp[-a(r/\sigma-1)] - \exp[-b(r/\sigma-1)]}{r/\sigma}\right] \times g_d^{PY}\left(\frac{r}{d_w},\eta_w\right)r^2\,dr$$

$$I_3 = 4\pi\rho\beta E\int_{d_w}^{r_m}\left[\frac{\exp[-a(r/\sigma-1)] - \exp[-b(r/\sigma-1)]}{r/\sigma}\right] \times g_d^{PY}\left(\frac{r}{d_w},\eta_w\right)r^2 dr$$

In Eq. (20), $z)$ is the Laplace transform of $rg_d^{PY}(r/d_w, \eta_w)$ and is given by Wertheim[12] as

$$G(z) = \frac{zL(z)}{12\eta_w[L(z)+S(z)e^z]} \qquad \ldots (22)$$

$$L(z)=12\eta_w[(1+\eta_w/2)z+(1+2\eta_w)] \quad \ldots (23)$$

$$S(z)=(1-\eta_w)^2z^3+6\eta_w(1-\eta_w)z^2+18\eta_w^2z-12\eta_w(1+2\eta_w) \quad \ldots (24)$$

$F(a)$ and $F(b)$ are given by[11]

$$F(z)=\frac{A}{zc_w}\{\exp[z(1-c_w)]-\exp[z(1-x_mc_w)]\}+\frac{B}{zc_w}\left[\left(1+\frac{1}{zc_w}\right)\exp[z(1-c_w)]-\left(x_m+\frac{1}{zc_w}\right)\exp[z(1-x_mc_w)]\right]+\frac{C}{zc_w}\left[\left\{1+\frac{2}{zc_w}+\frac{2}{(zc_w)^2}\right\}\exp[z(1-c_w)]-\left\{x_m^2+\frac{2x_m}{zc_w}+\frac{2}{(zc_w)^2}\right\}\exp[z(1-x_mc_w)]\right] \quad \ldots (25)$$

where

$$A=\alpha_0-\alpha_1+\alpha_2/2,\ B=\alpha_1-\alpha_2 \text{ and } C=\alpha_2/2 \quad \ldots (26)$$

α_0, α_1 and α_2 are given in Ref. 8.

The use of the DY potential model thus renders the evaluation of the integral I in an analytically exact form unlike the LJ potential model where the integrals I_1^n have been approximated[8].

2.3 Compressibility in the Random Phase Approximation

The RPA results for the compressibility can be obtained from the work of Evans and Sluckin[1]. The result is

$$1-\rho\tilde{C}(0)=\frac{(1+2\eta)^2+\eta^3(\eta-4)}{(1-\eta)^4}+\rho\beta\tilde{\varphi}_1(q=0) \quad \ldots (27)$$

where q is the wavevector and $\tilde{\varphi}_1(q=0)$ is the long wave limit of the Fourier transform of $\varphi_1(r)$

This is given by[1]

$$\tilde{\varphi}_1(q=0)=-15.797\varepsilon\sigma^3 \quad \ldots (28)$$

for the LJ case and

$$\tilde{\varphi}_1(q=0)=-15.793\varepsilon\sigma^3 \quad \ldots (29)$$

for the DY case[11]. Actual expression for $\tilde{\varphi}(q)$ for the DY case are given as:

$$\frac{\tilde{\varphi}_1(q)}{\pi\varepsilon\sigma^3}=\frac{4}{q^3\sigma^3}\left[qr_m\cos qr_m-\sin qr_m\right]+\frac{4\times2.0199}{q\sigma}\left[\frac{\exp[-a(r_m/\sigma-1)]}{a^2}(q\sigma\cos qr_m+a\sin qr_m)\left(1+\frac{q^2\sigma^2}{a^2}\right)^{-1}\right]-\frac{4\times2.0199}{q\sigma}\left[\frac{\exp[-b(r_m/\sigma-1)]}{b^2}(q\sigma\cos qr_m+b\sin qr_m)\left(1+\frac{q^2\sigma^2}{b^2}\right)^{-1}\right]$$

Eqs (10) and (27) can thus be used to obtain the compressibility values in the ERPA and RPA schemes respectively. Values of $1-\rho\tilde{C}(0)$ for the simple liquid argon at different temperatures are given in Table 1. Since the LJ and DY potential functions yield more or less the same values, the author has shown the results from the LJ potential model only. It is interesting to note that both the approximations (ERPA and RPA) yield almost exactly identical results for the inverse compressibility. This shows that the use of ERPA does not constitute any significant improvement over the RPA, at least for this particular long wave property. The reason for this is that the integrals $\int\varphi_1(r)r^2\,dr$ in $\tilde{\varphi}_1(q=0)$ of Eq. (28) and $\int\varphi_1(r)g_d(r)r^2\,dr$ of Eq. (13) differ only by a few per cent. The author has thus led to suggest that the following equation

$$\frac{p}{\rho kT}=\frac{1+\eta+\eta^2-\eta^3}{(1-\eta)^3}-7.8985\ \beta\varepsilon\rho\sigma^3 \quad \ldots (30)$$

obtained by integrating the RPA inverse compressibility relation (27) can be taken as a convenient equation of state for the simple liquids, provided that the diameter d is determined by the WCA criterion (since at fixed temperature d varies weakly[3] with density ρ, hence during integration with respect to ρ we may assume d to be constant). Nevertheless we should remember that the thermodynamic functions calculated through this route do not depend on the 'softness' of $\varphi_0(r)$, since these involve $\tilde{C}_0(0)$ which are hard sphere like by construction (Ref. 9). The RPA critical constants have already been discussed by Evans and Sluckin[1] and the author need not discuss them again.

2.4 Evaluation of Thermodynamic Properties

The equation of state (30) will now be utilized to verify the results for some real fluids, especially with respect to some easily measurable physical properties of simple liquids such as argon, nitrogen, oxygen and methane. The properties chosen are: (i) isothermal compressibility β_T, (ii) thermal expansion coefficient α_T, (iii) pressure variation of the bulk modulus C_1, (iv)

Table 1—Comparison of $1-\rho\tilde{C}(0)$ Values for Argon Obtained Using ERPA and RPA

Temp. K	$1-\rho\tilde{C}(0)$	
	ERPA	RPA
84	23.2419	23.2218
86	17.9450	17.9075
87	17.4988	17.4478
88	16.9869	16.9208
89	16.6450	16.5676
90	16.3865	16.3000

heat capacity $C_p(l)$, and (v) sound velocity C in the liquid. The expressions for these quantities are as follows (in all the calculations, the author has neglected the small density variation of the WCA diameter d during integrations and differentiations):

(i) Isothermal compressibility (β_T)

$$\beta_T = \frac{V}{RT}[1-\rho\tilde{C}(0)]^{-1} \qquad \ldots (31)$$

where $1-\rho\tilde{C}(0)$ is given by Eq. (27). V is the molar volume and R the universal gas constant.

(ii) Thermal expansion coefficient (α_T)

We know that

$$\alpha_T = \frac{1}{V}\left(\frac{\partial V}{\partial T}\right)_p = -\beta_T\left(\frac{\partial P}{\partial T}\right)_v \qquad \ldots (32)$$

Differentiating Eq. (30) with respect to temperature at constant volume, we get

$$\alpha_T = \frac{R\beta_T}{V}\left[\frac{1+\eta+\eta^2-\eta^3}{(1-\eta)^3} - \frac{(2+2\eta-\eta^2)6\eta\beta\varepsilon}{(1-\eta)^4}\,\frac{d'}{d}\right] \qquad \ldots (33)$$

where

$$d' = d'_B\left(1+\frac{\sigma_1}{2\sigma_0}\delta_\beta\right) + d_B\delta'_\beta\left(\frac{\sigma_1}{2\sigma_0}\right) \qquad \ldots (34)$$

$$d'_B = \frac{\partial d_B}{\partial(\beta\varepsilon)},\quad \delta'_\beta = \frac{\partial\delta_\beta}{\partial(\beta\varepsilon)}$$

d_B, δ_β, σ_0 and σ_1 are given in Ref. 8.

(iii) C_1 parameter

The pressure variation of bulk modulus C_1 is a very important (dimensionless) parameter[13,14] and serves as a severe test for the equation of state of liquids. In the present case C_1 is given by

$$C_1 = \left[\frac{\partial}{\partial P}\left(\frac{1}{\beta_T}\right)\right]_T = \frac{RT\beta_T}{V}\left[\left(\frac{1+11\eta+20\eta^2-12\eta^3+5\eta^4-\eta^5}{(1-\eta)^5}\right) - 31.594\beta\varepsilon\rho\sigma^3\right] \qquad \ldots (35)$$

(iv) Heat capacity $C_p(l)$

Following Yoshim[15], the heat capacity of liquids can be shown to be given by

$$C_p(l) = C_p(g) - R + \alpha_T Z_0 TR - \frac{6\eta R}{(1-\eta)^4}\left[(\beta\varepsilon)^2\left(\frac{d'}{d}\right)^2(4+9\eta-4\eta^2) + \left(\frac{\varepsilon}{k}\right)\left(\frac{d'}{d}\right)\alpha_T(2+2\eta-\eta^2) + (\beta\varepsilon)^2\left(\frac{d''}{d}\right) \times (2-3\eta+\eta^2)\right] \qquad \ldots (36)$$

where

$$d'' = d''_B\left(1+\frac{\sigma_1}{2\sigma_0}\delta_\beta\right) + \frac{\sigma_1}{\sigma_0}d'_B\delta'_\beta + \delta''_\beta d_B\left(\frac{\sigma_1}{2\sigma_0}\right) \simeq d''_B\left(1+\frac{\sigma_1}{2\sigma_0}\delta_\beta\right) \qquad \ldots (37)$$

$$Z_0 = \frac{1+\eta+\eta^2-\eta^3}{(1-\eta)^3},\quad d''_B = \frac{\partial d'_B}{\partial(\beta\varepsilon)},\quad \delta''_\beta = \frac{\partial\delta'_\beta}{\partial(\beta\varepsilon)} \qquad \ldots (38)$$

α_T and d' can be obtained from Eqs (33) and (34) respectively.

The contribution of the bracketted portion is, however, less than 1% and can therefore be neglected.

(v) Sound velocity (C)

Sound velocity C is given by

$$C^2 = \frac{\gamma V}{M\beta_T} \qquad \ldots (39)$$

where M is the molecular weight of the liquid, and $\gamma(C_p/C_v)$ the ratio of the heat capacities at constant pressure and constant volume. C_v may be obtained from the thermodynamic relationship

$$C_p - C_v = \alpha_T^2 TV/\beta_T \qquad \ldots (40)$$

when β_T, α_T and $C_p(l)$ are already known from Eqs (31), (33) and (36) respectively.

3 Results and Discussion

The calculations of the author are reported for (1) monatomic liquid-argon, (2) diatomic liquids—nitrogen and oxygen, and (3) symmetric polyatomic liquid methane in their liquid ranges at several temperatures. The values of the liquid densities required for the calculations are those quoted by Yoshim[15] and the references cited therein. The Lennard-Jones potential parameters ε/k and σ for the systems considered are given in Table 2. The calculation of the values of $C_p(l)$ requires the knowledge of the values of heat capacity $C_p(g)$ for gases. These values of $C_p(g)$ are also those quoted by Yoshim. The results for the calculations of β_T, α_T, C_1, $C_p(l)$ and C are given in Table 3 along with the observed values[15,19]. The values of the hard sphere fluid properties for the liquids are available in litera-

Table 2—Lennard-Jones Potential Parameters Used in the Calculations

Liquid	ε/k K	σ Å	Ref.
Ar	119.8	3.405	16
N_2	103.29	3.615	17
O_2	120.97	3.406	17
CH_4	147.4	3.7	18

Table 3—Variation of Thermodynamic Properties of Simple Fluids with Temperature

Liquid	Temp.	β_T		α_T		$C_p(l)$		C		C_1 parameter
	K	10^{-4}atm^{-1}		10^{-3}K^{-1}		cal/mol/K		m/sec		
		Calc.	Obs.	Calc.	Obs.	Calc.	Obs.	Calc.	Obs.	Calc.
Ar	84	1.78	1.93	3.75	4.45	9.38	10.49	875.1	860.2	7.92
	86	1.80	2.04	3.69	4.47	9.30	10.51	871.7	846.8	7.84
	87	1.84	2.10	3.70	4.49	9.29	10.52	864.9	840.0	7.81
	87.29*	1.84	2.10	3.69	4.50	9.28	10.52	864.2	—	7.80
	88	1.88	2.16	3.72	4.51	9.28	10.52	856.5	833.1	7.78
	89	1.91	2.22	3.71	4.53	9.26	10.54	851.5	826.4	7.74
	90	1.93	2.28	3.70	4.56	9.24	10.54	848.2	—	7.71
N_2	65	1.88	2.06	4.07	5.21	11.41	13.32	1005.3	975.0	8.20
	70	2.15	2.54	4.12	5.34	11.30	13.44	953.6	923.5	7.98
	75	2.46	3.03	4.20	5.49	11.22	13.50	905.1	873.0	7.79
	77.19*	2.57	3.30	4.20	5.56	11.18	13.56	889.7	—	7.71
	80	2.82	3.57	4.30	5.64	11.18	13.64	859.4	822.0	7.62
	85	3.23	4.11	4.43	5.81	11.16	13.70	816.4	772.0	7.46
	90	3.68	4.70	4.56	5.99	11.17	13.84	778.5	721.0	7.31
O_2	65	0.91	1.06	3.19	3.68	11.63	12.70	1193.9	1104.5	8.66
	70	0.99	1.19	3.15	3.73	11.42	12.77	1146.8	1066.0	8.42
	80	1.20	1.49	3.11	3.84	11.11	12.86	1059.2	988.0	8.01
	90	1.46	1.79	3.14	3.95	10.91	12.99	981.3	909.0	7.66
	90.13*	1.46	1.80	3.15	3.95	10.91	12.98	979.4	—	7.66
CH_4	102.6	1.88	1.32	3.09	3.11	12.40	13.1	1386.8		7.95
	108.1	2.08	1.46	3.13	3.25	12.35	13.2	1333.3		7.81
	111.7*	2.15	1.66	3.10	3.34	12.28	13.45	1315.8	—	7.71
	113.7	2.22	1.66	3.11	3.40	12.26	13.3	1301.1		7.66
	119.3	2.42	1.77	3.15	3.56	12.22	13.5	1258.3		7.52
	124.8	2.67	—	3.20	3.86	12.21	13.6	1214.3		7.40

* Boiling point of the liquid

ture[15,19]. Even though the C_1 parameter has a general value of around 8, it may be regarded as a constant characteristic of the liquid as confirmed by the calculations of the author.

It is seen from Table 3 that the magnitudes of the calculated values of β_T, α_T and C are more or less in good agreement with the observed values and are far better than the corresponding hard sphere results of Yoshim[15]. However, the agreement can be made to improve in the cases of α_T and $C_p(l)$ if the experimental values of β_T and α_T are inserted in Eqs (33) and (36) respectively. Another important thing to notice is that the trend of variation of the calculated properties with temperature does not correspond to that of their observed values in all cases. The isothermal compressibility β_T and sound velocity C reproduce the observed trend of temperature variation in a very good manner. But the observed trend of temperature variation of α_T is not so well reproduced by the calculations of the author. Also just like hard sphere fluids[15], the calculated values of $C_p(l)$ decrease with increase of temperature, contrary to the experimental results.

The disagreements may be due to inherent weakness of the derivation of the equation of state through the RPA. As mentioned earlier, the RPA (as well as the ERPA) does not correct the core DCF of hard sphere potential due to perturbation[20], which means that modifying the form of $\varphi_1(r)$ for r inside the hard core of the potential does not change $C_{HS}(r)$. Very recently McLaughlin and Young[21] have calculated the compressibility of argon and neon at several temperatures using the RPA and a more sophisticated mean density approximation (MDA). However, the MDA results are not much different from the RPA results. Thus it is gratifying to conclude that the present step is better than the pure hard sphere results and forms an important method in the formulation of the equation of state for simple fluids.

References

1 Evans R & Sluckin T J, *J Phys C (GB)*, 14 (1981) 2569.

2 Evans R, *Adv Phys (GB)*, **28** (1978) 143.
3 Weeks J D, Chandler D & Andersen H C, *J Chem Phys (USA)*, **54** (1971) 5237.
4 Jacobs R E & Andersen H C, *Chem Phys (Netherlands)*, **10** (1975) 73.
5 Carnahan N F & Starling K E, *J Chem Phys (USA)*, **51** (1969) 635.
6 Hansen J P & McDonald I R, *Theory of simple liquids* (Academic Press, London), 1976, 184.
7 Percus J K & Yevick G J, *Phys Rev (USA)*, **110** (1958) 1.
8 Verlet L & Weis J J, *Phys Rev (USA)*, **A5** (1972) 939.
9 Thiele E, *J Chem Phys (USA)*, **39** (1963) 474.
10 Foiles S M & Aschroft N W, *J Chem Phys (USA)*, **75** (1981) 3594.
11 Datta S K, *Pramana (India)*, in press.
12 Wertheim M S, *J Math Phys (USA)*, **5** (1964) 643.
13 Gopala Rao R V & Rao B S M, *Trans Faraday Soc (GB)*, **62** (1966) 2704.
14 Gopala Rao R V, *Indian J Pure & Appl Phys*, **5** (1967) 357.
16 Yoshim S J, *J Chem Phys (USA)*, **40** (1964) 3069.
16 Michels A, Wijker H & Wijker H K, *Physica (Netherlands)*, **15** (1949) 627.
17 Shukla K P, Singh S & Singh Y, *J Chem Phys (USA)*, **70** (1979) 3086.
18 Salter S J & Davis H T, *J Chem Phys (USA)*, **63** (1975) 3295.
19 Van Dael W, Van Itterbreek A, Cops A & Thoen J, *Physica (Netherlands)*, **32** (1966) 311.
20 Gaskell T, *Phys Lett (Netherlands)*, **65A** (1978) 421.
21 McLanghlin I L & Young W H, *J Phys C (GB)*, **15** (1982) 1121.

Indian Journal of Pure & Applied Physics
Vol 21, May 1983, pp 286-288

Experimental Study of Plasma Characteristics of Plasma Focus Devices

ANURAG SHYAM* & M SRINIVASAN
Neutron Physics Division, Bhabha Atomic Research Centre, Trombay, Bombay

Received 12 *July* 1982

Density, temperature and size of the plasma generated in a plasma focus device, operated on a relatively low energy and slow capacitor bank, were determined by measuring the intensity of bremsstrahlung emitted by this plasma in different spectral regions. The quantities thus obtained are compared with plasma properties of other plasma focus devices obtained on bigger and faster capacitor banks elsewhere, and scaling of plasma characteristics with bank parameters is inferred.

1 Introduction

The plasma focus[1] device is a high efficiency pinch device which produces plasma focus of a few mm diameter and a few cm length, with peak density and temperature $\sim 10^{19}$ electrons/cm^3 and $\sim 10^7$ K respectively and lasts for ~ 100 ns when a high powered electrical pulse of a few μs duration, generated by a capacitor bank, is discharged through it.

More than 20 laboratories are currently investigating plasma focus devices. The present experiments were conducted with a comparatively slower and low energy capacitor bank with a view to studying the scaling of device properties with electrical parameters of the capacitor bank. The characteristics of the capacitor bank named 'HEXA' (Ref. 2) are 16.8 μF capacity, 40 nH inductance, charging voltage variable up to 50 kV. The hydrogen filled plasma focus on which the experiments were conducted was of Mather type[1] with 11.8 cm long central and coaxial outer electrodes having diameters of 2.2 and 7.2 cm respectively.

The plasma formed in the device was characterized by experimentally studying the radiation emitted from it. The techniques used are described in the following sections:

2 Techniques for Determining Various Plasma Characteristics

2.1 Plasma Radiations

As is well known, a high temperature high density plasma emits copious amounts of bremsstrahlung radiation[3]. Since the plasma formed in the plasma focus device is optically thin, it transmits all the radiations generated by it and as the temperature of this hydrogen plasma is high, the recombination and line radiations are insignificant as compared to free-free radiation. The intensity as a function of photon energy of this free-free bremsstrahlung is given by the following relation[3] (assuming Maxwellian distribution of electrons):

$$\frac{dI}{dE}dE = Ag_{ff}\frac{n^2 V}{T^{1/2}}\exp(-E/T)dE \qquad \ldots(1)$$

where I is the intensity of the radiation, E (in eV) its energy, T the temperature (in eV), n the electron density, V the total volume of the "hot" plasma, g_{ff} the gaunt's factor for free-free bremsstrahlung, and A a constant. As evident from Eq. (1), the radiation emitted from the plasma has information about the dimensions (V), density (n), and temperature (T) of the plasma. Hence by using appropriate techniques (described in the next three sections), these quantities can be estimated.

2.2 Temperature

Since the radiation in the spectral region $E > T$ is most sensitive to T, T can be estimated by measuring the spectrum of the emission in this region. In the present studies, since T is of the order of a few keV, the radiation measured is in the soft X-ray range.

The spectrum of these soft X-rays was estimated by the well known foil transmission technique[4]. The attenuation of the X-rays was measured by six aluminium filters (thickness, 20, 50, 75, 100, 150 and 300 μm). Since the ratio of the attenuations through any two thicknesses is a function of temperature only, the plasma temperature can be deduced therefrom. Six, rather than two, attenuating foils were used so as to confirm that the distribution is Maxwellian and the impurity atoms are negligible (if temperatures obtained from all six attenuation ratios are identical).

As mentioned earlier, since the dense phase of the focus lasts only for ~ 100 ns, the intensity of the soft X-rays was measured by a detector with fast response time. A plastic scintillation detector (3 mm thick of NE 102A plastic mounted on a Philips 58 AVP photomultiplier tube) with FWHM of 5 ns for a $^{60}_{27}$Co gamma was used for this purpose. The output of this detector was recorded on a fast storage oscilloscope (Tektronix 7834).

2.3 Dimensions

In the spectral region $E \ll T$, the exponential term is unity and the intensity of the emitted radiation is not very sensitive to temperature [Eq. (1)] but is more sensitive to volume and density. For a plasma focus device, this condition is satisfied in the optical region ($E \sim 2$ eV) and because of the ease and accuracy with which visible light could be measured, this region was chosen for measurements. The intensity of light in the spectral range E to $(E + \Delta E)$ is given by

$$I = An^2 V \frac{\Delta E}{T^{1/2}} g_{ff} \qquad \ldots(2)$$

As can be seen from Eq. (2), to estimate n or V from the light output, the other parameters should be known. Generally, volume is measured by photographing the plasma. But since the hot phase of the plasma in the plasma focus device lasts only for ~ 100 ns, determination of the plasma volume would call for an ultrafast camera[5]. Such cameras are not readily available as they are very expensive. A new and simple method for deducing plasma dimensions and density without the use of a fast camera, for a plasma having an axis of symmetry, is described in what follows.

The plasma in the plasma focus device is approximately a cylinder. If this plasma is viewed by a slit collimator (Fig. 1) from direction perpendicular to its cylindrical axis, the intensity viewed by the detector will be

$$I_s = \frac{An^2 \Delta E}{T^{1/2}} g_{ff} \pi r^2 W \qquad \ldots(3)$$

where r is the radius of the plasma at the point it is being viewed and W the collimator slit width. If the same plasma at the same point is viewed through a pin hole collimator (with diameters much less than plasma radius), again perpendicular to the axis of the cylindrical plasma, aligned in such a way so as to view only the central part of the cylinder, then the intensity (I_H) will be

$$I_H = \frac{An^2 \Delta E}{T^{1/2}} g_{ff} 2\pi r a \qquad \ldots(4)$$

where a is the area of pin hole collimator. The radius (r) of the plasma can then be deduced from the ratio of the two intensities given by the following equation:

$$r = \frac{2a}{W} \frac{I_s}{I_H} \qquad \ldots(5)$$

If the plasma is also viewed by a pin hole collimator aligned axially (Fig. 1), the intensity (I_V) is given by

$$I_V = g_{ff} \frac{An^2 \Delta E}{T^{1/2}} al \qquad \ldots(6)$$

Then effective length (l) of the plasma can be estimated from the relation:

$$l = \frac{4\pi a}{W} \frac{I_V I_S}{I_H^2} \qquad \ldots(7)$$

Thus the plasma dimensions can be determined.

In the experiments conducted by us, the light emitted from plasma was again viewed by a fast detector—a chrome filter (bandwidth, 4500-5500 Å) mounted on a photomultiplier tube (Philips 58 AVP) and the signals were again recorded on the Tektronix fast oscilloscope. The slit collimator consisted of a pair of slits of 0.2 mm width, while the pin hole collimator was made up of two pin holes of 0.1 mm diameter. The alignment of the collimators was done by using a helium neon laser and mirrors.

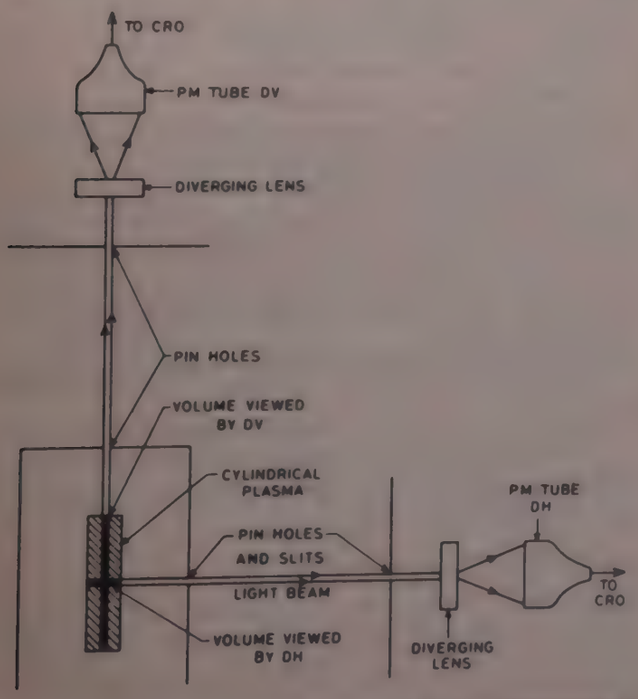

Fig. 1—Experimental set-up for deducing plasma dimensions and density without using fast camera

2.4 Density

Since r and T of the plasma are known, n can be estimated using Eqs (3) and (4) if the absolute intensity is known. This was ascertained by replacing the plasma by a standardized tungsten lamp and A in Eqs (2)-(4) and (6) was determined. Once A is known, n can be estimated from the following equation derivable from Eqs (3) and (4):

$$n = \left[\frac{WT^{1/2}}{4\pi a^2 A \Delta E g_{ff}} \right]^{1/2} \frac{I_H}{I_s^{1/2}} \qquad \ldots(8)$$

3 Experimental Results and Scaling

The peak values of n and T were determined at optimum filling pressures[6]. The length and diameter of the plasma were also determined at the same pressure and at the instant of peak density. Since the basic aim of this study was to study the behaviour of the device at low rates of change of current and low currents

Table 1—Properties of the Trombay Plasma Focus Device (TPF-1)

Charging voltage kV	Energy J	Current (C) kA	$\frac{dC}{dt}(\dot{C})$ 10^{11} A/s	Temp. 10^7 K	Density 10^{18} electrons/ cm^3	Diameter mm	Length cm
7	410	100	1.7	2.1	4	2.0	0.8
9	680	130	2.1	2.5	5	2.2	1.0
11.5	1110	160	2.7	2.6	7	2.3	1.4
13	1420	185	3.1	2.7	8	2.4	1.5
16	2150	230	3.8	3.1	10	2.6	1.8

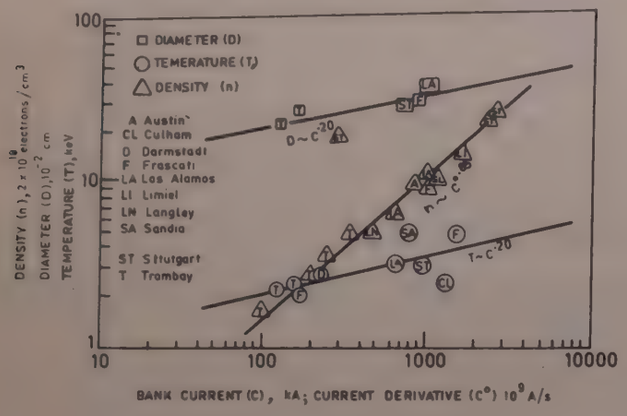

Fig. 2—Scaling of plasma focus properties

(energy), the experiment was conducted with charging voltages in the range 7-16 kV (100, 130, 165, 185 and 230 kA capacitor bank currents). The estimated values of temperature, density, diameter and length of the plasma are listed in Table 1.

Correlation studies were made between the plasma properties reported in Table 1 and the data collected from other sources[6-16] (density, temperature and diameter) and their respective capacitor bank electrical parameters (energy, current, voltage, dC/dt and their products). It was observed that while temperature and diameter correlated best with capacitor bank current (C) and scaled as $C^{0.2}$ and $C^{0.2}$ respectively, the plasma density correlated with $\frac{dC}{dt}(\dot{C})$ and scaled as $(C)^{0.85}$ (Fig. 2).

4 Conclusion

Scaling law derived from plasma focus theory predicts the temperature and diameter dependence on current[17] as $C^{0.15}$ and $C^{1.1}$ respectively. Calculations[18] also predict the scaling of density as $(\dot{C})^{2.0}$. These exponents of scaling laws derived theoretically are different from the experimentally obtained ones. This suggests that the present theories about plasma focus phenomenon are not totally adequate and require further refinement.

References

1 Mather J W, *Methods of experimental physics*, Vol 9B (Academic Press, New York) 1971, 187.

2 Shyam A, Auluck S K H, Pal P K & Srinivasan M, *Indian J Pure & Appl Phys*, **20** (1982) 647.

3 Podgorny I M, *Topics in plasma diagnostics* (Plenum Press, New York) 1971.

4 Jahoda F C, *Phys Rev (USA)*, **119** (1960) 843.

5 Lukyanov V I, *Proc 2nd UN Int Conf on Peaceful Uses of Atomic Energy* (United Nations, Geneva) **32** (1958) 358.

6 Mather J W, *Plasma Phys and Controlled Nucl Fusion Res* (International Atomic Energy Agency Publication, Austria), **2** (1966) 389.

7 Beckner E H, *J Appl Phys (USA)*, **37** (1966) 4944.

8 Long J W & Peacock N J, *Conference on Pulsed High Density Plasma*, Los Alamos Scientific Laboratory (USA) Report LA-3770, C-5, 1966.

9 Baconnet J P, Cesari G, Coudeville A & Watteau J P, CEA-CONF-1204 (Commissariat a e'Energie Atomique Report, Limiel, France), 1968.

10 Bernstein M J, *Phys Fluids (USA)*, **13** (1970) 2858.

11 Krompholz H, Michel L, Schonbach K H & Fischer H, *Appl Phys (Germany)*, **13** (1977) 29.

12 Decker G, Nahrath B, Oppenlander T, *et al.*, *Plasma Phys and Controlled Nucl Fusion Res* (International Atomic Energy Agency Publication, Austria), **3** (1976) 441.

13 Decker G & Wienecke R, *Physica C (Netherlands)*, **82** (1976) 155.

14 Bernard A, Garconnet J P, Jolas A, *et al.*, *IEEE Int Conf on Plasma Science*, Montreal, 1979 (Institute of Electric and Electronic Engineers, New York) 1979.

15 Bernard A, *Pulsed high beta plasmas* (Pergamon Press, New York) 1976, 69.

16 Maissonier C, Rep 75/3/E (Centro Gas Ionizzati, Frascati, Italy) 1975.

17 Imshennik V S, Filippov N V & Fillippova T I, *Nucl Fusion* (International Atomic Energy, Austria), **13** (1973) 929.

18 Decker G, Flemming L, Kaeppeler H J, *et al.*, *Plasma Phys (GB)*, **22** (1980) 245.

Indian Journal of Pure & Applied Physics
Vol 21, May 1983, pp 289-292

Freezing Points of Pure Tin & Zinc as Defining Temperature Standards

K D BAVEJA* & RAM KRISHAN
Thermometry Section, National Physical Laboratory, New Delhi 110012

Received 12 *October* 1982; *revised received* 9 *February* 1983

An apparatus to maintain the equilibrium state of the freezing/melting of tin and zinc over long periods of time and hence useful for calibration of platinum resistance thermometers is described. Uniform temperature is established inside the well of the graphite crucible and the slope of the flat portion of the melting/freezing curve is ±0.2 mK and lasts for nearly 90 min.

1 Introduction

The melting/freezing points of pure metals are assigned definite temperature values on the International Practical Temperature Scale (IPTS). The apparatus described here realizes the thermal equilibrium state of the freezing/melting of the spec-pure tin and zinc under 1 normal pressure to a high precision (±0.0002°C) required for the calibration of standard platinum resistance thermometers (SPRT). This work is a part of the programme to realize and maintain a National Temperature Scale according to the definition of the IPTS.[1-3]

2 Experimental Details

2.1 Apparatus

The basic design of the apparatus for realizing mp/fp of pure metals is similar to that followed in other laboratories[4-6]. Fig. 1 shows the tin or zinc point furnace containing the metal holder.

The graphite crucible, made of pure synthetic graphite, was designed to hold spec-pure metal, about 1500-1700 g, in the annular space and is contained in a pyrex glass mould. The graphite crucible also has a central re-entrant well for admitting standard platinum resistance thermometer through a thin walled SS tubing closed at the lower end. Four stainless steel radiation shields, acting also as heat shunts, are supported by the SS tubing in the region above the crucible. The inner space in the pyrex mould below and above the graphite crucible is filled with fine glass wool.

A suitably designed brass cap, containing a water condenser, is sealed at the top of the pyrex glass mould with piecin wax. The provision of the condenser maintains the piecin joint at room temperature preventing any leakage. The glass mould is connected to pumps and a mercury manometer through a large thermostated volume. The hermetically leak-tight system can be filled with pure dry argon/helium gas.

The graphite crucible is in the central uniform temperature region of the furnace. The metal-holder is surrounded by a heavy brass cylinder of large thermal inertia. The graphite crucible is suitably insulated against thermal losses as shown in Fig. 1.

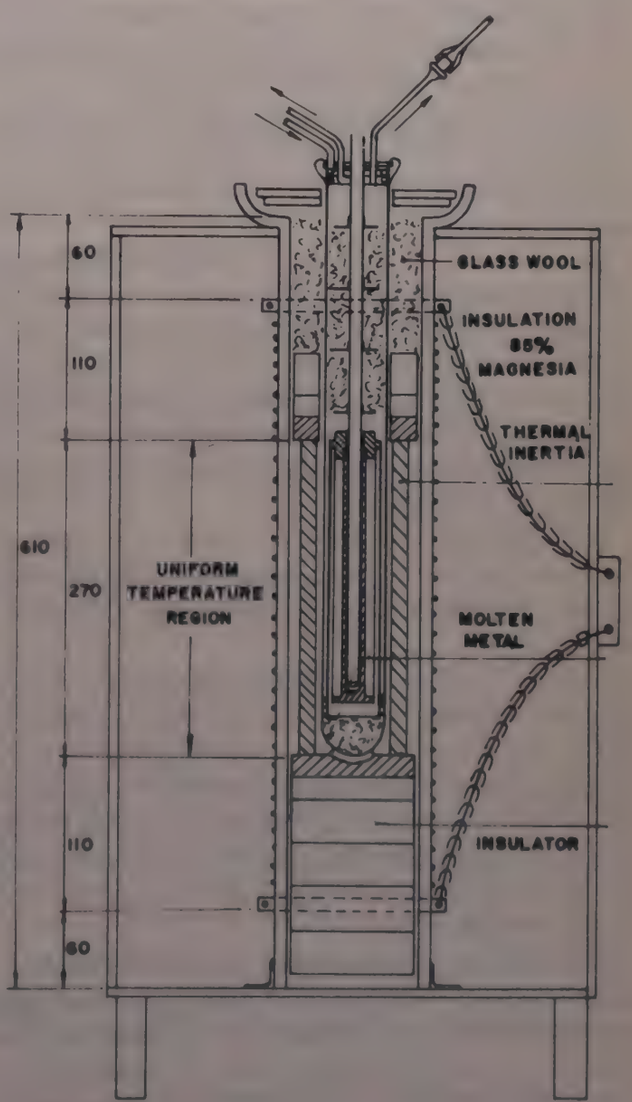

Fig. 1—Furnace assembly

The power supply (230 V, 50 Hz) from mains is fed into an automatic servo voltage regulator; its output of 230 V ± 0.5% is next fed into another servo voltage regulator and the stabilized output (230 V ± 0.25%) finally to the furnace through a variac.

2.2 Filling of the Graphite Crucible

The cleaning of the metal-holder parts and filling of the graphite crucible under vacuum with 1500-1700 g of pure metal follows the procedure adopted by the previous workers[4-6].

The system after thorough evacuation and degassing is filled with pure dry argon/helium gas at 1 normal atmospheric pressure when the crucible is close to the mp/fp of the pure metal.

2.3 Melting/Freezing Curves of Tin and Zinc

Starting with an initial temperature slightly lower than the melting point, the input power is increased to obtain a temperature rise of 0.5°C/hr. The level of the molten metal is about 170-180 mm above the top of the sensor of the SPRT in the re-entrant well. The design of the metal-holder and furnace assembly provide uniform temperature over the entire length of the space in the re-entrant well within the crucible.

Measuring the resistance of the SPRT at intervals of few minutes, the plot of the resistance versus time is drawn and the flat portion of the curve indicates the melting process.

In Fig. 2; V_1, V_2, V_3 and V_4 indicate decreasing voltage inputs, i.e. decreasing rates of heating. The corresponding melting curves are illustrated qualitatively by broken curves (m_1—m_1, m_2—m_2, m_3—m_3 and m_4—m_4) yielding increasing periods of melting. Obviously, when the rate of heating (V_1) is rather high, superheating and negligible width of flat region (m_1—m_1) are obtained.

For realizing the freezing point one starts the experiment a few degrees higher than the mp of the metal. The molten metal in the crucible is allowed to cool 1-2°C/hr.

In Fig. 3, the power input to the furnace is set at different voltages say V_1, V_2, V_3, V_4, V_5 (where $V_1 < V_2 < V_3 < V_4 < V_5$) the corresponding rates of cooling of the metal would be faster for V_1 and slower for successive values of V_n. The corresponding freezing curves are illustrated qualitatively by broken curves A—A, B—B, C—C, D—D, or D′—D′ and E—E, or E′—E′ respectively.

Curve A—A illustrates the trace when cooling is rather fast and freezing introduced when the super-cooling was small; the latent heat released may even raise the temperature slightly above the freezing point for some time and no definite flat portion may be realised due to the fast cooling rate. The flat portion of curve B—B lasts for more than an hour corresponding to slower rate of cooling.

For still slower rate of cooling for the voltage setting V_3, the flat region of the curve C—C may last even less than an hour. It would be observed that here the freezing was introduced in a greater undercooled state than in case of curve B—B. If the freezing was introduced at still lower undercooled state, the curve traced would be C′—C′, the latent heat then released was not sufficient to raise the temperature of the assembly to the freezing point of the metal. The remaining freezing point curves are similarly explained for voltages V_4 and V_5.

As tin tends to super-cool by more than 10°C, the molten metal is allowed to undercool only by 0.5 to 1°C before the nucleation is introduced in the melt. This is achieved by taking out the SPRT and inserting a brass rod (at room temperature) for intimate contact for 2 to 3 min with the inner surface of the well and then putting the SPRT back.

Uniform temperature is soon established in the well within 10-20 min and usually the flat portion of the freezing curve for tin, as monitored by the SPRT, lasts for 45 to 90 min (Fig. 4).

In the case of zinc, the super-cooling effect is less than a degree celcius, so introducing the brass rod for a

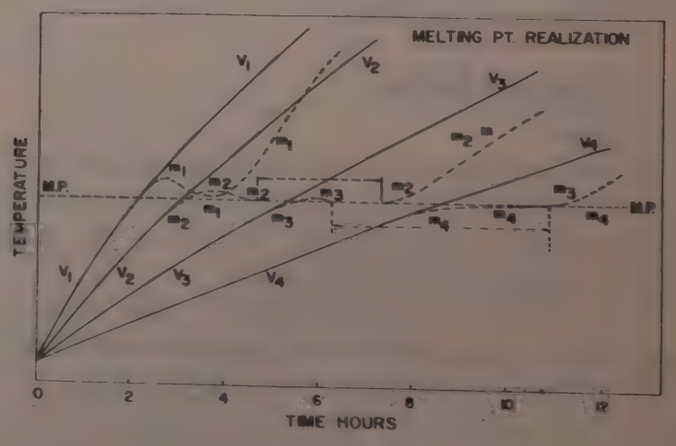

Fig. 2—Melting point curves

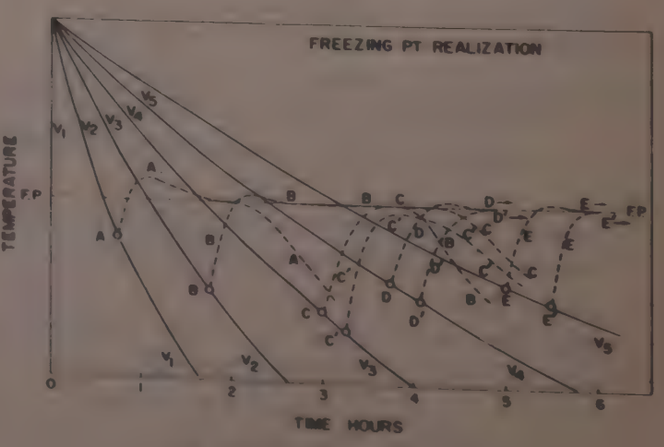

Fig. 3—Freezing point curves

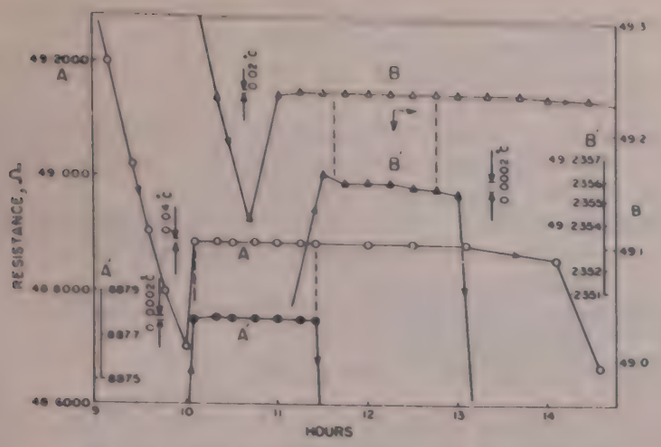

Fig. 4—Typical freezing point curves of spec-pure tin

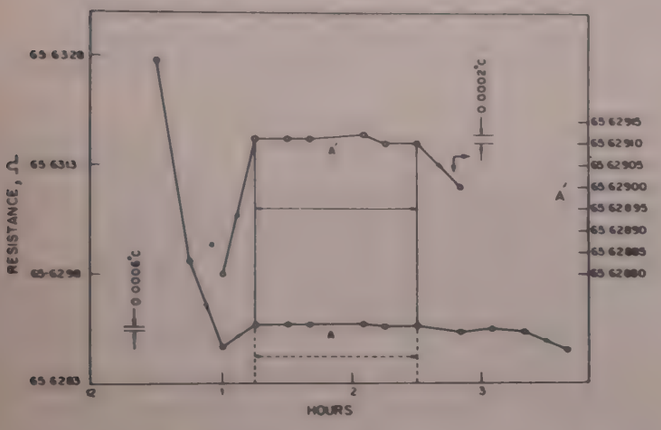

Fig. 5—Typical freezing point curve for spec-pure zinc

few seconds was adequate to induce nucleation. Fig. 5 shows a typical curve at the zinc point for one of our SPRTs.

The inset curves A′ and B′ in Figs 4 and 5 show the flat region of the curves corresponding to the freezing process on an expanded scale. Any fluctuation of the resistance of the thermometer in the flat region is small and less than 0.0002°C in the case of both tin and zinc.

2.4 Resistance Measurement

The resistance in these experiments was measured with an ER thermometer bridge (Leeds & Northrup Co, USA) and a Null-detector (Leeds & Northrup Co, USA 9828-2) to a precision of 10^{-5} Ω. Usual corrections for bridge errors and self-heating effect were applied.

3 Results

Since the melting/freezing point of a pure metal is not very sensitive to overhead atmospheric pressure[7], it was sufficient to ensure that this pressure did not vary by more than a few mm of mercury by controlling the room temperature within ±2°C. In our system, the argon pressure, reduced to same ambient room temperature, remained constant for several months. With helium, the pressure drop noticed was less than 2 mm in 4 weeks.

During the flat plateau of the freezing curve, the ambient temperature around the aluminium head of the SPRT was raised by about 2°C. It was observed that this had negligible effect on the resistance of the thermometer. This effect in any case did not exceed 0.2 mK showing the height of the melt (about 220 mm) in the crucible was sufficient to nullify the cold-conduction down the stem, leads and radiation effect from the ambient temperatures.

In some of the experiments, we induced freezing/nucleation in the tin melt by using a short brass rod, about 50-60 mm instead of brass rod of 220 length, so that freezing process was initiated in the melt, close to the well only in the bottom portion or near the top region. This was done for the introduction of non-uniform freezing in the melt on its surface in the proximity of the re-entrant well. Contrary to expectation, no larger slope or fluctuation in temperature in the flat region of the freezing curve was observed. Perhaps the re-introduction of SPRT itself (with stem usually at lower temperature) helped rapid establishment of the uniform temperature in the well and freezing progressed uniformly.

Only small variations in temperature of the order of 0.2 mK in about 45-90 min during freezing process is observed. This also indicates that the metal (source—Johnson Mathey & Co, UK or Commin Co, Canada) was highly spec-pure.

It has been observed that for realizing a good flat plateau during melting, the rate of heating has to be much slower than the rate of cooling required to realize a good plateau during freezing. Apparently the reason may be that the melting process of the metal begins on the outer surface and may not be uniform over the entire height. However, this could not be investigated.

4 Conclusion

The main feature of the apparatus is the incorporation of a water-condenser in the cap of the metal-holder. This helps hold the piecin wax joint leak tight and the 'Fixed Point' functional continuously, over a long period.

The effects of the varying rates of heating, cooling and of undercooling before nucleation on the flat plateau of the mp or fp curves discussed here show that it is necessary to have optimum control on the rate of heating or cooling for getting a good plateau.

The experimental set-up is good enough to allow realizing the melting/freezing point for a duration of 45-90 min and the slope of the plateau of the curve not exceeding 0.2 mK.

Due to varying oxidation state of the PRT sensor affecting the stability of a SPRT, the reproducibility of

the melting/freezing points of pure metals can be relied to 0.5 mK only.

Acknowledgement

The authors sincere thanks are to Mr S K Nijhawan, Mr V P Sharma and Mr Mansa Ram for general assistance during the set-up.

References

1 Stimson H F, International Practical Temperature Scale of 1948: Text revision of 1960, *NBS Monograph* (*USA*), **37** 1961.

2 International Practical Temperature Scale of 1968, *Metrologia* (*Germany*), **5** (1969) 35-44.

3 Amended edition of International Practical Temperature Scale of 1975, *Metrologia* (*Germany*), **12** (1976) 1-17.

4 Barber C R & Horsford A, *Proc R Soc London Ser A* (*GB*), **247** (1958) 214.

5 Furukwa G T, Riddle J L & Bigge W R, cited in *Temperature—Its measurement & control in science & Industry* (Reinhold, New York), Vol. 4, Part I, 1972, 247.

6 Preston Thomas S, cited in *Temperature—Its measurement and control in science & industry* (Reinhold, New York) Vol 2, 1955, 169.

7 Mc Laren E H, *Can J Phys* (*Canada*), **35** (1957) 1086; **36** (1958) 585; **37** (1959) 422; **38** (1960) 100.

8 Berry R J, *Metrologia* (*Germany*), **10** (1974) 145.

Indian Journal of Pure & Applied Physics
Vol 21, May 1983, pp 293-297

Effect of Matrix on the Magnetic Enhancement of Spectral Lines in the dc Arc

M A EID*, A A FAKHRY, K M ELBEHERY & M S HASHEM
Physics Department, National Research Centre, Cairo, Egypt

Received 11 *October* 1982

Five matrices of different ionization potentials, containing traces of different elements were prepared. The optimal arcing conditions were determined. Application of the magnetic field revealed a relation between the ionization potential of the matrix and the magnetic enhancement factor of spectral lines. Matrices of high ionization potentials caused remarkable magnetic enhancement of the spectral lines, while those having low ionization potentials showed decrease in the intensity of spectral lines on application of the magnetic field to the arc. Moreover, it was found that the changes in the temperature and the electron pressure of the arc plasma, induced by the application of the magnetic field, may be one of the reasons for the magnetic enhancement of spectral lines.

1 Introduction

The application of external magnetic fields of different configurations to the dc arc, for increasing the spectrochemical sensitivity, has attracted the attention of many investigators[1-4]. In many cases, the magnetic field enhances the emission of spectral lines and hence provides new possibilities for the detection of extremely small amounts of elements. Vukanovic *et al.*[1,2] attributed the observed intensity enhancement to the increase of the residence time of the particles in the plasma.

Leushacke and Nickel[5] used trace amounts of elements in a graphite base and a homogeneous magnetic field to study the magnetic enhancement of spectral lines. They found that the maximum intensification was obtained when the concentrations of the elements were near the limit of detection. Harisonov and Zadgorska[6] studied the effect of a non-homogeneous magnetic field on an arc burning in different gases differing in their ionization potentials. They found that the enhancement of the spectral lines by the application of the magnetic field depends on the ionization potential of the gas and attributed it to the increase of the number of ions in the arc plasma.

As an extension in this field, it is of interest to study the effect of matrices of different ionization potentials on the magnetic intensification of spectral lines.

2 Experimental Details and Results

2.1 Experimental Arrangement

The arc was placed in a radially symmetric non-homogeneous magnetic field. The field was produced by a water-cooled electromagnet coil provided with an iron core whose upper end has a conical shape of solid angle $\pi/2$. The axis of the arc was in coincidence with that of the magnet. The magnetic induction B and its vertical gradient dB/dz, which could be varied by changing the current in the magnet coil, were measured at different heights from the pole.

A medium quartz spectrograph Q24 (Carl-Zeiss Jena) was used, with a slit width of 10 μm, to obtain the spectra. The spectra were recorded on ORWO photographic plates type WO 3 and the intensities of the spectral lines were evaluated from characteristic curves obtained by the preliminary curve method.

2.2 The Elements under Investigation

The elements selected for the present investigation can be divided according to their volatility[7] into three groups:

(a) volatile: In, Sn, Ag, Cu and Zn,
(b) medium volatile: Al, Mn, and Mg, and
(c) involatile: B and Be.

In each group, representative elements with different ionization potentials are chosen. A mixture of these elements is added to spec-pure graphite powder in such a concentration that for each element the most sensitive lines appear in the spectrum of the arc. This mixture will be referred to as the 'O' mixture. Table 1 gives the concentrations of the elements in the 'O' mixture, their ionization potentials and the wavelengths of the spectral lines used for the investigations.

2.3 Factors Affecting the Magnetic Enhancement of Spectral Lines

The magnetic enhancement of spectral lines is a function of some experimental variables; these are: the concentration of the element, the arc current, the shape

*Present address: Science and Mathematics Centre, POB 2375 Dammam, Saudi Arabia.

of the electrodes, the arc gap, and the applied magnetic induction. In order to achieve the optimal working conditions, the effect of all these variables on the enhancement factor I/I_0 was studied. The variables I and I_0 are the line intensities corrected for background, with and without magnetic field respectively. This investigation was carried out using a graphite matrix. The SnI line at 2839.99 Å was taken as a test line. The results of this investigation can be summarized as follows:

2.3.1. *Effect of the concentration of the element*—The previously mentioned 'O' mixture of elements was diluted with spec-pure graphite powder in different ratios and then I/I_0 of the test line was determined. The result is shown in Fig. 1, which shows that the maximum enhancement corresponds to a dilution of 1:9. This result is in agreement with that reported by Leushacke and Nickel[5].

2.3.2. *Effect of arc current*—The effect of the arc current on the enhancement factor I/I_0 of the test line is shown in Fig. 2. It is obvious that the optimal value of the arc current is 8 A.

Table 1—Ionization Potentials Spectral Lines and Concentrations of the Elements in the 'O' Mixture

Element	Ionization potential eV	Spectral line, Å	Conc. %
In	5.79	3039.36	0.0012
Sn	7.34	2839.99	0.0053
Ag	7.57	3382.89	0.0007
Cu	7.72	3273.46	0.0007
Zn	9.39	3345.02	0.0012
Al	5.98	3092.71	0.0032
Mn	7.43	2798.27	0.0050
Mg	7.64	2852.13	0.0006
B	8.30	2497.73	0.0036
Be	9.32	3321.34	0.0022

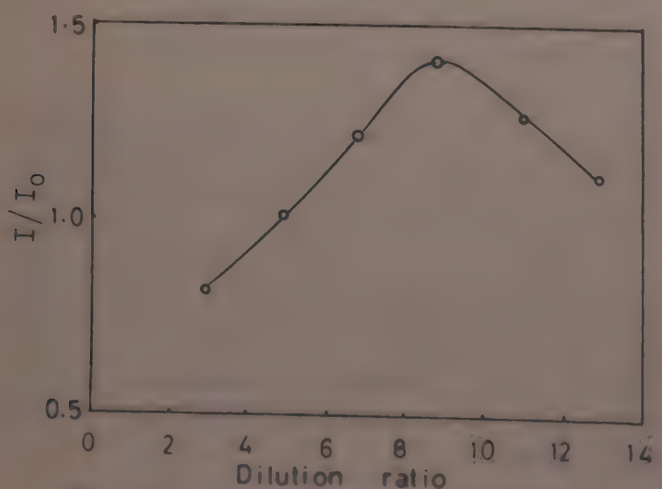

Fig. 1—Dependence of the magnetic enhancement factor I/I_0 of the test line SnI 2839.99 Å on the dilution ratio of the 'O' mixture [Arc current 6 A, crater diameter 4 mm, crater depth 4 mm, cathode: pointed, arc gap: 2 mm, magnetic induction: 11 mT, height of arc gap from the magnet pole: 5 cm]

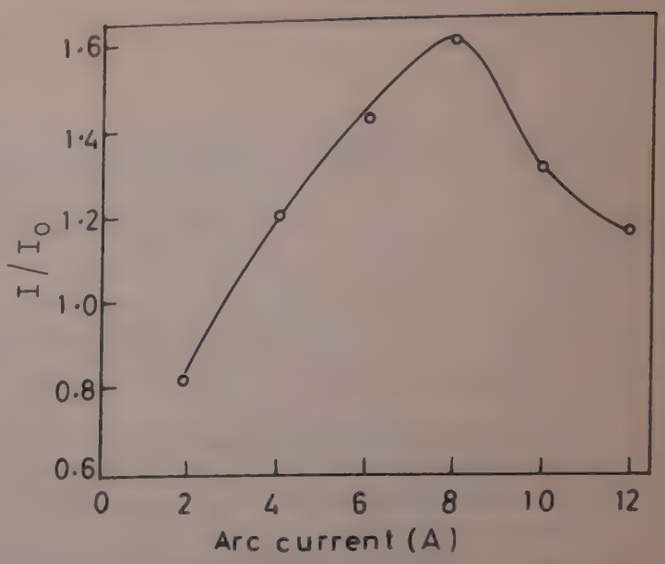

Fig. 2—Effect of arc current on the magnetic enhancement factor I/I_0 of the test line SnI 2839.99 Å

Table 2—Dependence of the Magnetic Enhancement Factor I/I_0 of the Test Line SnI 2839.99 Å On the Shape of the Anode

[arc current: 8 A, cathode: pointed, arc gap: 2 mm, magnetic induction: 11 mT, height of arc gap from the magnet pole: 5 cm]

Crater depth, mm	I/I_0 for crater diameters of		
	2 mm	4 mm	5.2 mm
2	1.30	1.60	1.71
4	1.88	2.55	2.65
6	1.50	2.11	2.21

2.3.3. *Effect of the shape of the electrodes*—The effects of the lactors governing the shape of the lower electrode (anode) namely, the internal diameter and the depth of its cavity on the enhancement factor I/I_0 of the test line were studied. The results are given in Table 2. From these results, one can see that I/I_0 exhibits a maximum at a crater depth of 4.0 mm which increases gradually with the increase of the internal diameter of the crater. Meanwhile, with increase in the crater diameter it was found that the arc started to wander and consequently fluctuations in the spectral line intensity were observed. For the purpose of the present investigation, the optimal crater diameter was taken to be 4.0 mm.

Three types of counter electrodes were used. The first two are the preformed 100 u and L3963 electrodes. The third electrode is a graphite rod 5 mm diameter pointed at its end to form a cone with solid angle of 24°. The effect of the shape of these types of counter electrodes on I/I_0 of the test line and the corresponding relative standard deviation, using five measurements at an optimal arc current of 8 A indicated that the highest enhancement with the least standard deviation is obtained using the pointed counter electrode.

Fig. 3 shows the effect of the arc gap on the enhancement factor I/I_0 of the test line. It can be seen that maximum enhancement is obtained with an arc gap of 4.0 mm.

2.3.4. *Effect of the magnetic field on the intensity of spectral lines*—Fig. 4 shows the enhancement of the intensity of the test line as a function of the magnetic induction B at different heights z from the magnetic pole. It can be seen that the maximum intensification of the spectral lines is achieved at a magnetic induction of 7 mT and a height of arc gap from the magnet pole of 5 cm. This corresponds to an induction vertical gradient of 1.9 mT/cm. It was found that this result holds true for the spectral lines of all elements under investigation.

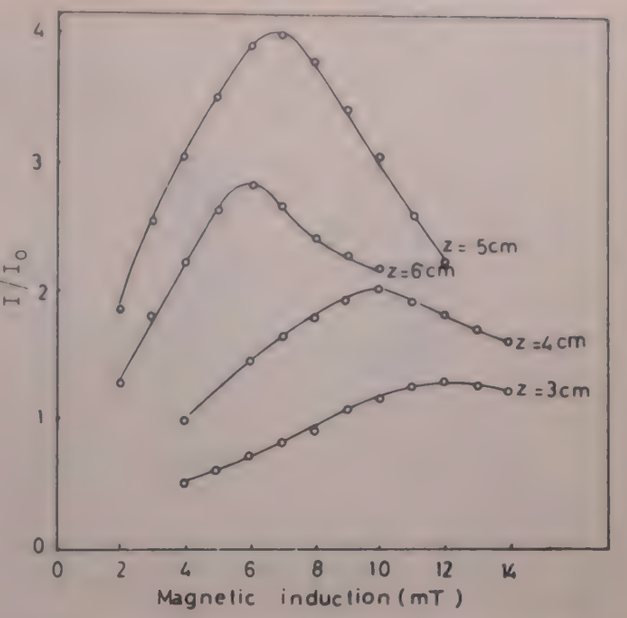

Fig. 4—Dependence of the magnetic enhancement factor I/I_0 of the test line SnI 2839.99 Å on the magnetic induction B and the height z of the arc gap from the magnet pole

2.4 Effect of Matrix on the Magnetic Enhancement of Spectral Lines and on the Changes of the Plasma Parameters

The matrices chosen for this investigation are BaO, CuO, SiO_2, As_2O_3 and graphite. The choice is based on the ionization potential of their cations, which are 5.21, 7.70, 8.35, 10.05 eV respectively and that for graphite which is 11.30 eV. The charge of the electrode consisted of 70% matrix, 20% spec-pure graphite powder and 10% of the 'O' mixture. For each matrix, eight electrodes were prepared; four of them to be arced with magnetic field and four without. So, each intensity value was obtained as the average of four readings. The optimal arcing conditions, achieved previously, for the graphite base were conducted to study the effect of the different matrices on the magnetic enhancement of the spectral lines of the different elements as well as on the changes in the plasma parameters of the arc, induced by the magnetic field. The magnetic enhancement factor I/I_0, for each element in the mixture, was determined from the spectra. Moreover, the excitation temperature and the electron pressure with and without magnetic field were measured. The excitation temperature was determined from the intensity ratio of the zinc atom line pair ZnI 3072.06 Å/ZnI 3075.90 Å [Ref. 8]. The electron pressure was determined from the intensity ratio of the ion-atom line pair of magnesium MgII 2795.53 Å/MgI 2779.83 Å [Ref. 9].

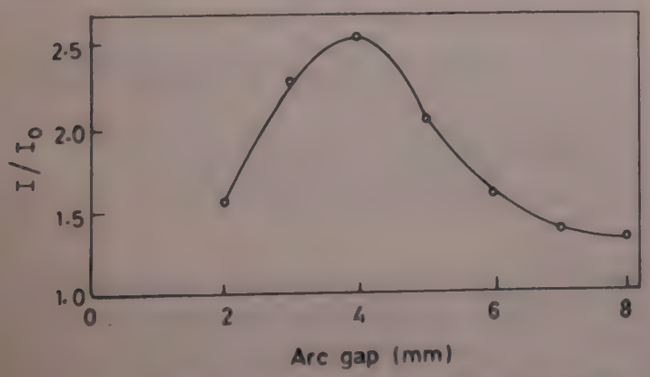

Fig. 3—Effect of arc gap on the magnetic enhancement factor I/I_0 of the test line SnI 2339.99 Å

The results of this investigation are shown in Tables 3 and 4. Table 3 gives the effect of the matrix on the I/I_0 ratio for the different elements. The ionization potential of the matrix is also given (Table 3). Table 4

Table 3—Effect of Matrix On the Enhancement Factor I/I_0 of Spectral Lines of Different Elements

Matrix	V_i, eV	I/I_0 Volatile				Medium volatile				involatile	
		In	Sn	Ag	Cu	Zn	Al	Mn	Mg	B	Be
BaO	5.21	0.68	0.36	0.44	0.95	0.34	0.63	0.49	0.58	0.26	0.54
CuO	7.70	0.81	0.40	0.40	—	0.37	0.73	0.60	0.67	0.49	n.d.
SiO_2	8.51	0.89	0.54	0.22	0.19	0.61	0.81	0.70	0.70	0.51	n.d.
As_2O_3	10.05	0.51	1.46	1.01	1.01	0.70	1.49	1.81	1.67	0.73	0.78
graphite	11.30	4.31	3.80	2.31	2.11	1.00	4.22	2.00	3.11	1.31	1.30

n.d. means the line was not detected in this matrix.
V_i is the ionization potential of the matrix.

Table 4—Effect of Magnetic Field on Temperature and Electron Pressure of the Arc Plasma using Different Matrices

Matrix	I/I_0 SnI 2839.99 Å	T, K			$P_e \times 10^{-3}$ atm.		
		0	7 mT	ΔT	0	7 mT	ΔP_e
BaO	0.36	5620	5760	140	2.03	1.22	−0.81
CuO	0.40	6100	6260	160	3.06	2.34	−0.72
SiO_2	0.54	6120	6220	100	0.99	0.40	−0.59
As_2O_3	1.46	6100	6200	100	0.92	1.21	+0.31
graphite	3.80	6210	6510	300	1.08	2.48	+1.30

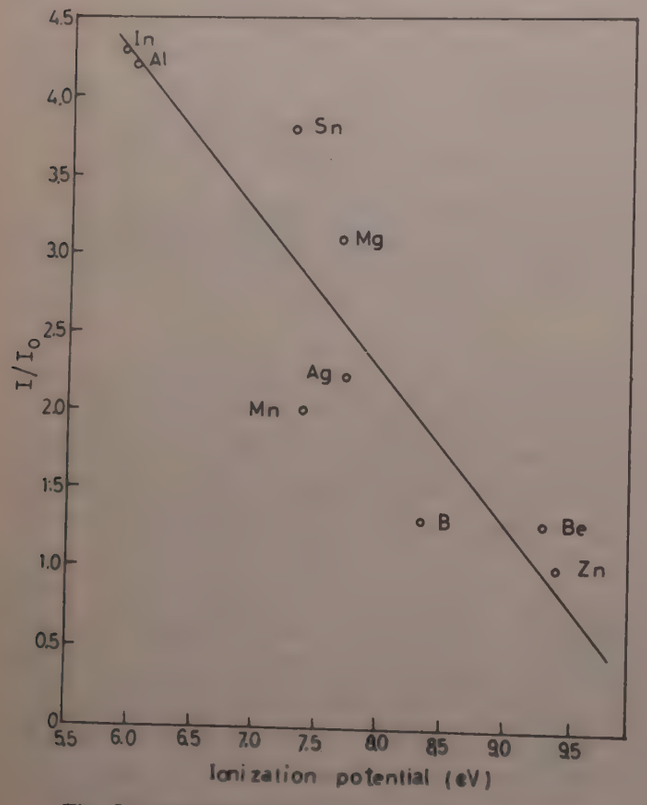

Fig. 5—Dependence of the magnetic enhancement factor I/I_0 on the ionization potential of the element

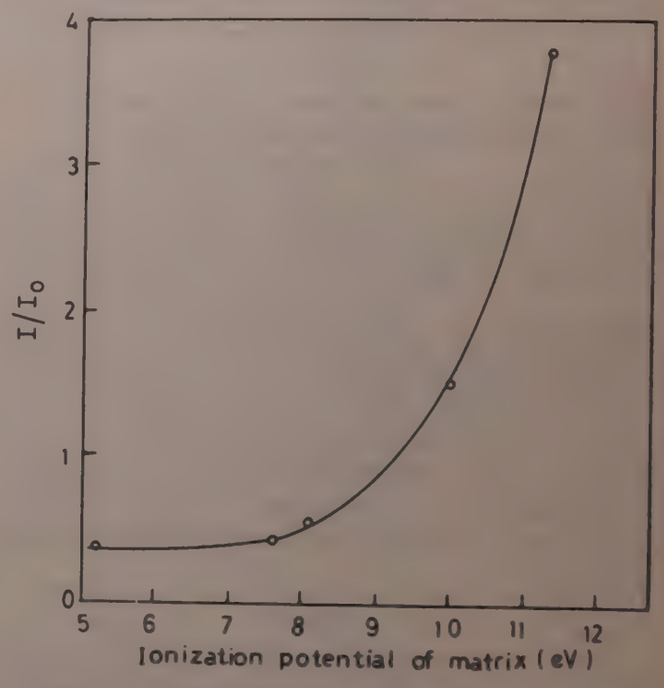

Fig. 6—Dependence of the magnetic enhancement factor I/I_0 of the test line SnI 2839.99 Å on the ionization potential of the matrix

gives the effect of the magnetic field on the excitation temperature and the electron pressure in presence of the different matrices. The changes in these quantities, due to the application of the magnetic field, are also given in Table 4. The enhancement factor I/I_0 of the test line SnI 2839.99 Å is given in Table 4 for convenient comparison.

3 Discussion and Conclusions

From the results of the present work, the following relations (with few exceptional cases) can be found:

(1) The involatile elements have the least response to the magnetic field, as given in Table 3.

(2) The magnetic enhancement factor I/I_0, using a certain matrix, depends on the ionization potential of the element and, in general, it decreases as the ionization potential of the element increases. This relation is shown in Fig. 5 for the graphite matrix.

(3) The magnetic enhancement factor, for all elements, depends remarkably on the ionization potential of the matrix. A value of I/I_0 greater than unity is obtained only with As_2O_3 and graphite, while the other matrices affect in depressing the intensity of the spectral lines, when the magnetic field is applied. The relation between the magnetic enhancement factor I/I_0 and the ionization potential of the matrix is shown in Fig. 6 for the test line SnI 2839.99 Å. This is the main conclusion of this work, which can be useful in detecting trace amounts of elements by the application of magnetic field to the dc carbon arc.

(4) The application of the magnetic field causes a slight increase in temperature for all matrices. In spite of the fact that the increase in temperature is small and shows no regular dependence on the ionization potential of the matrix, the highest increase in

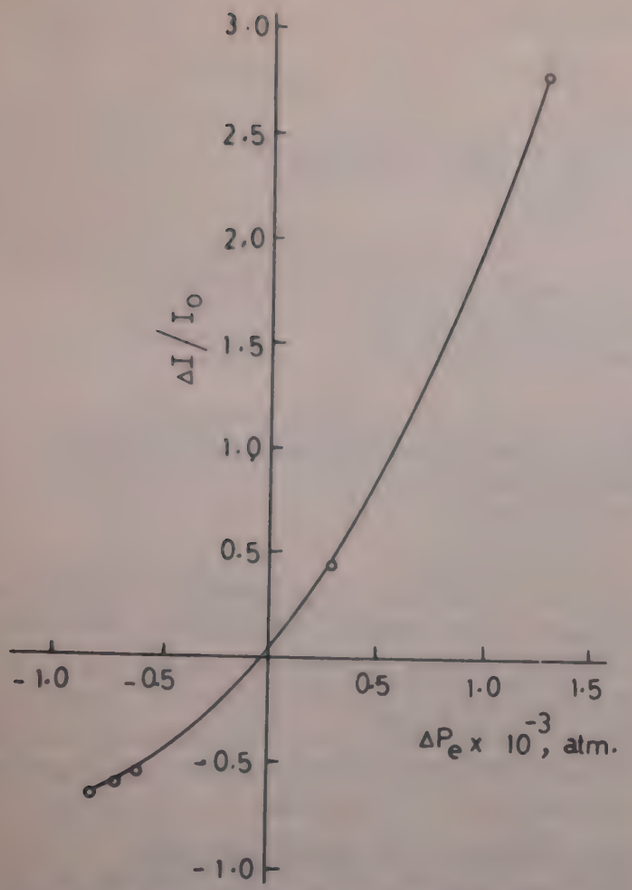

Fig. 7—Relation between the relative change in intensity $\Delta I/I_0$ of the test line SnI 2839.99 Å and the change in electron pressure ΔP_e, induced by the magnetic field

temperature is obtained with the graphite matrix of the highest ionization potential and the highest enhancement factor.

The changes in the electron pressure, induced by the application of the magnetic field, show some regular dependence on the ionization potential of the matrix. In the presence of matrices of low ionization potential, the application of the magnetic field causes a decrease in the electron pressure. These matrices depress the intensity of the spectral lines of all elements present. On the other hand, matrices of high ionization potential cause an increase in the electron pressure when the magnetic field is applied. These matrices enhance the emission of the spectral lines. A relation is obtained between the relative change in intensity $\Delta I/I_0$ of the test line SnI 2839.99 Å and the change in the electron pressure ΔP_e, induced by the magnetic field. This is illustrated in Fig. 7.

From the results of this investigation, it may be concluded that one of the reasons for the magnetic enhancement of spectral lines can be the changes in the plasma parameters induced by the magnetic field.

References

1 Vukanovic V & Georgijevic V, *J Anal Chem USSR (USA)*, **225** (1967) 137.

2 Vukanovic V, Georgijevic V, Vukanovic D & Todorovic M, *Spectrochim Acta Vol. B (GB)*, **24** (1969) 555.

3 Todorovic M, Vukanovic V & Georgijevic V, *Spectrochim Acta Vol B (GB)*, **24** (1969) 571.

4 Krasnobaeva N, Charisanov Ju & Zadgorska Z, *Spectrochim Acta Vol B (GB)*, **24** (1969) 473.

5 Leushacke D F & Nickel H, *Spectrochim Acta Vol B (GB)*, **26** (1971) 409.

6 Harisonov Yu & Zadgorska Z, *Spectrochim Acta Vol B (GB)*, **25** (1970) 29.

7 Ahrens L H & Tayler S R, *Spectrochemical analysis* (Addison Wesley, London) 1961, 82.

8 Boumans P W J M, *Theory of spectrochemical excitation* (Hilger & Watts, London) 1966, 108.

9 Boumans P W J M, *Theory of spectrochemical excitation* (Hilger & Watts, London) 1966, 175.

Indian Journal of Pure & Applied Physics
Vol 21, May 1983, pp 298-302

A Microprocessor Based Internal Friction Measurement System

K NEELAKANTAN, DIPENDRA CHOWDHARY, B PURNIAH* & RADHA RANGANATHAN
Reactor Research Centre, Kalpakkam 603 102, Tamil Nadu

Received 8 *September* 1982

A microprocessor-based system for internal friction measurements is described. The system is built around a National Semiconductors' SC/MP microprocessor and can handle set-ups covering a wide range of frequency and temperature. Experimental parameters like initial temperature, temperature increment/decrement, number of temperature steps, etc. can be specified by the user and thereafter the experiment is fully controlled by the system.

1 Introduction

The study of internal friction in solids provides a convenient means of obtaining information about the thermally-activated defect motion in solids. Examples are the Snoek, Zener and Bordoni relaxations which occur due to interstitials, substitutionals and dislocations respectively[1]. The type and orientation of the defect can be identified by the characteristic dependence of the internal friction Q^{-1} (or damping) on temperature and frequency, given by

$$Q^{-1} = A\omega\tau/(1+\omega^2\tau^2) \quad \ldots(1)$$

where ω is the angular frequency of oscillation of the sample and τ the relaxation time for the process giving rise to internal friction. A is a constant which contains information regarding the concentration of defects, their strength to cause damping, etc.

The relaxation time τ is strongly temperature dependent through the Arrhenius relation

$$\tau = \tau_0 \exp(H/k_B T) \quad \ldots(2)$$

where H is the activation energy for the process, T the temperature, k_B the Boltzmann constant, and τ_0 the frequency factor. It may be seen from Eq. (1) that, for each process, the maximum ($\omega\tau = 1$) will occur for a particular choice of frequency and temperature range [as dictated by Eq. (2)]. The wide variation in ω and T entails the use of different experimental arrangements. Further, to obtain the Debye curve completely [Eq. (1)], one has to perform the measurement of damping (using for example the free decay method[1]) at different temperatures. The process becomes extremely tedious especially if one is dealing with low frequencies. The large amount of data that has to be handled at once underscores the need for some kind of automation.

This paper describes a microprocessor-based measurement system that facilitates performing experiments covering frequency and temperature ranges of 0.1-10 kHz and 4-1000 K respectively. This choice of parameters enables one to perform experiments covering a large number of relaxations covering point defects, dislocations and grain boundaries. Similar automated systems have been described earlier[2-4], but the present one differs from these in that the logic is not hardwired. Functional requirements are met through software programming, thus lending flexibility and ease in system design.

2 Block Diagram and Control Algorithm

The block diagram of the system is shown in Fig. 1. The different ranges of frequencies and temperatures give rise to four convenient combinations. Each set-up has its temperature controller* and capacitance transducer (which also incorporates the excitation circuit). The output of the transducer is coupled to the peak detector (to record the oscillation amplitude) and an analog to digital converter (ADC-2) through the multiplexer, while the amplified temperature sensor voltage is directly fed to the CPU from the multiplexer using ADC-1. The CPU, in addition, has main memory (where the program is stored) and a keyboard and printer as the I/O devices.

Before proceeding with the description of the control algorithm, we present the sequence of operations to be performed at each temperature. These are: (a) Controlling the temperature, (b) exciting oscillations to a preset level, (c) recording the peak to peak amplitudes of the decaying oscillations, (d) measuring the time period, and finally (e) computing the damping (log decrement) and printing out the values of temperature, log decrement and time period. The sequence (b) to (e) is gone through thrice at each temperature before proceeding to the next temperature.

The main philosophy behind the algorithm is that temperature control is the main program while the

*The temperature controller is used in the 'LINE' mode wherein it accepts signals from the microprocessor to switch on or switch off the power to the heater. The comparison etc. is performed in the microprocessor using the stored calibration curve for each sensor.

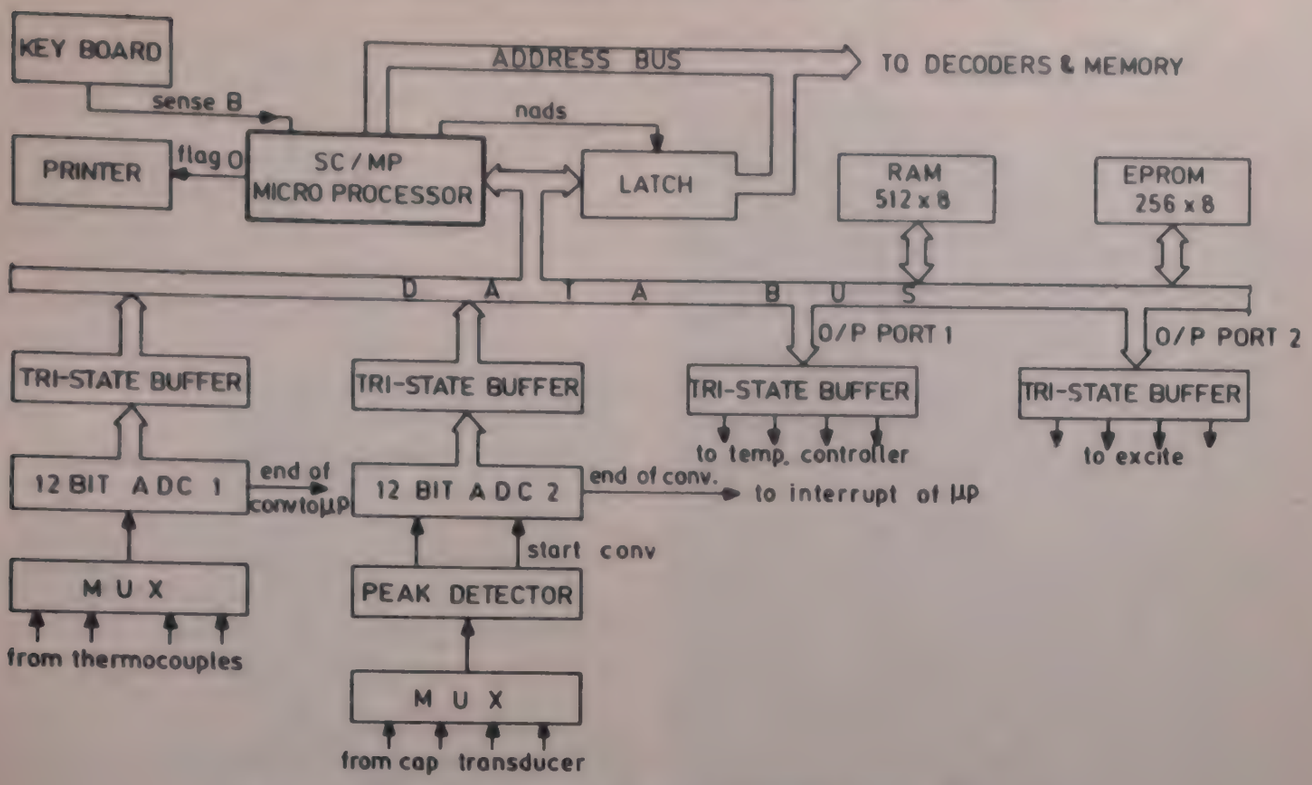

Fig. 1—Microprocessor-based internal friction measurement system: Block diagram

other tasks like excitation, data acquiring, computation, etc. are subroutines incorporated into the interrupt service routine and are executed only when needed.

The flow chart of the temperature control routine is shown in Fig. 2. Upon 'cold starting', the system initializes its registers and waits for the user to enter the experimental parameters. These are the starting temperature, temperature step size, number of temperature steps, sensor type, etc. (however as a default option, certain typical values for these parameters are assumed). Once this step is completed, the system latches each of the four temperature channels (inputs) sequentially, and at each channel it initiates analog to digital conversion of the amplified sensor voltage. These digital values are then stored. All these voltage readings are converted into temperature (linearized) and a difference table of ΔT's (difference between current temperature at which a reading is to be taken, T_{set} and T_{actual}) is prepared. The sign of ΔT is used to switch ON or OFF the power to the heater in each channel. This process is continued till any one of the ΔT's is zero. This implies that the particular set-up has reached the set temperature and is ready. Next the DATA flag is set and the interrupt of the microprocessor is 'enabled' (The data flag has been used so that subsequently when $\Delta T = 0$ for the other channels, the microprocessor does not attend to them till this one is disposed of). The appropriate experimental set-up is then given an excite input and the corresponding data channel (transducer output) is

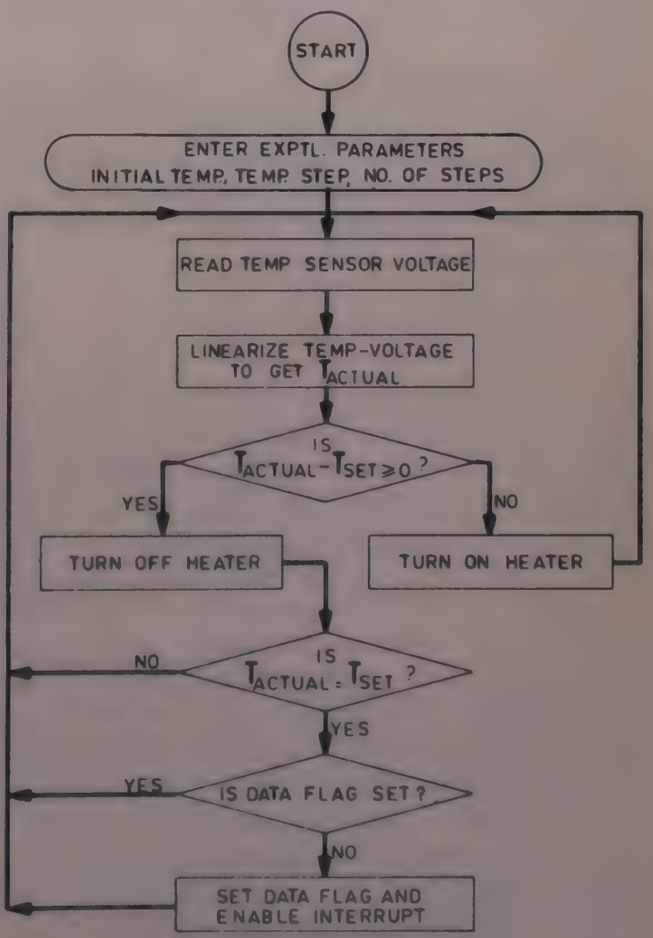

Fig. 2—Temperature control routine and main program of the system: Flow chart

latched. The system then continues with the temperature control algorithm.

It may be noted that the actual collection of data takes a short time (≈30 sec for a frequency of 1 Hz) compared to the time taken to raise or lower the temperature of the sample. This fact is utilized in attending to each set-up ('servicing'). The servicing is in terms of which set-up has reached the desired temperature first. However, in the event of two channels showing $\Delta T = 0$, the set-up with the lower address designation is given priority. Thus in the long run, all experimental set-ups will get equal attention provided the thermal time constants are not grossly mismatched.

We now proceed to discuss the sequence of operations once a particular channel has reached its current T_{set}. A method to ensure smooth excitation of oscillations is that the sample be excited repeatedly till the p-p amplitude reaches a preset value (This can be varied if needed). This is accomplished by the use of another flag, the data acquisition flag (DAQ) in the interrupt service routine (Fig. 3). A check is first made on the DAQ flag and if it is not set, the system proceeds with the excitation, i.e. an excite pulse is generated after each positive peak. Otherwise amplitudes of 68 positive and negative peaks (34 p-p values, A_i) are then recorded, each recording being an interrupt by the data.

After acquiring all the data (i.e. the p-p values corresponding to the channel which has reached T_{set}), the first four peak values (2 cycles) are ignored as these may correspond to transients. The value of the log decrement δ is then calculated from the remaining data points by an averaging formula[5]

$$\delta = (1/N)\left\{\ln \sum_{i=1}^{N-1} A_i - \ln \sum_{i=N+1}^{2N-1} A_i\right\} \quad \ldots(3)$$

Next, the time period is read in and the results are printed out along with the channel number. The DAQ flag is then reset and the experiment is repeated two more times. At the end of three iterations, the DATA flag is reset. The system finally checks for any erroneous condition (e.g. poor vacuum) and prints out a condition code before proceeding to increment temperature and perform data acquisition the next time it meets $\Delta T = 0$ (either for this channel or any other channel). The condition code has been used purely as an indicator and no corrective action is taken.

Before setting the next temperature on a particular channel, a check is made whether the experiment is over or not, i.e. whether the temperature cycle has been gone through fully. This is done as follows: The number of temperature steps is compared with the user-specified value. If the two are unequal, the step count is incremented and the experiment proceeds. If

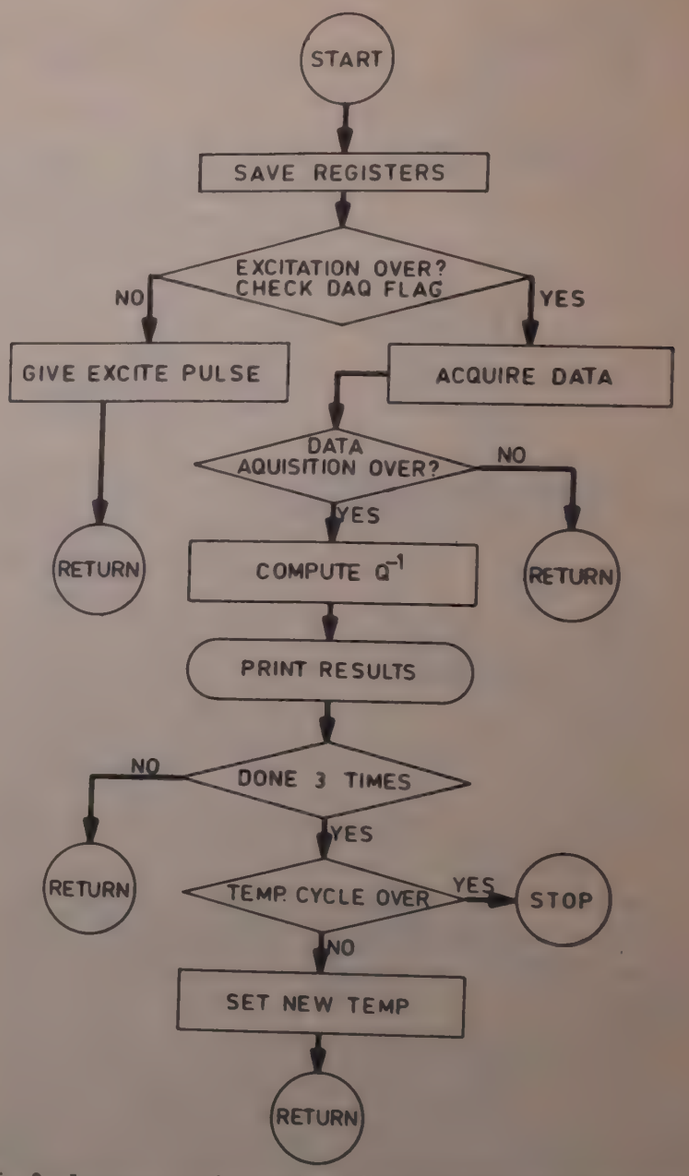

Fig. 3—Interrupt service routine (All RETURNS are to the main program)

they are equal, the temperature increment δT is checked to see if it is negative (This option has been included so that a heating-cooling type run can be done). If it is positive, the step number is set to zero and the increment is negated. Otherwise the experiment is over and the message is printed out.

The computation and printout take only about five seconds so that temperature control is quite effective. However, higher speeds of data acquisition may not be compatible with such an interrupt service structure. In such cases, a direct memory access (DMA) controller will have to be added and the microprocessor will be interrupted only after all the data have been acquired. This entails only minor changes in the interrupt service routine.

It may be observed that the initialization of the experimental parameters has to be done for all four set-ups right in the beginning. However, a situation may arise wherein one of the set-ups has to be hooked on after the microprocessor has begun operations (e.g. a malfunction has just been set right in one set-up). This

drawback has been taken care of to a certain extent by having a 'LOCAL' mode on each of the temperature controllers which will keep the temperature at their current values. The fourth set-up can now be connected and the system appropriately re-initialized before changing the controllers to the 'LINE' mode.

3 Hardware

3.1 Transducer

The typical strain amplitude of the sample is in the range 10^{-6}-10^{-8}. A capacitive transducer has been employed in our set-up and the corresponding change in capacitance works out to be in the range 10^{-2}-10^{-4} pF. We have used the ratio transformer principle to measure these small changes in capacitance[6]. The ratio transformer and associated circuitry are depicted in Fig. 4. The rms current at the point A is given by

$$i_A = (V_0/\sqrt{2})(C_1 - C_2)\omega_0 \qquad \ldots(4)$$

where $\pm V_0 \sin \omega_0 t$ is the voltage appearing across the secondary of T_1. The output is thus proportional to the difference in the capacitance of the two arms (which are attached appropriately to the mechanical part). Slow variations in $(C_1 - C_2)$ can be tracked provided the frequency of such variations is much smaller than ω_0. We have chosen a frequency of 10 kHz which allows tracking variations up to 100 Hz.

The current i_A is typically a few picoamperes for $C_1 - C_2 \sim 10^{-3}$ pF and $V_0 = 2V$. This current can be converted into a voltage which is measured using a lock-in amplifier. As shown in Fig. 4, the current to voltage conversion is achieved through the FET input op amp NE536 which has an input resistance of $10^{12}\,\Omega$ and a 2 pA input bias current. This allows for a 1 MΩ feedback resistor to be placed without saturating the op amp. The circuit layout was made symmetric to reduce any capacitance mismatch.

The heart of the ratio transformer bridge is the bifilar wound transformer T_1 on a CEL HP2A ferrite core of size 26 × 16 mm. The primary had 500 turns of 38 SWG copper wire while the secondaries had 250 + 250 turns. Extreme care was exercised during the winding to ensure that the two secondaries are as closely matched as possible.

3.2 Automation Hardware

The control system is based on a 8 bit SC/MP microprocessor (National Semiconductors, USA). A schematic diagram of the system configuration has already been shown in Fig. 1. The data entry by the operator is via the keyboard and results are printed out on a printer which uses a serial ASCII code. The keyboard has only the hexadecimal characters and three command keys. The ASCII codes are generated in parallel and then fed to the sense B input of the microprocessor at 110 baud to simulate the operation of a teletypewriter.

The 16 bit address is formed from the address pins (12 LSB address bits) and from the data bus. The address decoding is made simple by reserving address lines for specific devices, as for example, the address line 15 is reserved for the temperature sensor channels and 13 for the capacitor transducer channels.

The input channels have been divided into four groups; the thermocouple input channels which are slow and require an integrating type ADC and the fast channels which are connected to a fast ADC via a peak detect/peak locate circuit using ADC's with conversion times of ~10 msec. While this at present caters for the low frequency experiments, a 12 bit successive approximation ADC (conversion time ~20 μsec) is to be used with the medium frequency set-ups.

The peak locate signal from the peak detector[7] is used to initiate conversion on the signal channels and the same pulse is fed to a timer circuit to measure the time period of the oscillations. The conversion on the temperature channels is initiated under software control. The end of conversion from the signal channel ADC is used to interrupt the processor to read in the peak data.

The temperature controllers are of the on-off type and the heater powers are switched on or off depending on the control signal from the microprocessor. This is achieved by means of a triac circuit and the control signals for the temperature controller are latched on to output port 1. The output port 2 forms the excite signal port and, whenever a particular set-up is to be set into oscillation, the bit corresponding to that set-up is made high. In addition, a digital input port 3 is provided to enable the processor to detect abnormal conditions.

The memories consist of 512 bytes of RAM of which the first 256 bytes are used for data (peak values) storage and the remaining 256 bytes are used to store the experimental parameters, intermediate results and as a scratchpad. The program memory is in the form of EPROMs. The communication with the processor for reading in data, printing results, etc. is done via the KIT BUG program[8].

4 Automation Software

We now proceed to give the details of two routines that have been used in the main program and the interrupt service routine (Section 2). These are the temperature linearization routine (to convert voltage to temperature) and the log routine.

The linearization of the sensor voltage is done as follows: The calibration curve of temperature versus voltage (or resistance in the case of RTD) is divided into a number of segments (32 in the case of K type thermocouples). The temperatures at the end points

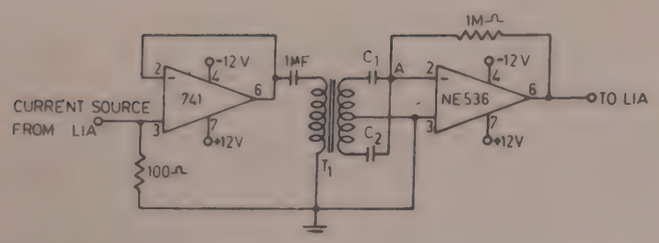

Fig. 4—Ratio transformer bridge and associated circuitry

are stored in a look-up table and temperature is computed by the formula

$$T_x = [(T_f - T_i)(V_x - V_i)/(V_f - V_i)] + T_i \qquad \ldots(5)$$

where V_f, V_i, T_f, T_i are the voltages and temperatures at the end points and T_x is the temperature corresponding to the voltage V_x. The above scheme gives an accuracy of about 0.5% for the K type thermocouple. Temperature control is achieved by comparing this temperature T_x with the set temperature value stored in the RAM. The temperature control output is set low or high depending on the result of this comparison.

The value of δ is calculated by the relation given in Eq. (3). The sums are computed using multibyte arithmetic and then the logarithm of these sums is calculated. The sums are first represented as a fraction, X (the sums are first left justified by shifting and the number of shifts is noted). The logarithm is computed by multiplying the given number by certain constants whose logarithms are known, such that the product approaches unity, i.e.

$$X f_1^a f_2^b f_3^c \ldots f_n^m \equiv 1 \qquad \ldots(6)$$

and hence

$$\ln X = -(a \ln f_1 + b \ln f_2 + \ldots + m \ln f_n) \qquad \ldots(7)$$

The factors f_1, f_2, etc. are chosen such that the multiplication becomes a trivial shift and add. The values of their logarithms are stored as decimal numbers and the result is obtained directly as a BCD number which is printed out after conversion to the ASCII code.

The conversion of numbers from binary to BCD and then to ASCII is done very easily by the use of the decimal ADD instruction of the microprocessor and adding 30 to the resulting BCD code.

5 Results and Performance

The reproducibility of the δ values was found to be better than 2%. This was determined by repeatedly taking a large number of δ values at the same temperature. The lowest value of $Q^{-1} = \delta/\pi$ measurable was 5×10^{-5} (This is typical of most systems).

Temperature stability was found to be ± 0.2 K up to 600 K and ± 2 K thereafter.

Further, a complete temperature run was made on copper of commercial grade purity. The sample was a wire of 0.7 mm diameter $\times 50$ mm long and was annealed *in situ* at 400°C for 2 hr. The results are shown in Fig. 5. It can be seen that the temperature at which the peak occurs is in the range for the grain boundary relaxation in Cu. The high temperature rise is due to the background contribution[1]. The actual peak is obtained by subtracting the estimated background damping from the measured total spectrum.

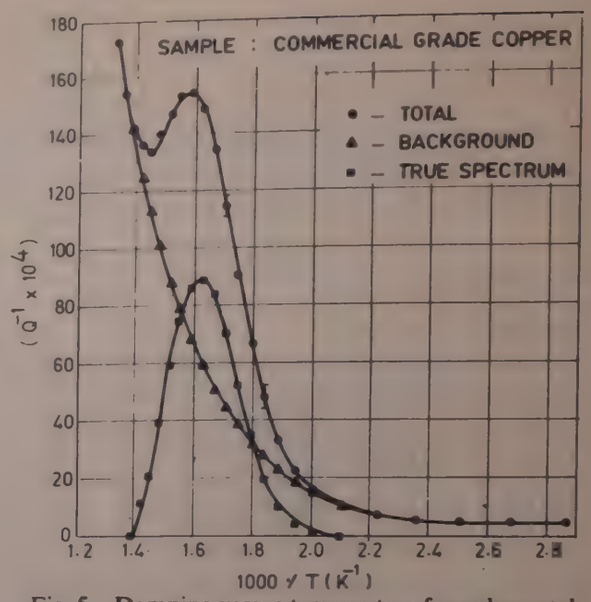

Fig. 5—Damping versus temperature for polycrystalline commercial grade copper [Frequency of oscillation 1 Hz]

6 Conclusion

We have described a very flexible system for measuring the internal friction in materials. It can handle a wide range of frequencies and temperatures. An experiment in the low frequency, high temperature region has demonstrated the capabilities of the system.

Acknowledgement

Thanks are due to Mr V R Seshadri and Mr S Chandrasekharan for providing us with a custom-built peak detect, ADC and temperature controller. We would also like to thank Dr G Venkataraman for suggesting this work and evincing keen interest during various stages of its progress.

References

1 Nowick A S & Berry B S, *Anelastic relaxation in crystalline solids* (Academic Press, New York) 1972.
2 Smith D L, Winieck A L & Lee R K, *J Phys E (GB)*, 3 (1970) 715.
3 Grandchamp P A & Fornerod R C, *J Phys E (GB)*, 3 (1970) 223.
4 Brozel M R & Leak G M, *J Phys E (GB)*, 11 (1978) 53.
5 Aghili Kermani H, O'Brien T, Armeniades C D & Roberts J M, *J Phys E (GB)*, 9 (1976) 887.
6 Jones R V & Richards J C S, *J Phys E (GB)*, 6 (1973) 589.
7 Seshadri V R, Ramaswamy Pillai B, Subramanian V & Neelakantan K, *J Inst Eng (India), Electron & Telecommun Eng Div*, 63 (1982) 30.
8 *SC MP Kit User's Manual* (National Semiconductors, USA) 1976.

NOTES

Indian Journal of Pure & Applied Physics
Vol 21, May 1983, pp 303-305

On the Exchange Repulsion in Ionic Solids

USHA PURI*
S M College, Bhagalpur

Received 23 *September* 1982

The exchange repulsion between ions in ionic solids is discussed. Analytical form of the orbitals constructed by Clementi suggests many exponential terms which constitute the interacting potential. An approximate form is suggested and limitations are discussed.

The Born-Mayer exponential form ($Ae^{-r/\rho}$) for the repulsive energy between closed shells has been used in the study of properties of ionic solids[1,2]. Here ρ is a parameter. Although simple in form and supported by the quantum mechanical calculations[3-8], it is empirical in nature[9,10]. It has a limitation for small values of r, the distance between the ions. In fact, the Born repulsive interaction may consist of several terms partly attractive and partly repulsive[10]. Unsold[11] and Bruck[12] have shown that the energy has a form $\pi(r)e^{-\gamma r}$ where $\pi(r)$ is a polynomial and γ is a parameter. Similar is the nature of the expression given by Heitler and London[4]. The Born-Mayer form can be taken as an approximation to this with $\pi(r)$ a constant.

Recently, Gordon and Kim[13] have given *a priori* calculation of intermolecular forces between closed shell molecules. Their approach predicts remarkably well the distance (σ) at which the potential crosses zero as well as the distance between nuclei at the potential minimum, in case of rare gases. The interaction energy between ions of the alkali halides is expressed as [Eq. (17) of Gordon and Kim[13]]:

$$-\frac{1}{R}+\int_0^\infty 4\pi r_1^2 dr_1 \int_0^\infty 4\pi r_2^2 \rho_a(r_1)\rho_b(r_2) I \qquad \ldots(1)$$

where $$I=\frac{Z_aZ_b+1}{(Z_a-1)(Z_b-1)}\cdot\frac{1}{R}+F(R,r_1,r_2)$$
$$-\frac{2Z_b}{(Z_b+1)}\frac{1}{R+r_1+|R-r_1|}$$
$$-\frac{2Z_a}{(Z_a-1)}\frac{1}{R+r_2+|R-r_2|}$$

and

$$F(R,r_1,r_2)=\frac{2}{R+r_1+|R-r_1|} \quad \text{for } r_2<|R-r_1|$$
$$=\frac{1}{2}\left(\frac{1}{r_1}+\frac{1}{r_2}\right)-\frac{R}{4r_1r_2}-\frac{(r_1-r_2)^2}{4r_1r_2R}$$
$$\text{for } |R-r_1|<r_2<|R+r_1|$$
$$=\frac{1}{r_2} \quad \text{for } r_2>R+r_1$$

where R is the distance between the ions a and b, r_1 and r_2 refer to the distances from them, Z_a and Z_b their atomic numbers. The electronic charge densities (ρ_a and ρ_b), of the ions can be obtained in analytical form by use of atomic orbitals constructed by Clementi[14] which are given as

$$\psi_{i\lambda\alpha}=\sum_p \chi_{p\lambda\alpha} C_{i\lambda p} \qquad \ldots(2)$$

where p refers to the pth basis function of symmetry $\lambda(\lambda$ corresponds to quantum number l), α indicates the subspecies and i refers to the orbital symmetry λ, and

$$\chi_{\lambda p\alpha}=R_{\lambda p}(r)Y_{\lambda\alpha}(\theta,\varphi)(\theta,\varphi)$$

where

$$R_{\lambda p}=[2(n_{\lambda p})!]^{-1/2}(2\xi_{\lambda p})^{n\lambda p+1/2}$$
$$\times r^{n\lambda p-1}e^{-\xi_{\lambda p}\cdot r}$$

Here, r refers to the distance, $n_{\lambda p}$ is an integer $\geq\lambda+1$ and $Y_{\lambda\alpha}$ are the spherical hermonics. The exponent $\xi_{\lambda p}$ has been chosen so as to give the best energy using process of optimization. The quantities $C_{i\lambda p}$, $n_{\lambda p}$ and $\xi_{\lambda p}$ are numbers and can be obtained from the Tables of atomic wavefunction[14].

Use of Eq. (1) coupled with Eq. (2) leads to a sum of large number of exponential terms for the interaction energy which can be expressed as

$$\sum_{i=1}^{m} A_i\frac{e^{-\lambda_i r}}{r}+\sum_{j=1}^{Q} B_j e^{-\lambda_j r}$$
$$+\sum_{k}^{P} C_k r e^{-\lambda_k r}+\ldots\sum_{s=1}^{R} O_s r^s e^{-\lambda_s r} \qquad \ldots(3)$$

where A_i, B_j, C_k, O_s, λ_i, λ_j, λ_k, λ_s are constants; m, Q, P, R are the integers up to which the series is to be summed up. They are related to the number of basis functions used by Clementi[14].

It may be noted that Eq. (3) contains a term of the type $e^{-\lambda r}/r$ which may be essential to account for infinite repulsive energy in case the ions are brought sufficiently near. This type of potential was first suggested by Hellman[15] for metals and later used by Varshni and Shukla[16] for alkali hydrides. Puri and Srivastava[17] have used this form for alkali halides. In fact, a form of the type

$$Ae^{-\alpha r}/r+Be^{-\beta r}+De^{-\delta r} \qquad \ldots(4)$$

may be a better approximation but such a form is linked with the difficulty of evaluating the parameters A, B, D, α, β and δ. If equilibrium conditions are used for the purpose, one is constrained to limit the form to one term only, either the first or the second term of Eq.

(4), as the third term alone is unrealistic. Since in most computations, one is concerned with the properties in equilibrium state, the first or the second term of Eq. (4), which are respectively screened Coulomb potential (SCP) of Hellman[15] and Born-Mayer's (B-M) form, may yield good results[17,18] in case of alkali halides. But wherever distances lower than the equilibrium distance between the ions such as that in the computation of 'σ' (Table 1) at which the potential crosses zero, are involved, SCP form may show better performance as the B-M form has a limitation for small values of r[10,19]

Also, in case of alkali and heavy metal halide molecules, results of dissociation energy (Table 2) with this form (SCP) agree well with the sophisticated calculations of Matcha[20], who has used linear combination of atomic orbitals wavefunctions for alkali halide molecules. Polarization functions with suitable angular behaviour to describe the distortions accompanying molecule formation have been included in the basis set which comprises atomic orbitals.

Further, the SCP form gives a value of the Schottky defect formation energy for KBr greater than that for KCl. This observation is in agreement with the experimental observation[21] (Table 3). The results of calculations of Boswarva and Lidiard[22] and Rao and Rao[23] through the Born-Mayer form are in the reverse order.

Goodisman[24] has suggested the division of the potential for the whole range of r into three groups:

(a) $r < a$

(b) $r > a$

(c) intermediate range, where a takes certain suitable values of r. Although we believe that such an approach will be quite appropriate, there is difficulty of joining the potentials at the boundary and it may not always be easy.

Thomas-Fermi-Dirac method, which is an approximate version of density functional method, has also been applied[25] in case of cohesive energy of KBr. The method has not given results.

While using the commonly prevalent forms of potential to cesium and lithium halide crystals, a point to be noted is that these metals are the two extremes of alkali group; as such their electronic configurations are also of two extremes. Whereas lithium has the first s-closed shell unshielded by p-electrons, cesium has many s and p closed shells. Therefore, their behaviours are expected to be somewhat different from those of other alkali group metals. Phonon spectra of lithium[26] and thermoelectric power of cesium[27] are typical examples. In case of cesium compounds, the situation is complicated on account of the closed shell electron wavefunctions ranging to distances much beyond the equilibrium distance of halide crystals.

The penetration of wavefunction into the regions of halide ions modifies the distribution of electrons giving rise to polarization effects. The effect is increased when the halide ions have also long ranging wavefunction of closed shell electrons such as iodine. In other words, the overlap interaction in case of cesium iodide will be the longest amongst alkali halide crystals and in such a situation no single potential form can be expected to give good results.

Table 1—Calculated Values of σ (in au) of Ionic Pairs

System	SCP	B-M	Gordon and Kim[13]
NaCl	2.05	2.01	2.06
KCl	2.33	2.39	2.27

Table 2—Values of Dissociation Energy

[in kcal mol]

Molecule	Matcha[20]	SCP
LiCl	109.58	104.77
LiBr	95.97	90.71
NaF	111.65	107.5
NaCl	91.58	93.32
KF	110.39	115.62
KCl	95.34	98.80

Table 3—Energy (in eV) of Schottky Defect Formation

Crystal	Exptl [Ref. 21]	SCP	B-L [Ref. 22]	R-R [Ref. 23]
KCl	2.22	2.09	2.05	2.11
KBr	2.53	2.21	1.92	1.87

References

1 Barr L W & Lidiard A B, *Physical chemistry: solid state physics*, Vol. 10, edited by H Erying, D Henderson and W Jost (Academic Press, New York) 1970, 152.

2 Tosi M P, *Solid state physics*, Vol. 16, edited by F Seitz and D Turnbull (Academic Press, New York) 1964, 1.

3 Slater J C, *Phys Rev (USA)*, **32** (1928) 349.

4 Heitler W & London F, *Z Phys (Germany)*, **44** (1927) 455.

5 Pauling L, *Z Kristallogr (Germany)*, **67** (1928) 377.

6 Sakamoto Y & Ishiguro M, *Prog Theor Phys (Japan)*, **15** (1956) 37.

7 Bleik W E & Mayer J, *J Chem Phys (USA)*, **2** (1934) 252.

8 Ref. 2, p. 35.

9 Fowler R H, *Statical mechanics* (Cambridge University Press, Cambridge) 1966, 295.

10 Ref. 1, p. 195.

11 Unsold A, *Z Phys (Germany)*, **43** (1927) 563.

12 Bruck H, *Z Phys (Germany)*, **51** (1928) 707.

13 Gordon K G & Kim Y S, *J Chem Phys (USA)*, **56** (1972) 3122.

14 Clementi E, *Tables of atomic functions* (IEM Corporation, California) 1965.

15 Hellman H, *J Chem Phys (USA)*, **3** (1935) 61 & *Acta Physica Chem (URSS)*, **1** (1934) 913.

16 Varshni Y P & Shukla R C, *Rev Mod Phys (USA)*, **35** (1963) 130.

17 Puri U & Srivastava P L, *J Chim Phys (France)*, **74** (1977) 1034.

18 Puri U, *Indian J Pure & Appl Phys*, **15** (1977) 387.

19 Torrens I M, *Interatomic potential* (Academic Press, New York) 1972, 61.

20 Matcha R L, *J Chem Phys* (*USA*), **47** (1967) 4595, 5295; **48** (1967) 335; **49** (1968) 1264; **53** (1970) 485.

21 Franklin A D, *Point defects in solids*, Vol. 1, edited by J H Crawford (Jr) and L M Slifkin (Plenum Press, New York) 1971, 1.

22 Boswarva I M & Lidiard A B, *Phill Mag* (*GB*), **16** (1967) 805.

23 Rao K J & Rao C N R, *Phys Status Solidi* (*Germany*), **28** (1968) 157.

24 Goodisman J, *Diatomic interaction potential theory*, Vols I & II, (Academic Press, New York) 1973.

25 Alonso J A & Iniquez P, *De An Fiz* (*Spain*), **74** (1978) 48.

26 Smith H C, Dolling G, Nicklow R H *et al*, *Inelastic scattering of neutrons in solids and liquids* (*IASA*), **1** (1968) 149.

27 Sinha N N & Srivastava P L, *Phys Status Solidi b* (*Germany*), **90** (1978) 369.

Indian Journal of Pure & Applied Physics
Vol 21, May 1983, pp 306-307

Phosphors for Solar Cells: Tb-doped Lanthanum Fluoride & Th-doped Calcium Tungstate

V N SAXENA*

Institute of Armament Technology, Girinagar, Pune 411 025

Received 1 *September* 1982; *revised received* 7 *December* 1982

Fluorescent wavelength-shifting by cold emission of phosphors exhibiting 'quantum-counter-action' (QCA), popularly called summation of photons, has been proposed to enhance the conversion efficiency of silicon solar cells for AM1 use. The absolute quantum efficiency (number of visible photons produced divided by the number of IR photons absorbed) and the optical efficiency (light transmitted into the solar cell compared to light incident on the fluorescent sheet) of terbium-doped lanthanum fluoride and thulium-doped calcium tungstate have been measured. It has been verified that there is an optimum screen thickness of the phosphors which is a function of the incident wavelength.

The photovoltaic effect was first reported by Becquerel in 1839 and only in 1954, an RCA group[1] claimed a conversion efficiency of 6%. In the later years, vigorous efforts have been made to use different materials like silicon, gallium arsenide, indium phosphate, gallium phosphide, aluminium arsenide and even some organic substances[2] to achieve higher conversion efficiency. Most of the photovoltaic work has been done in the visible region of the solar spectrum. Loferski's formula[3] for the maximum efficiency of the solar cell indicates that most of the visible photons should be used up to produce electron-hole pairs and that the IR beyond 1.0 μm only heats the solar cells. The solar cell efficiency decreases with the increasing temperature[4], leading to the loss of photovoltage to the extent of 2 mV/°C. It is with this in mind that the author thought of using 'quantum-counter-action' (QCA) of a few prospective phosphors as efficient solar cells.

Literature shows that Hovel[5] has enhanced the conversion efficiency by 2% by fluorescent wavelength shifting on the solar cells, using commercially available plexiglass. However, there is an overlap between the absorption and emission bands resulting in a little re-absorption of the emitted radiation energy, i.e. a sort of self-absorption. In order to look for an up-conversion phosphor having a reasonable high quantum efficiency (number of visible photons produced divided by the number of IR photons absorbed) and also high optical efficiency (light transmitted into the solar cell compared to light incident on the fluorescent sheet), absolute values of these parameters were measured using Bruner's method[6], with a few experimental modifications.

Terbium-doped lanthanum fluoride was prepared from spectroscopically pure oxide obtained from M/s Johnson Mathey Chemical Ltd, UK. Varying thicknesses of thin film of this phosphor were deposited on microscope cover slides used as substrates. Both vacuum evaporation and chemical deposition techniques were employed, and the values of areal density were computed[6] and the quantum efficiency calculated in absolute terms at various IR radiations along with optical efficiency. IR lamp was used with interference filters purchased from Oriel Corp., USA. Similar observations were made for thulium-doped calcium tungstate phosphors (Table 1). The excitation spectra of these phosphors were taken with various concentrations of thulium.

A Reeder thermopile made of gold, purchased from Charle's M Reeder and Co., Michigan, USA, and blackened with evaporated colloidal gold, was used to measure the incoming IR. The details of this thermopile are given elsewhere[7]. A specially

Table 1—Values of Areal Density, Absolute Quantum Efficiency and Optical Efficiency

Sample number	Areal density mg/cm^2	Absolute quantum efficiency	Optical efficiency
Terbium-doped (0.05% by weight) lanthanum fluoride			
1	4.33	0.065	0.055
2	3.21	0.062	0.058
3	7.05	0.053	0.052
4	1.54	0.060	0.032*
5	0.79	0.054	0.042
6	2.42	0.048	0.038
7	0.042	0.064	0.052
8	0.850	0.058	0.048
9	1.30	0.074	0.063
10	0.520	0.083	0.074
Thulium-doped (0.06% by weight) $CaWO_4$			
1	3.48	0.066	0.052
2	1.62	0.048	0.016†
3	5.46	0.054	0.042
4	3.84	0.048	0.044
5	2.54	0.062	0.054
6	0.79	0.057	0.043
7	0.42	0.064	0.062
8	1.52	0.074	0.068
9	1.32	0.086	0.074
10	0.56	0.065	0.060

*Looks good for QCA on solar cell
†Prospective candidate for QCA on solar cell

constructed RCA 931A photomultiplier-type photometer was used to measure the intensity of the luminescent flux coming from the back of the phosphor screen. The inter-calibration was accomplished in such a way that the final results were independent of the absolute intensity of either instrument, i.e. the Reeder thermopile and the photomultiplier-type photometer. Appropriate corrections for the absorption and scattering of light within the sample were made.

Both the phosphors exhibited QCA to convert IR into the visible luminescence as a function of sensitizer concentration for constant condition of excitation. The energy transfer in such trivalent rare earth ions takes place either by one or more transfers because the multiplets associated with these are spaced conveniently and a number of these have long lifetimes and show strong fluorescence. Concentration quenching has also been observed. The absolute quantum efficiency is not very high, but the optical efficiency is not discouragingly low either. The existence of an optimum thickness is an encouraging sign for its use on the solar cells. The IR has more than 40% of the solar energy at AM1. Its conversion into luminescent visible radiation has two-fold advantages and is worth trying on the silicon solar cells. In addition to their quantum and optical efficiencies, the absorption coefficients for the IR, direct visible flux and the visible radiations produced as a result of QCA, refractive indexes and also any chemical aging effects, etc., are to be thoroughly investigated.

The work was carried out at the Laboratory for Atmospheric and Space Physics (LASP), University of Colorado, Boulder, Colorado, USA, and the funds were provided partly by NASA. The author wishes to place on record his thankfulness to the Director and the Dean, IAT, Pune, for publishing this work.

References

1 Rappaport P, *Phys Rev (USA)*, **93** (1954) 246; *RCA Rev (USA)*, **17** (1956) 100.

2 Mukherjee T K, *Photocurrents and photopotentials in organic solids*, paper presented at the 6th IEEE Conference, Cocoa Beach, Florida, USA, 28-30 March 1967.

3 Loferski J J, *J Appl Phys (USA)*, **27** (1956) 707.

4 Shirland F A, *Adv Energy Conversion (USA)*, **6** (1966) 201.

5 Hovel H J, Hodgson R T, Woodall J M, *Solar Energy Mater (Netherlands)*, **2** (1979) 19.

6 Bruner E C (Jr), *J Opt Soc Am (USA)*, **59** (1969) 204.

7 Brown T G, Chasmar P K, Fellget T, *J Scient Instrum (GB)*, **30** (1953) 195.

Indian Journal of Pure & Applied Physics
Vol 21, May 1983, pp 308-310

Specific Heat Anomaly of $CoSiF_6.6H_2O$, $MnSiF_6.6H_2O$ and $NiSiF_6.6H_2O$ at the Phase Transition Points

M P SINHA*
Department of Physics, Bihar Institute of Technology, Sindri, Dhanbad 828 123
and
S K DUTTA ROY
Cryogenic Engineering Centre, Indian Institute of Technology, Kharagpur (WB)

Received 15 *July* 1982

The specific heats of $CoSiF_6.6H_2O$, $MnSiF_6.6H_2O$ and $NiSiF_6.6H_2O$ are measured in the temperature region 100-300 K using a pulse heating technique. In all the three compounds it is found that specific heat has anomalous temperature dependence around the structural transition point. The data are analyzed using the asymptotic power law.

The results of a study of temperature dependence of specific heat around the structural transition point[1-3] in hydrated cobalt, manganese and nickel fluosilicate single crystals are presented in this note. Using these data, the nature of the critical singularity near the structural transition point has been investigated. Further, very little information[4] is available about the anomalous specific heat in the critical region where the crystal symmetry changes from one form to the other. It is, therefore, presumed that an analysis of the critical region specific heat data of the above compounds by the asymptotic power law formula would categorize the critical parameters and suggest the order of phase transition[5].

The samples used in this investigation were single crystals with elongated c-axis and were prepared using the same method described in an earlier communication[6] by one of the present authors. The microcrystals were mounted in a silver calorimeter of internal diameter 2.5 cm, wall thickness 0.25 cm and length 3.2 cm. This was placed inside a radiation shield provided with an outer vacuum case (10^{-5} mm of Hg) immersed in a liquid nitrogen bath. The 'heat pulse' technique following the method of Cole *et al.*[7] was adopted for the measurement of specific heat. Both, the power input and the temperature of the system were measured with the help of a copper resistance heater thermometer calibrated against a copper-constantan thermocouple. The temperature measuring accuracy was $\sim 10^{-3}$ K. In principle, specific heat is calculated from the mean energy input to the sample and the effective rise in the temperature ΔT, of the sample due to a single heat pulse. ΔT is determined as the difference between the equilibrium temperatures of the system at the beginning and at the end of the heat pulse. The equilibrium temperatures are calculated from[8]:

$$\ln(T-T_s)=\ln(T^m-T_s)-\beta t \qquad \ldots (1)$$

where T^m is the instantaneous temperature of the calorimeter just at the end of the heat pulse, T_s the temperature of the radiation shield and β^{-1} the time taken by the system for attaining the equilibrium temperature. The final equilibrium temperature between the calorimeter and the sample was recognized as the value of T at time $t=\beta^{-1}$. From a plot of T versus t and $\log(T-T_s)$ versus t in the fore-rating and in the after-rating periods, the equilibrium temperatures were determined[9]. The reproducibility of the experimental data and the accuracy of the apparatus were checked by measuring the temperature dependence of C_p of polycrystalline ammonium chloride through the transition point. The experimental data agreed within 1% of those of Simon *et al.*[10]

Specific heats C_p in the temperature interval 100-300 K for $CoSiF_6.6H_2O$, $MnSiF_6.6H_2O$ and $NiSiF_6.6H_2O$ are shown in Figs. 1(a), 1(b) and 1(c) respectively. The plot in Fig. 1(a) shows that there are

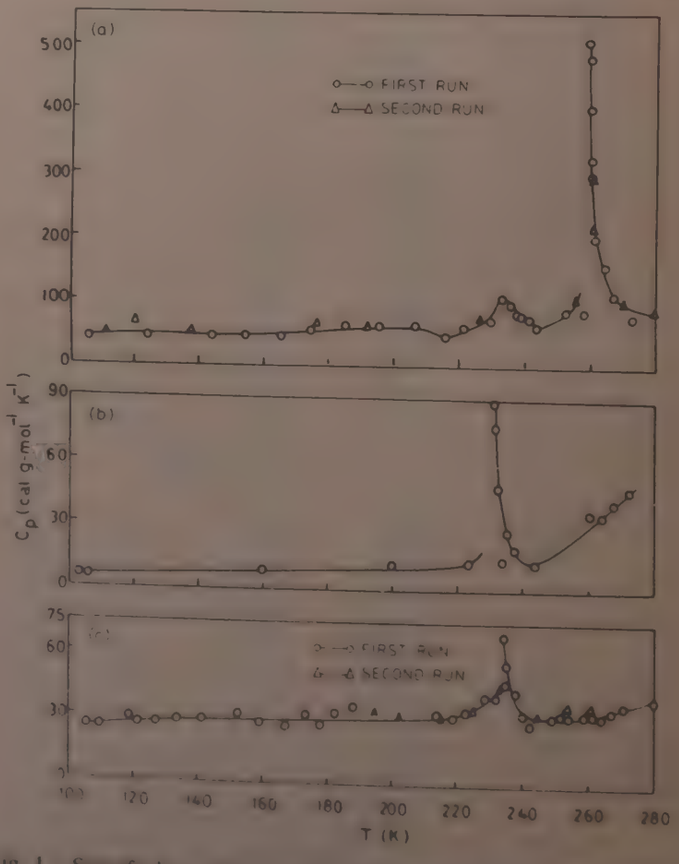

Fig. 1 — Specific heat of (a) $CoSiF_6.6H_2O$, (b) $MnSiF_6.6H_2O$ and (c) $NiSiF_6.6H_2O$ as a function of temperature in the region 100-300 K

Table 1—Critical Parameters in the Phase Transition Region for $T > T_c$

Name of compound	T_c, K	α	Range of agreement*	A	B	E
$CoSiF_6.6H_2O$	259.02	0.34	$6\times10^{-3} > t > 7\times10^{-4}$	37.15	64.7	77.71
$MnSiF_6.6H_2O$	230.5	0.41	$1\times10^{-2} > t > 2\times10^{-3}$	3.75	10.12	11.52
$NiSiF_6.6H_2O$	234.15	0.32	$2\times10^{-3} > t > 2\times10^{-4}$	2.46	34.41	43.4

* Range of agreement between the experimental data and calculated C_p from Eq. (2)

two transition points in $CoSiF_6.6H_2O$ at critical temperatures $T_c(I) \sim 231$ K and $T_c(II) \sim 259$ K, respectively. The transition temperature $T_c(II)$ is well within the limit of error with the value determined earlier in our laboratory using continuous heating technique[11]. $T_c(II)$ also coincides with the transition temperature $T_c(h)$ obtained from magnetic anisotropy data during heating cycle. Figs 1(b) and 1(c) indicate that in $MnSiF_6.6H_2O$ and in $NiSiF_6.6H_2O$ the transition temperatures are 230 and 234 K respectively. The transition point in $MnSiF_6.6H_2O$ agrees well within the limit of error to the transition temperature $T_c(h)$ obtained from the optical absorption data[2]. The transition in $NiSiF_6.6H_2O$ is similar to the magnetic transition observed in $Ni(ClO_4).6H_2O$ [Refs 12, 13]. These confirm the presence of hysteresis effect during the structural transitions in $CoSiF_6.6H_2O$ and $MnSiF_6.6H_2O$. A comparison of the specific heat data for the compounds reveals that the shape of the curve around the transition point in $MnSiF_6.6H_2O$, $NiSiF_6.6H_2O$ and around $T_c(II)$ in $CoSiF_6.6H_2O$ has characteristic similarities. In the region $T < T_c$, the specific heat rises sharply with temperature whereas in the region $T > T_c$, the specific heat decreases at a comparatively slower rate with temperature. The shape of the curve in the critical region resembles a mirror image of λ-shaped C_p versus T curve obtained near the critical temperature in magnetic transitions[14,15].

Recent theoretical advances in the description of critical behaviour within the critical region suggest that the specific heat of a system is expected to obey the asymptotic form[16],

$$C_p = At^{-\alpha} + B + Et \qquad \ldots (2)$$

where $t = (T - T_c)/T_c$, and A, α, B and E are constants to be determined from experimental data. The first asymptotic term in Eq. (2) corresponds to a singularity at $T = T_c$ and other terms represent the background contribution and are assumed to be linear in temperature[17]. The critical region parameters determined from the experimental data are shown in Table 1. It is worthwhile to note that the parameter fitting is for $T > T_c$ only. At $T < T_c$, the variation of specific heat with temperature is very sharp and it has not been possible to obtain more than one point in this

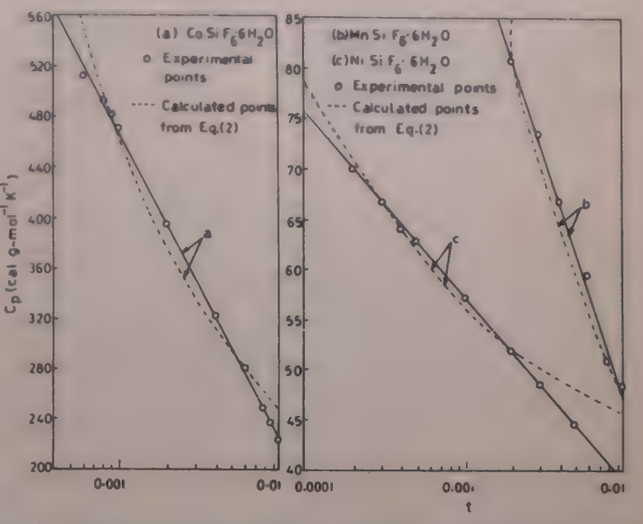

Fig. 2—Specific heat of (a) $CoSiF_6.6H_2O$, (b) $MnSiF_6.6H_2O$ and (c) $NiSiF_6.6H_2O$ as a function of reduced temperature t in the vicinity of the phase transition for $T > T_c$

region. Table 1 also shows the calculated critical temperature and the ranges of agreement between the experimental data and the specific heat C_p calculated from Eq. (2). Fig. 2 shows the variation of C_p with reduced temperature t plotted in a log scale in the transition region. Experimental points when joined together indicate a linear variation while calculated curve shows deviation from linearity. This deviation probably arises from the assumption of linear temperature dependence of the background contribution in Eq. (2). The experimental plot in Fig. 2 does not show any rounding off near the transition temperature and for small positive values of the critical exponent α, the logarithmic singularity of specific heat is obtained for each sample. The specific heat in the vicinity of first transition $T_c(I)$ in $CoSiF_6.6H_2O$ has not been analyzed using Eq. (2) because the experimental data do not give meaningful variation of C_p versus $\log t$ and cause a large percentage error in the calculation of critical parameters.

In conclusion we give an evidence for logarithmic singularity in the specific heat of paramagnetic compounds around a structural transition point. A similar observation has been made by Sinha *et al.*[4] in case of the other paramagnetic compounds around their structural transition points. It is presumed that the present results support that structural transition has a second order origin.

References

1 Dutta Roy S K, Ghosh B & Kar S, *J Phys & Chem Solids (GB)*, **32** (1971) 857.

2 Tsujikawa I & Courture L, *J Phys Radium*, **16** (1965) 430.

3 Sinha M P & Pal A, *Nuclear Phys & Solid State Phys Symp India*, **17C** (1974) 298.

4 Sinha M P, Pal A & Dutta Roy S K, *J Phys C(GB)*, **9** (1976) 2783.

5 Kadanoff Leo P, Gotze W, Hamblen D *et al.*, *Rev Mod Phys (USA)*, **39** (1967) 395.

6 Dutta Roy S K & Ghosh B, *J Phys & Chem Solids (GB)*, **29** (1968) 1511.

7 Cole A G, Hutchens J D, Robie R A & Stout J W, *J Am Chem Soc (USA)*, **82** (1960) 4807.

8 Parkinson D H & Quarrington J E, *Proc Phys Soc (London Ser A)*, **67** (1954) 569.

9 Sinha M P & Pal A, *Indian J Phys*, **50** (1976) 695.

10 Simon F, Simson O V & Ruheman M, *Z Phys Chem, (Germany)*, **129** (1927) 339.

11 Dutta Roy S K, Ghosh B, Kar S & Kaul S N, *J Phys & Chem Solids (GB)*, **33** (1971) 755.

12 Choudhury B K, *J Phys C (GB)*, **7** (1974) 3962.

13 Choudhury B K & Ghosh D, *Nuclear Phys & Solid State Phys Symp India*, **16C** (1974) 381.

14 Kornblit A & Ahlers G, *Phys Rev B (USA)*, **8** (1973) 5163.

15 Kornblit A & Ahlers G, *Phys Rev B (USA)*, **11** (1975) 2678.

16 Fisher M E, *Rep Prog Phys (GB)*, **30** (1967) 615.

17 Gjaki M, Kida J & Watanabe T, *J Phys Soc Jpn (Japan)*, **39** (1975) 588.

18 Ikeda H, Hatta I, Ikushima A & Uryu N, *J Phys Soc Jpn (Japan)*, **39** (1975) 825.

Indian Journal of Pure & Applied Physics
Vol 21, May 1983, pp 311-312

Normal Coordinate Analysis & Molecular Constants of some Pyramidal XYZ_2-type Molecules

S MOHAN*, K G RAVIKUMAR & S GUNASEKARAN
Division of Applied Sciences, Anna University, Madras Institute of Technology, Chromepet, Madras 600044

Received 12 *January* 1982; *accepted* 6 *January* 1983

A fresh study of the harmonic potential constants, compliance constants and vibrational mean amplitudes has been attempted in some pyramidal XYZ_2 cases (C_s) using the kinetic constants method.

The kinetic constants[1-5] relating to molecules have been studied at length and these provide interesting results concerning molecular dynamics. The kinetic constants have been advantageously utilized in solving the secular equation, governing potential constants. The molecules of pyramidal XYZ_2-type belongs to C_s point group having six fundamental frequencies under two species ($4A' + 2A''$). The present investigation has been undertaken to obtain the reasonable set of molecular constants for some pyramidal XYZ_2-type molecules using the most general quadratic valence force field. In addition to potential constants, other molecular constants such as compliance constants[6] and the vibrational mean amplitudes[7] of bonded as well as non-bonded distances are evaluated at 298.16 K and reported in this note. The knowledge of these constants are essential to understand the behaviour of these molecules.

The symmetry coordinates used in the present investigation are taken from Ref. 8. The most general quadratic potential energy function has been considered and the F matrix elements have been obtained as follows:

A' type:

$$\begin{pmatrix} f_D & d f_{D\beta} & \sqrt{2} f_{Dd} & \sqrt{2Dd}\, f_{D\alpha} \\ & d^2 f_\beta & \sqrt{2} d f_{d\beta} & \sqrt{2Dd^3}\, f_{\alpha\beta} \\ & & f_d + f_{dd} & \sqrt{Dd}\,(f_{d\alpha} + f'_{d\alpha}) \\ & & & Dd\,(f_\alpha + f_{\alpha\alpha}) \end{pmatrix}$$

A'' type:

$$\begin{pmatrix} f_d - f_{dd} & \sqrt{Dd}\,(f_{d\alpha} - f''_{d\alpha}) \\ & Dd\,(f_\alpha - f_{\alpha\alpha}) \end{pmatrix}$$

The elements of kinetic energy matrix[9] are used to calculate the kinetic constants of these molecules.

The method of kinetic constants seeks to relate the off-diagonal elements to the diagonal elements of the F-matrix through the relation:

$$\frac{F_{ij}}{F_{jj}} = \frac{k_{ij}}{k_{jj}} \quad (i < j;\ i, j = 1, 2, 3, 4)$$

The compliance constants are also calculated by the Decius method[6].

Using Cyvin's equation $\Sigma = L\,\Delta\,L'$, the symmetrized mean square amplitudes and hence the valence mean square amplitude quantities for both the bonded and the non-bonded distances are evaluated at 298.16 K using the present set of force constants.

The structural parameters and the harmonic frequencies used in the present work are taken from literature[10,11]. The kinetic constants and the valence potential constants of the molecules are presented in Tables 1 and 2 respectively. It is interesting to note that

Table 1 — Values of Kinetic Constants (10^{-23} g)

Molecule	k_D	k_d	k_{dd}	k_{Dd}	k_α	k_β	$k_{\alpha\alpha}$	$k_{\alpha\beta}$	$k_{D\alpha}$	$-k_{D\beta}$	$k_{d\alpha}$	$-k'_{d\alpha}$	$k_{d\beta}$
$AsHD_2$	0.1652	0.3259	0.0003	0.0002	0.1096	0.1628	0.0011	0.0002	0.0015	0.0001	0.0029	0.0001	0.0043
$AsDH_2$	0.3258	0.1783	0.0132	0.0002	0.1096	0.0712	0.0001	0.0007	0.0029	0.0001	0.0016	0.0004	0.0011
$AsHT_2$	0.1652	0.5200	0.0389	0.0002	0.1230	0.2081	0.0014	0.0007	0.0017	0.0002	0.0002	0.0002	0.0094
$AsTH_2$	0.4818	0.1783	0.0132	0.0002	0.1230	0.0712	−0.0003	0.0008	0.0048	0.0002	0.0018	0.0000	0.0011
$AsDT_2$	0.3255	0.5197	0.0385	0.0006	0.1943	0.2181	0.0003	0.0010	0.0051	0.0003	0.0081	0.0002	0.0094
$AsTD_2$	0.4820	0.3259	0.0003	0.0005	0.1943	0.1628	−0.0007	0.0003	0.0075	0.0003	0.0051	0.0003	0.0043

Table 2 — Values of Force Constants (10^5 dynes/cm)

Molecule	f_D	f_d	$-f_{dd}$	f_{Dd}	f_α	f_β	$-f_{\alpha\alpha}$	$f_{\alpha\beta}$	$f_{D\alpha}$	$-f_{D\beta}$	$f_{d\alpha}$	$-f'_{d\alpha}$	$f_{d\beta}$
$AsHD_2$	2.6937	3.4271	0.1061	0.0024	0.2628	0.7376	0.0421	0.0003	0.0029	0.0005	0.0069	0.0015	0.0696
$AsDH_2$	3.0583	2.1044	0.5310	0.0022	0.2281	0.2466	0.0539	0.0011	0.0046	0.0003	0.0033	0.0007	0.0152
$AsHT_2$	2.7693	2.2471	1.0691	0.0005	0.1994	0.4920	0.0610	0.0007	0.0018	0.0011	0.0083	0.0024	0.0197
$AsTH_2$	2.8349	2.8316	0.9466	0.0011	0.3347	0.4318	0.0240	0.0023	0.0138	0.0007	0.0048	0.0005	0.0051
$AsDT_2$	3.2174	2.3458	0.6098	0.0017	0.2448	0.6250	0.0469	0.0010	0.0052	0.0009	0.0102	0.0017	0.0291
$AsTD_2$	3.4152	2.6148	0.2028	0.0009	0.2649	0.3756	0.0411	0.0029	0.0087	0.0008	0.0043	0.0041	0.0316

Table 3—Values of Compliance Constants (Å/m dynes)

Molecule	n_D	n_d	n_{dd}	$-n_{Dd}$	n_α	n_β	$n_{\alpha\alpha}$	$-n_{\alpha\beta}$	$-n_{D\alpha}$	$n_{D\beta}$	$-n_{d\alpha}$	$n'_{d\alpha}$	$-n_{d\beta}$
$AsHD_2$	0.3271	0.5346	0.0381	0.0003	0.7259	0.2526	0.1162	0.0003	0.0036	0.0002	0.0021	0.0001	0.0077
$AsDH_2$	0.3270	0.5077	0.1280	0.0003	0.8633	0.7545	0.2040	0.0043	0.0037	0.0002	0.0023	0.0015	0.0101
$AsHT_2$	0.3272	0.5755	0.2739	0.0001	0.8285	0.1246	0.3148	0.0006	0.0022	0.0001	0.0105	0.0052	0.0048
$AsTH_2$	0.2893	0.7451	0.3851	0.0001	0.5626	0.4305	0.3562	0.0038	0.0020	0.0001	0.0047	0.0025	0.0057
$AsDT_2$	0.3101	0.4577	0.1193	0.0003	0.7884	0.2979	0.1512	0.0013	0.0035	0.0002	0.0082	0.0023	0.0151
$AsTD_2$	0.2929	0.3852	0.0303	0.0005	0.7192	0.4959	0.1117	0.0006	0.0038	0.0003	0.0022	0.0021	0.0151

Table 4—Values of Mean Amplitudes of Vibration (10^{-2}Å) 298. 16 K

Molecule	l_D $(X-Y)$	l_d $(X-Z)$	l_p $(Y\ldots Z)$	l_q $(Z\ldots Z)$
$AsHD_2$	8.8533	7.2927	15.1453	12.7990
$AsDH_2$	7.9362	8.8430	14.7773	14.7781
$AsHT_2$	8.7714	6.5792	14.2793	11.9297
$AsTH_2$	6.6569	8.3665	13.8342	15.5342
$AsDT_2$	7.8348	6.8434	12.7785	12.6163
$AsTD_2$	6.6171	7.7660	12.7546	12.9721

the major stretching kinetic constants k_D of As—H is half that of As—D and one third that of As—T. The stretch-stretch interaction kinetic constants k_{Dd} and k_α practically remain the same for the isotopic pairs. The interaction kinetic constants, viz. $k_{D\beta}$ and $k'_{d\alpha}$ are uniquely negative in all the cases.

As the mass of the Z atom increases, the major stretching force constant f_D increases. This trend can be noticed in $AsHD_2$, $AsHT_2$; $AsDH_2$, $AsDT_2$ and $AsTH_2$, $AsTD_2$. The stretch-stretch interaction force constant f_{dd}, angle-angle interaction force constant $f_{\alpha\alpha}$ and the bond-angle interaction force constants $f_{D\beta}$ and $f'_{d\alpha}$ assume negative sign in all these cases.

The compliance constants for the molecules under consideration are listed in Table 3. These constants are invarient to the choice of coordinates defining the force field and they may be used as a measure of the bond strengths and interactions instead of force constants as pointed out by Decius[6] and Jones[12]. Further, it may be noticed that the compliance constants exhibit trends opposite to that of the force constants.

The vibrational mean amplitudes for both the bonded and non-bonded distances at 298.16 K reported in Table 4 are in the expected range. It may be noted that l_D remains same in isotopically substituted molecules, viz. $AsHD_2$, $AsHT_2$; $AsDH_2$, $AsDT_2$ and $AsTH_2$, $AsTD_2$. It may be added that a decreasing trend is noticed in l_d when the mass of the Z atom increases as per the order cited.

The authors are thankful to Prof. S Sathikh, Director, Madras Institute of Technology, for his kind and constant encouragement and facilities given to carry out this research work.

References

1 Mohan S, *Bull Soc Chem Belg (Belgium)*, **52A** (1977) 747.
2 Mohan S, *Proc Indian Acad Sci Sect A*, **88** (1979) 351.
3 Mohan S, *Acta Phys Pol A (Poland)*, **57** (1980) 433.
4 Mohan S & Ravikumar K G, *Indian J Pure Appl Phys*, **18** (1980) 857.
5 Mohan S & Rajaram S, *Indian J Pure & Appl Phys*, **19** (1981) 620.
6 Decius J C, *J Chem Phys (USA)*, **38** (1963) 241.
7 Cyvin S J, *Molecular vibrations & mean square amplitudes* (Elsevier, Amsterdam) 1968.
8 Venkatesvaralu K & Rajalakshmi K V, *J Sci Ind Res (India)*, **24** (1962) 349.
9 Wilson E B, Decius J C & Cross P C, *Molecular vibrations* (McGraw-Hill, New York) 1955.
10 Reading F P, Horning D F, *J Chem Phys (USA)*, **23** (1955) 1053.
11 Cleveland F, Sundaram S, Thiagarajan C, *J Mol Spectros (USA)*, **5** (1960) 307.
12 Jones L H, *Inorganic vibrational spectroscopy*, Vol I (Marcel Dekker, New York) 1971.

Indian Journal of Pure & Applied Physics
Vol 21, May 1983, pp 313-316

Superposition of Potentials for Diatomic Molecules

S V BIRAJDAR
S B College of Science, Aurangabad 431 001
and
P L SARDESAI & S H BEHERE*
Department of Physics, Marathwada University, Aurangabad 431 004

Received 16 *August* 1982

The potential functions for diatomic molecules suggested by Iyer and Sharma [*Indian J Pure & Appl Phys*, **17** (1979) 615] are reinvestigated. A new potential function is also suggested. The α_e and $\omega_e x_e$ values of a few diatomic molecules are calculated using the newly suggested potential function and these values are compared with the experimental values. The new function gives better agreement as compared to the potential functions suggested by Iyer and Sharma.

The importance of potential functions for the diatomic molecule is well known. Various molecular constants like dissociation energy and anharmonicity constants can be calculated using the potential functions. Recently, Iyer and Sharma[1] suggested two potential functions which are superimpositions of potential functions of Morse[2] and Rydberg[3]. The values of α_e and $\omega_e x_e$ using these functions are also reported. However, the derivations for α_e and $\omega_e x_e$ seem to be incorrect, and hence we have re-examined these functions for the calculations of α_e and $\omega_e x_e$. The potential functions suggested by Iyer and Sharma are as follows:

$$U(r)=\frac{D_e}{2}\left\{[1-\exp(-b\rho)]^2 - \left[1+\frac{b\rho}{2}\right]\exp\left(-\frac{b\rho}{2}\right)-1\right\} \quad \ldots (1)$$

$$U(r)=\frac{D_e}{2}\left\{[1-\exp(-b\rho)]^2-[1+b\rho]\exp(-b\rho)-1\right\} \quad \ldots (2)$$

where $\rho=r-r_e$ and b is a parameter.
The $\omega_e x_e$ and α_e evaluated by Iyer and Sharma are

$$\left.\begin{aligned}\alpha_e&=[0.873\,\Delta^{\frac{1}{2}}-1]\,\frac{6B_e^2}{\omega_e}\\ \omega_e x_e&=[4.34\,\Delta]\,\frac{W}{\mu_A r_e^2}\end{aligned}\right\}$$ Using potential function (1)

$$\left.\begin{aligned}\alpha_e&=[0.833\,\Delta^{\frac{1}{2}}-1]\,\frac{6B_e^2}{\omega_e}\\ \omega_e x_e&=[5.416\,\Delta]\,\frac{W}{\mu_A r_e^2}\end{aligned}\right\}$$ Using potential function (2)

Calculation of α_e and $\omega_e x_e$—The potential functions (1) and (2) were differentiated up to fourth degree which is essential for the calculation of α_e and $\omega_e x_e$. In both cases the first derivative at $r=r_e$ is zero, which is in accordance with the required criterion for extremum. The successive values of differentials at $r=r_e$ are as follows:

	Potential (1)	Potential (2)
$U^{II}(r_e)$	$\frac{D_e}{2}\cdot\frac{9}{4}b^2$	$\frac{D_e}{2}\cdot 3b^2$
$U^{III}(r_e)$	$-\frac{D_e}{2}\cdot\frac{25}{4}b^3$	$-\frac{D_e}{2}\,8b^3$
$U^{IV}(r_e)$	$\frac{D_e}{2}\cdot\frac{227}{16}b^4$	$\frac{D_e}{2}\cdot 17b^4$

Following Varshini[4],

$$\alpha_e=-\left[\frac{Xr_e}{3}+1\right]\frac{6B_e^2}{\omega_e}$$

where $X=\dfrac{U^{III}(r_e)}{U^{II}(r_e)}$ ... (3)

and

$$\omega_e x_e=\left[\frac{5}{3}X^2-Y\right]\frac{W}{\mu_A}$$

where $W=2.1078\times10^{-16}$; $Y=\dfrac{U^{IV}(r_e)}{U^{II}(r_e)}$ ... (4)

Inserting values of proper derivatives in Eqs (3) and (4), we obtain

$$\left.\begin{aligned}\alpha_e&=[1.2346\,\Delta^{\frac{1}{2}}-1]\,\frac{6B_e^2}{\omega_e}\\ \omega_e x_e&=\frac{11.65\,\Delta\,W}{\mu_A\cdot r_e^2}\end{aligned}\right\}$$ Using potential function (1)

$$\left.\begin{aligned}\alpha_e&=[1.0264\,\Delta^{\frac{1}{2}}-1]\,\frac{6B_e^2}{\omega_e}\\ \omega_e x_e&=\frac{8.247\,\Delta\,W}{\mu_A r_e^2}\end{aligned}\right\}$$ Using potential function (2)

These relations for α_e and $\omega_e x_e$ derived in the present note using potential functions (1) and (2) are used to calculate α_e (Table 1) and $\omega_e x_e$ (Table 2) for a number of diatomic molecules. In these calculations, instead of using the values of Δ (Sutherland parameter) for various molecules given by Varshini[4], the values of Δ were recalculated using the molecular constants from a recent bibliography of Huber and Herzberg[5], and are reported in Table 3.

A new potential function—A new potential function which is also a combination of Morse's and Rydberg's

Table 1—Values of α_e for Different Diatomic Molecules

Molecule	α_e (Expt l)	Potential (1)		Potential (2)		Present Potential (5)	
		α_e (Calc.)	Error %	α_e (Calc.)	Error %	α_e (Calc.)	Error %
Br_2	0.0003187	0.0005629	+76.0	0.0004470	+40.26	0.0004160	+31.0
CH	0.534	0.7496	+40.4	0.5493	+2.86	0.4963	−7.05
Cl_2	0.00149	0.002429	+73.5	0.001912	+36.59	0.001767	+26.24
CO	0.01750	0.02271	+29.7	0.017146	−2.04	0.015675	−10.45
CdH	0.2180	0.4730	+116.97	0.3708	+70.12	0.3438	+57.74
H_2	3.0620	2.0824	−31.99	0.8799	−71.26	0.5623	−81.63
HBr	0.2333	0.3504	+50.23	0.26398	+13.16	0.2411	+3.34
HCl	0.3072	0.4364	+42.07	0.3248	+5.7	0.2954	−3.84
HF	0.7980	0.9222	+15.56	0.6596	−17.33	0.5899	−26.08
HI	0.1688	0.2659	+57.53	0.2030	+20.24	0.1863	+10.39
HgH^+	0.2060	0.2678	+30.02	0.2008	−2.5	0.1931	−6.26
I_2	0.0001138	0.0001994	+75.20	0.0001592	+39.88	0.0001486	+30.55
ICl	0.0005354	0.0008746	+63.34	0.0006928	+29.39	0.0006447	+20.4
Li_2	0.007040	0.01435	+103.0	0.01063	+50.95	0.009646	+37.02
K_2	0.0001650	0.0005631	+241.0	0.0004327	+162.25	0.0003983	+141.38
N_2	0.01732	0.02685	+55.02	0.02060	+18.99	0.01896	+9.4
NO	0.01710	0.02552	+49.21	0.01973	+15.36	0.01819	+6.4
Na_2	0.0008736	0.002034	+133.0	0.001539	+76.17	0.001408	+61.19
OH	0.7242	1.0027	+38.45	0.7368	+1.74	0.6667	−7.9
O_2	0.01593	0.02345	+47.5	0.01816	+14.21	0.01676	+5.4
P_2	0.00149	0.002351	+57.82	0.001836	+23.2	0.001699	+14.00
SO	0.005736	0.008115	+41.47	0.006289	+9.6	0.005807	+1.20
ZnH	0.2500	0.5638	+125	0.4406	+76.25	0.4081	+63.20
AuAl	0.000668	0.0007488	+12.09	0.0005713	−14.52	0.000524	−21.55
GeSe	0.0002890	0.0004146	+43.47	0.0003217	+11.33	0.0002972	+2.8
He_2^+	0.2240	0.3242	+44.76	0.2386	+6.5	0.2159	−3.62
Si_2	0.001350	0.001896	+40.43	0.001463	+8.3	0.001349	−00.09

potential functions can be formed as

$$U(r)=\frac{D_e}{2}\{[1-\exp(-a\rho)]^2 - [1+b\rho]\exp(-b\rho)+1\} \quad \ldots (5)$$

where a and b are Morse's and Rydberg's parameters respectively, and $a^2=\frac{K_e}{2D_e}$ and $b^2=\frac{K_e}{D_e}$ which means that $a=\frac{b}{\sqrt{2}}$ or $b=a\sqrt{2}$.

The above suggested potential function can be written either in Morse's or in Rydberg's form.

In Morse's form

$$U(r)=\frac{D_e}{2}\{[1-\exp(-a\rho)]^2 - [1+a\sqrt{2}\rho]\exp(-\sqrt{2}a\rho)+1\} \quad \ldots (6)$$

In Rydberg's form

$$U(r)=\frac{D_e}{2}\left\{\left[1-\exp\left(-\frac{b\rho}{\sqrt{2}}\right)\right]^2 - [1+b\rho]\exp(-b\rho)+1\right\} \quad \ldots (7)$$

Potential function (5) satisfies all the required criteria. At $r=r_e$, in the potential functions (5), (6), (7), $U(r_e)=0$ as the last term is $\frac{D_e}{2}$, whereas in the potential functions (1) and (2), $U(r_e)=-D_e$ as the last term is $-\frac{D_e}{2}$. This has no effect on the evaluation of α_e and $\omega_e x_e$ which need the successive differentiations and the last term being only an adjustable constant its derivative is zero. The values of successive differentials at $r=r_e$ are:

	Morse's form	Rydberg's form
$U^{II}(r_e)$	$\frac{D_e}{2}\cdot 4a_2$	$\frac{D_e}{2}\cdot 2b^2$
$U^{III}(r_e)$	$-\frac{D_e}{2}\left[\frac{3}{2}+\sqrt{2}\right]4a^3$	$-\frac{D_e}{2}\left[\frac{3}{\sqrt{2}}+2\right]b^3$
$U^{IV}(r_e)$	$\frac{D_e}{2}\cdot 26a^4$	$\frac{D_e}{2}\cdot\frac{13}{2}b^4$

By calculating the values of X and Y and using relations (3) and (4), the values of α_e and $\omega_e x_e$ are evaluated. Although Eqs. (6) and (7) look different, they are basically the same; naturally the relations for α_e and $\omega_e x_e$ derived either by Eq. (6) or Eq. (7) are the same. Thus the potential function (5) gives

$$\alpha_e=(0.9714\,\Delta^{\frac{1}{2}}-1)\frac{6B_e^2}{\omega_e} \quad \ldots (8)$$

Table 2—Values of $\omega_e x_e$ for Different Diatomic Molecules

Molecule	$\omega_e x_e$ (Exptl)	Potential (1)		Potential (2)		Potential (5)	
		$\omega_e x_e$ (Calc.)	Error %	$\omega_e x_e$ (Calc.)	Error %	$\omega_e x_e$ (Calc.)	Error %
Br_2	1.0774	2.398	+122.0	1.69	+57.0	1.57	+46.0
CH	63.0	101.37	+60.90	71.76	+13.90	66.61	+5.70
Cl_2	2.67	5.39	+102.00	3.82	+43.00	3.54	+32.0
CO	13.28	18.92	+42.00	13.40	+1.00	12.43	−6.00
CdH	46.30	106.00	+128.00	75.09	+62.00	69.63	+50.00
H_2	121.33	182.00	+49.00	130.15	+7.20	120.80	−0.2
HBr	45.22	80.73	+78.00	57.17	+26.00	53.00	+17.00
HCl	52.82	87.47	+65.00	61.90	+17.28	56.80	+8.00
HF	89.88	120.06	+33.58	85.02	−5.40	78.83	−12.83
HI	39.64	75.64	+90.0	53.56	+35.0	49.67	+25.0
HgH^+	40.90	59.55	+45.60	42.16	+3.07	39.10	−4.38
I_2	0.614	1.33	+117.0	0.0450	+52.0	0.876	+43.0
ICl	1.501	3.06	+104.0	2.16	+44.0	2.01	+34.0
Li_2	2.610	5.25	+101.0	3.717	+42.0	3.44	+32.0
K_2	0.2829	0.7354	+159.9	0.5205	+84.0	0.4832	+70.8
N_2	14.32	25.34	+77.0	17.94	+25.0	16.64	+16.0
NO	14.08	24.72	+75.0	17.51	+24.4	16.23	+15.0
Na_2	0.7254	1.56	+115.0	1.108	+52.8	1.028	+42.0
OH	84.88	136.36	+60.6	96.56	+13.7	89.54	+5.4
O_2	11.98	21.61	+80.4	15.30	+27.7	14.19	+18.4
P_2	2.83	3.73	+31.87	2.64	−6.5	2.45	−15.0
SO	5.60	10.97	+96.0	7.77	+38.7	7.20	+28.0
ZnH	55.14	122.81	+122.0	86.97	+57.0	80.6	+46.0
AuAl	1.1630	1.4891	+28.03	1.0541	−9.6	0.9784	−15.86
GeSe	1.36	1.5052	+10.68	1.066	−21.62	0.9896	−37.43
He_2^+	35.30	52.70	+49.3	37.31	+5.69	34.61	−1.95
Si_2	2.02	3.34	+65.40	2.36	+17.08	2.19	+8.68

Table 3—Values of Δ for Different Diatomic Molecules

Molecule	State	Δ (Varshini)	Δ (Present calculations)	$\Delta^{\frac{1}{2}}$	$\frac{6B_e}{\omega_e}$	$\frac{W}{\mu_A r_e^2}$
Br_2	$X\,^1\Sigma$	20.09	20.0536	4.4781	0.0001243	0.010267
CH	$X\,^2\pi$	4.814	4.814	2.1941	0.4387	1.80763
Cl_2	$X\,^1\Sigma$	16.12	15.18	3.896	0.0006377	0.0305
CO	$X\,^1\Sigma$	7.752	6.728	2.594	0.010314	0.24155
CdH	$X\,^2\Sigma$	15.23	13.677	3.6982	0.13265	0.66556
H_2	$X\,^1\Sigma$	2.073	2.0757	1.1441	5.04828	7.6089
HBr	$X\,^1\Sigma$	6.654	6.5478	2.559	0.162297	1.05842
HCl	$X\,^1\Sigma$	5.669	5.6651	2.3802	0.22512	1.32455
HF	$X\,^1\Sigma$	3.813	3.9332	1.9832	0.63669	2.6202
HI	$X\,^1\Sigma$	7.881	7.9349	2.8169	0.10732	0.81829
HgH^+	$X\,^1\Sigma$	—	6.18267	2.4865	0.129403	0.82682
I_2	$X\,^1\Sigma$	24.58	24.513	4.951	0.00003906	0.0046737
ICl	$X\,^1\Sigma$	17.74	18.411	4.291	0.0002035	0.014274
Li_2	$X\,^1\Sigma$	5.408	5.3577	2.3147	0.0077246	0.08410
K_2	$X\,^1\Sigma$	9.107	8.8970	2.9828	0.0002099	0.007095
N_2	$X\,^1\Sigma$	8.662	8.7072	2.9508	0.010157	0.24985
NO	$X\,^2\pi$	9.995	9.9622	3.1563	0.008808	0.213176
Na_2	$X\,^1\Sigma$	6.864	6.9469	2.6357	0.0009025	0.01934
OH	$X\,^2\pi$	5.003	4.9502	2.2249	0.574014	2.364515
O_2	$X\,^3\Sigma$	10.26	10.2655	3.2040	0.007935	0.180754
P_2	$X\,^1\Sigma$	12.25	12.2409	3.4987	0.0007084	0.026159
SO	$X\,^3\Sigma$	25.81	10.4532	3.2331	0.0027127	0.090127
ZnH	$X\,^2\Sigma$	12.62	12.6228	3.5529	0.16651	0.83516
AuAl	$X\,^1\Sigma$	-	7.86886	2.8051	0.0003040	0.016243
GeSe	$X\,^1\Sigma$	—	10.7315	3.27589	0.00013626	0.0120463
He_2^+	$X\,^1\Sigma$		5.01755	2.2399	0.183686	0.90162
Si_2	$X\,^3\Sigma$	—	9.60141	3.0986	0.0006707	0.02987

$$\omega_e x_e = \frac{7.655\,\Delta W}{\mu_A r_e^2} \qquad \ldots (9)$$

The values of α_e and $\omega_e x_e$ using relations (8) and (9), i.e. potential (5) are calculated and compared with the experimental values (Tables 1 and 2).

Discussion—It was needed to revise the values of Δ for the molecules under consideration as very recent and authentic data[5] of molecular constants compared with those of Varshini[4] had become available. The values of Δ obtained by the present calculations are close to those of Varshini (Table 3) except for SO. Instead of N_2(ii), CO(ii), Cd(iii) and NO(ii) reported by Varshini[4], we have included a few other molecules, viz. GeSe, AuAl, Si_2 and He_2^+. Instead of HgH, HgH^+ molecule is selected as the $\omega_e x_e$ and α_e are to be derived from interpolation of ΔG_v and B_v values. These alterations change the average % errors in α_e and $\omega_e x_e$ using Morse and Rydberg potentials, which are not explicitly reported in this note for the sake of brevity. The average % errors in α_e for Morse and Rydberg functions using these randomly selected molecules are ± 25.98 and ± 22.39 respectively (Varshini's Table XI)[4]. The average % errors in α_e using potentials (1) and (2) are ± 66.73 and ± 32.33 respectively, whereas it is ± 26.54 only when potential (5) is used (Table 1), which is in close agreement with the values derived from Morse and Rydberg potentials.

In the case of $\omega_e x_e$ (Table 2), the average % errors for Morse and Rydberg potential functions using revised Δ are ± 26.82 and ± 19.92 respectively; whereas the average percentage errors using potentials (1) and (2) and (5) are ± 81.12, ± 30.48 and ± 24.48 respectively.

Conclusions

It can be concluded that the superposition of Morse and Rydberg potential functions suggested by Iyer and Sharma has not given very remarkable improvement in the calculations of α_e and $\omega_e x_e$, however the potential function (5) suggested in the present paper gives better agreement in comparison with the potential functions suggested by Iyer and Sharma.

References

1 Iyer R & Sharma L K, *Indian J Pure & Appl Phys*, **17** (1979) 615.
2 Morse P M, *Phys Rev (USA)*, **34** (1929) 57.
3 Rydberg R, *Z Phys (Germany)*, **80** (1933) 514.
4 Varshini Y P, *Rev Mod Phys (USA)*, **29** (1957) 664.
5 Huber K P & Herzberg G, *Constants of diatomic molecules* (Van Nostrand Reinhold Co, New York), 1979.

Indian Journal of Pure & Applied Physics
Vol 21, May 1983, pp 317-318

Effect of Screening on Reaction Rates of ${}_1^1H(p\beta^+\nu){}_1^2H$ in Stellar Interiors

A E Md KHAIROZZAMAN*
B N College, Dhubri 783 324

Received 11 *June* 1982; *accepted* 28 *December* 1982

The screened p-p reaction rates to form ^2H have been studied considering the effect of screening on nuclear reaction rates in stellar interiors. The screening effect appreciably augments the reaction rates at the lower end of hydrogen burning temperature. As the rates are greater, mean life of the star in this phase of evolution will be shorter. The screened rates give us a new set of data to reinvestigate the luminosity, mean life and relative abundance of ^2H.

In the main sequence stars, the thermal pressure due to the hydrogen burning reaction establishes a balance with the gravitational pressure. A good study on various aspects of the reaction such as Coulomb barrier penetration, etc was made by Burbidge *et al.*[1] At a temperature of the order 10^6-10^7K, hydrogen burning becomes dominant. The transmutation of hydrogen to deuteron is given by:

$${}_1^1H + {}_1^1H \rightarrow {}_1^2H + \beta^+ + \nu \qquad \ldots(1)$$

The neutrino quickly escapes from the star and positron combines with an electron to give gamma radiation, $\beta^+ + \beta^- \rightarrow \gamma$ which feeds the radiation field in the star.

Burbidge *et al.*[1] considered the p-p reaction and calculated the energy generation rate without considering the screening effect. The recent works of Van Horn and Salpeter[2] and Itoh *et al.*[3] tempt one to recalculate the reaction rates considering the screening effect. Therefore, we took up the re-study of the screened p-p reaction rates to form ^2H in the present note.

Screening effect and its evaluation—The reaction rate is enhanced when the screening effect of the electron clouds is considered. The presence of electron clouds reduces the Coulomb barrier and hence the rate is multiplied. Van Horn and Salpeter[2] defined a dimensionless parameter Γ, to define weak ($\Gamma < 1$) and strong ($\Gamma > 1$) screening effects. Γ is given by

$$\Gamma = \frac{z^2 e^2}{akT} \qquad \ldots(2)$$

where

$$a = \left(\frac{3}{4\pi n_e}\right)^{1/3} \text{ is the mean ionic distance} \qquad \ldots(3)$$

n_e is the number density of electrons,

n_e is the number density of electrons in plasma, but represents number density of ions in case of hydrogen plasma, and z, e and k are respectively atomic number, electronic charge and Boltzmann's constant.

We may write

$$n_e = \rho N_A \frac{X}{A} \text{ for hydrogen plasma} \qquad \ldots(4)$$

where ρ is the density, N_A the Avogadro number, X the fractional abundance, $A = 1$ for hydrogen ions.

Taking $\rho X = 10^2\ \mathrm{g\,cm^{-3}}$, we get

$$n_e = 6.025 \times 10^{25} \qquad \ldots(4a)$$

We find that $\Gamma \ll 1$. So the reaction is in weak screening regime.

For nuclei to react, it is necessary that they should be able to approach each other closely. If the nuclei are to approach a distance r, the kinetic energy for their relative motion must be $\frac{z_1 z_2 e^2}{r}$. The mean thermal energy is $\frac{3kT}{2}$ and the energy of relative motion is $3kT$ when they approach (Amburtsumayan[4]). Hence

$$E = 3kT = \frac{z_1 z_2 e^2}{r} \qquad \ldots(5)$$

where $r = 10^{-11}$ cm, the upper limit at which the nuclei react.

If we take the interaction distance to be 10^{-11} cm then the particles will have to possess an energy to overcome the Coulomb barrier which is given by

$$\frac{z_1 z_2 e^2}{r} = 23.04 \times 10^{-9} \text{ erg}$$

$$= 14.4 \text{ keV} \qquad \ldots(6)$$

In the range of temperature proper for p-p reaction, the thermal energy cannot be that high. In the range of temperature 10^6-10^7 K, the reaction will take place through quantum mechanical tunnelling. (at about 12 million Kelvin degrees $kT = 1$ keV). Therefore, we take $kT = 0.1$ keV, 0.2 keV, 0.3 keV, etc. to find the weak screening enhancement factor.

Further, using

$$k = \frac{1\text{ eV}}{1.16 \times 10^4\text{ K}} = \frac{1\text{ keV}}{1.16 \times 10^7\text{ K}} \qquad \ldots(7)$$

temperatures in T_6 ($T_6 = T/10^6$) units are obtained. The mean ionic distance is obtained by using the value of n_e from Eq. (4a) in Eq. (3) as 0.158×10^{-8} cm. Thus Γ becomes equal to $0.091\ kT$.

As our reaction is in weak screening regime, we use the enhancement factor, $\exp(3^{1/2}\Gamma^{3/2})$ from Itoh *et al.*[3]

Putting $Y = \exp(3^{1/2}\Gamma^{3/2})$ and taking logarithms on both sides, we find

$$\log Y = 0.75\left(\frac{0.091}{kT}\right)^{3/2} \quad \ldots(8)$$

$$= C T_6^{-3/2} \quad \ldots(9)$$

where C is a constant.

Reaction and energy generation rates—The equation for unscreened reaction rate (R) is obtained from the work of Burbidge *et al.*[1] as obtained in the book by Cohen[5].

$$R = 7.20 \times 10^{-19} n_1 n_2 \left[\frac{z_1 z_2 M_1 M_2}{M_1 + M_2}\right]^{-1} S_0 \tau^2 e^{-\tau}$$

$$= 1568.187 \times 10^9 \tau^2 e^{-\tau} \quad \ldots(10)$$

where

$$\tau = 42.48\left(\frac{z_1^2 z_2^2 M_1 M_2}{M_1 + M_2}\right)^{1/3} T_6^{-1/3}$$

$$= 42.48\,(\tfrac{1}{2} T_6^{-1})^{1/3} \quad \ldots(10a)$$

$S_0 = 3 \times 10^{-22}$ keV barn (Cohen[5]), $n_1 = n_2 = 6.025 \times 10^{25}$ for p-p reaction.

The logarithm of unscreened rate is

$$\log R = 12.2 + 2\log_{10}\tau - 0.43\tau \quad \ldots(11)$$

The logarithm of screened rate (R) is

$$\log R^* = 12.2 + 2\log_{10}\tau - 0.43\tau + \log Y \quad \ldots(12)$$

Further the energy generation rates are given by

$$\left.\begin{aligned} E &= \frac{Q}{\rho} R \text{ erg g}^{-1}\text{s}^{-1} \text{ (unscreened)} \\ E^* &= \frac{Q}{\rho} R^* \text{ erg g}^{-1}\text{s}^{-1} \text{ (screened)} \end{aligned}\right\} \quad \ldots(13)$$

where Q is the disintegration energy.

$Q = 1.443$ MeV (Ref. 6)

$= 2.308 \times 10^{-6}$ erg

The logarithms of energy generation rates are given by

$$\left.\begin{aligned} \log_{10} E &= -7.6366 + \log_{10} R \text{ (unscreened)} \\ \log_{10} E^* &= -7.6366 + \log_{10} R^* \text{ (screened)} \end{aligned}\right\} \quad \ldots(14)$$

Using Eqs (7), (9), (10a), (11), (12), (13) and (14) the values of various parameters have been calculated and presented in Table 1.

Discussion—The enhancement factor decreases as the temperature increases. The screening effect at the lower end of temperature is appreciably high. At higher temperature, the screened and unscreened rates are almost same. We can observe from Eqs (2), (3) and (4) that

$$\frac{\Gamma T}{\rho^{1/3}} = \text{constant} \quad \ldots(15)$$

It appears from Eq. (15) that for the same screening effect at higher temperature, the density should be high. At constant density condition, the weak screening enhancement factor is given by

$$Y = \text{constant.}\ 10^{T_6^{-3/2}} \quad \ldots(16)$$

The screened rates differ greatly from those of Burbidge *et al.*[1] at the lower end of hydrogen burning temperature. The results in Table 1 will be helpful to find rnean life, luminosity and abundance of ^{2}H in main sequence star. The abundance can numerically be alculated through Harm and Schwarzschild's scheme[7].

Table 1—Reaction and Energy Generation Rates as Function of Temperature

kT keV	$T_6 = T/10^6$	$\log R$	$\log R^*$	$\log E$	$\log E^*$
0.1	1.16	1.4147	2.0658	−6.2219	−5.5708
0.2	2.32	4.048	4.2782	−3.5886	−3.3584
0.3	3.48	5.327	5.4522	−2.3095	−2.1844
0.4	4.64	6.1247	6.2068	−1.5119	−1.4298
0.5	5.80	6.6758	6.7340	−0.9608	−0.9026
0.6	6.96	7.1002	7.14459	−0.5364	−0.462

The author gratefully acknowledges the financial assistance from the University Grants Commission, New Delhi.

References

1 Burbidge E M, Burbidge G R, Fowler W A & Hoyle F, *Rev Mod Phys (USA)*, **29** (1957) 547.
2 Salpeter E E & Van Horn H M, *Astrophys J (USA)*, **155** (1969) 183.
3 Itoh N, Totsuji H & Ichimaru S, *Astrophys J (USA)*, **218** (1977) 477.
4 Amburtsumayan V A, *Theoretical astrophysics* (Pergamon Press, London) 1962.
5 Cohen B L, *Concepts of nuclear physics* (Tata McGraw-Hill, New Delhi) 1975.
6 Harwit M, *Astrophysical concepts* (John Wiley, New York) 1973.
7 Harm R & Schwarzschild M, *Astrophys J (USA), Suppl*, 3 (1955) 1.

Indian Journal of Pure & Applied Physics
Vol 21, May 1983, p 319

B System of SnBr Molecule

P M SHAH, A B DARJI* & N R SHAH
Department of Physics, M S University of Baroda, Baroda 390002

Received 17 *July* 1982

The spectrum of tin monobromide in the range 3250-2950 Å has been excited in high frequency discharge and recorded in the plane grating spectrograph at a dispersion of 3.6 Å/mm. The vibrational analysis has been carried out and the following constants have been evaluated:

$\nu_e = 33064.6\ cm^{-1}$
$B^2\Sigma$: $\omega'_e = 298.12\ cm^{-1}$; $\omega'_e x'_e = 2.56\ cm^{-1}$
$X^2\Pi_{1/2}$: $\omega''_e = 247.00\ cm^{-1}$; $\omega''_e x''_e = 0.77\ cm^{-1}$

The spectrum of tin monobromide is known to be consisting of four groups of bands. Sharma and Venkateswarlu[1] excited a group of bands in the range 6400-5100 Å in an uncondensed transformer discharge and assigned an electronic transition $A^2\Sigma^+ \rightarrow X^2\Pi_{1/2}$. Jevons and Bashford[2] excited the spectrum in heavy current discharge source and reported four groups of bands, viz. 4255-3709 Å, 3428-3021 Å, around 3600 Å and 2930-2850 Å. Oldershaw and Robinson[3] reported a group of bands below 2500 Å in absorption. Jevons and Bashford[2] reported seven bands in the region 3160-3020 Å and seven bands in 3430-3260 Å. They arranged these bands as the members of $\Delta v' = 0$ progression by taking the bands at 33091.0 and 30631.5 cm^{-1} as the (0,0) bands of $^2\Sigma \rightarrow {}^2\Pi_{1\ 2}$ and $^2\Sigma \rightarrow {}^2\Pi_{3/2}$ subsystems respectively. It is obvious from their work that as they could not observe any sequence members of the above progressions, they could not carry out a complete vibrational analysis and hence could not report vibrational constants for the $B^2\Sigma$ state of the SnBr molecule. This note reports a detailed vibrational analysis and the vibrational constants of the $B^2\Sigma \rightarrow X^2\Pi_{1/2}$ system.

The spectrum of SnBr molecule has been excited in a high frequency discharge tube using a pure sample of $SnBr_4$. The bands developed strong intensity in whitish colour of the discharge which was maintained by external heating. The spectrum in the region 3250-2950 Å has been recorded in the second order of a plane grating spectrograph (Carl-Zeiss) at an inverse dispersion of 3.6 Å/mm on ORWO WU-3 plates by giving an exposure of about 1 hr. Measurements of the band heads were made on an Abbe comparator and the error of measurement does not exceed $\pm 0.1\ cm^{-1}$.

The spectrum in the region 3250-2950 Å reveals the presence of strong violet degraded bands. In addition to the bands already reported by Jevons and Bashford[2], eleven additional bands have been observed. The bands have been analyzed by taking the (0,0) band at 33089.8 cm^{-1} and the following vibrational constants have been evaluated:

$\nu_e = 33064.6\ cm^{-1}$
$B^2\Sigma$: $\omega'_e = 298.12\ cm^{-1}$; $\omega'_e x'_e = 2.56\ cm^{-1}$
$X^2\Pi_{1/2}$: $\omega''_e = 247.00\ cm^{-1}$; $\omega''_e x''_e = 0.77\ cm^{-1}$

Table 1—Band Head Data of $B^2\Sigma \rightarrow X^2\Pi_{1\ 2}$ System of SnBr

Rel. intensity	Wavenumber in vacuum, cm^{-1}	Assignment v', v''	$\Delta\nu = \nu_{obs} - \nu_{calc}$ cm^{-1}	Wavenumber reported by Ref. 2 cm^{-1}
1	33953.0	3,0	−0.3	—
2	33670.4	2,0	−0.2	—
2	33382.8	1,0	+0.1	—
2	33136.9	1,1	−0.3	—
6	33089.8	0,0	0.0	33091.0
5	33893.0	1,2	−0.3	—
10	32845.1	0,1	+0.8	32846.5
8	32600.6	0,2	+0.2	32601.9
3	32409.6	1,4	−0.5	—
6	32357.9	0,3	−0.1	32361.2
3	32170.6	1,5	0.0	—
3	32117.4	0,4	+0.2	32121.8
4	31878.0	0,5	+0.1	31880.0
3	31640.2	0,6	+0.1	31646.0(?)
2	31403.4	0,7	−0.5	—
2	31169.5	0,8	+0.3	—
3	30936.3	0,9	+0.2	—

The difference between the observed and calculated wavenumbers does not exceed $\pm 0.8\ cm^{-1}$. Table 1 includes the band head data of the $B^2\Sigma \rightarrow X^2\Pi_{1/2}$ system of SnBr molecule. The ground state constants derived from the present analysis agree well with those reported by earlier workers. The system may be ascribed to an electronic transition $B^2\Sigma \rightarrow X^2\Pi_{1\ 2}$ as suggested by previous workers.

Two additional bands have been observed at 30911 cm^{-1} and 31242.2 cm^{-1} which may be taken as the 1,0 and 2,0 bands of the $B^2\Sigma \rightarrow X^2\Pi_{3\ 2}$ system. However, as no more bands have been observed, it is not possible to present here complete vibrational analysis of this component of the system.

The authors are thankful to Prof. M M Patel for his valued suggestions.

References

1 Sharma P R K & Venkateswarlu P. *J Molec Spectrosc (USA)*, **17** (1965) 203-209.
2 Jevons W & Bashford L A. *Proc Phys Soc London (GB)*, **49** (1937) 554-557.
3 Oldershaw G A & Robinson K. *Trans Faraday Soc (GB)*, **67** (1971) 2499-2504.

Indian Journal of Pure & Applied Physics
Vol 21, May 1983, pp 320-322

Effect of Dielectric Constant on EDTA-Metal Chelates—An Ultrasonic Study

G L N SASTRY*
Department of Physics, T J P S College, Guntur 522006

Received 8 *November* 1982

Employing a single-crystal, variable-path interferometer, five EDTA-metal chelates, viz. EDTA + $CrCl_3$, EDTA + $ZnSO_4$, EDTA + $CoCl_2$, EDTA + $SrCl_2$, and EDTA + KNO_3 have been studied at 30°C and pH = 3.5 using 90%-10% water-dioxane mixture as solvent. The condition for a metal ion to form a chelate with EDTA under experimental conditions has been deduced in terms of radius of the metallic cation and valency of the cation. The experimental results have been discussed on the basis of Bjerrum's theory of ion association. The results on these chelates in water-dioxane mixture have been compared with those obtained when water was used as solvent. The present studies have been found to be in agreement with those obtained in the case of six other EDTA-metal chelates studied earlier by the author. Lower dielectric constant of the medium has been found to be favourable for the extent and scope of chelation.

A chelate is a ring structured stable complex ion. EDTA is well known for its capacity to form chelates with metals. Ultrasonic studies of EDTA-metal chelates, though limited, have proved quite interesting in view of their wide scope. Various workers[1-4] worked on these lines but their studies have little scope for systematization. The author attempted a systematic study on these EDTA-metal chelates, especially in regard to the influence of various factors like valency (z), radius of metallic cation (r), temperature (T), dielectric constant (ε), etc., on the process of ion-association in EDTA-metal chelation. The results pertaining to some metals have already been published[5-8]. The present note reports the results obtained with some other metallic salts using water-dioxane mixture as solvent to study the influence of low dielectric constant on chelation.

EXPERIMENTAL DETAILS

Mixtures studied—Using disodium salt of EDTA, five mixtures, namely, (1) EDTA + $CrCl_3$, (2) EDTA + $ZnCl_2$, (3) EDTA + $CoCl_2$, (4) EDTA + $SrCl_2$ and (5) EDTA + KNO_3 have been studied. It has been established by earlier studies[5] that EDTA cannot form a chelate with KNO_3 using water as solvent. In the present investigation, EDTA + KNO_3 mixture has also been included and studied with a view to knowing whether the present solvent of less dielectric constant can give any scope for EDTA to form a chelate with KNO_3 also.

Preparation of solutions—Using double distilled water and distilled AnalaR sample of dioxane, a stock solution of 90%-10% water-dioxane mixture has been prepared. This mixture has been used as the solvent in the preparation of EDTA-metallic salt mixtures in different molar proportions adopting Job's method[9] of continuous variation. Using the water-dioxane mixture as solvent, equimolar stock solutions of individual EDTA and metallic salts of 0.1 *M* each have been prepared. The total molarity of the mixture has been kept constant at 0.1 *M* in all cases of metallic salts.

Temperature and pH—All the mixtures have been studied at a constant temperature of 30 ± 0.1°C and *p*H = 3.5 using a thermostat of NBE type and a pH meter of CL 44 type (Toshniwal Co.). The pH has been maintained constant at 3.5 for the reasons explained in an earlier paper[6].

Velocity determination—A single-crystal, variable-path interferometer working at 2 Mc/s (model made by NPL, New Delhi) capable of yielding velocity measurements to an accuracy of 0.013% has been used for the determination of ultrasonic velocity by the usual well-established interferometric method.

Density determination—A bicapillary pyknometer and an accurate analytical balance capable of measuring the mass to an accuracy of 0.0001 g (0.01%) have been used for density determination.

Calculation of compressibility—Using the values of ultrasonic velocity (v) and density (d), the adiabatic compressibility (β) in each mixture and at different molar proportions has been calculated using the formula $\beta = 1/v^2 d$

RESULTS AND DISCUSSION

It has been observed that the coloured metallic ions formed deeply coloured chelates and colourless metallic ions colourless chelates at 1:1 molar ratio between EDTA and metallic salt. The variation of adiabatic compressibility with molar fraction of the metallic salt in each mixture has been illustrated in Fig. 1. Whereas in four mixtures, β deviated from linearity having a maximum deviation at 0.5 molar fraction, i.e. at 1:1 molar ratio between EDTA and metallic salt (Fig. 1), in the case of fifth mixture, viz. EDTA + KNO_3, it varied linearly[8] with molar fraction of the metallic salt. The values of excess compressibility (β^E) at different molar fractions in the case of each mixture have been noted from the concentration variation curves of compressibility as explained in an

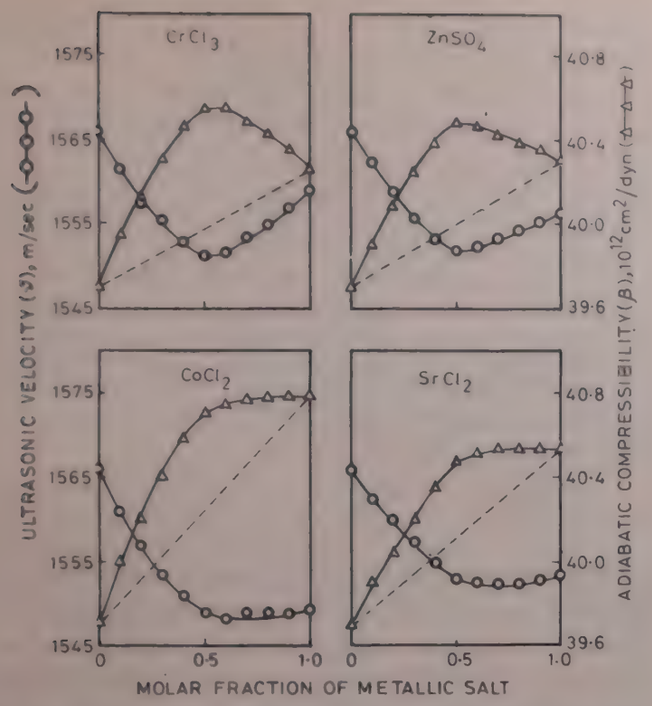

Fig. 1 Variation of v and β with molar fraction of the metallic salt in EDTA-metal chelates in water-dioxane mixture

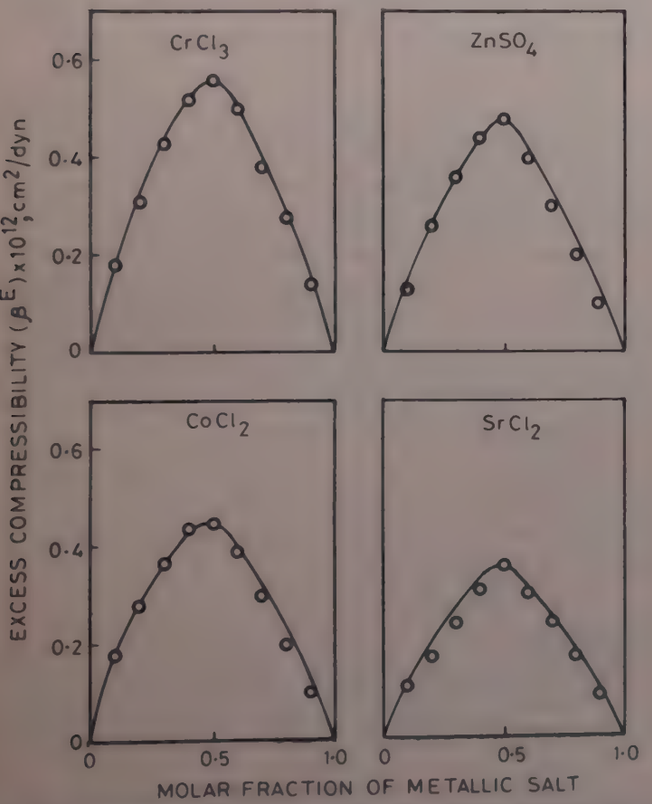

Fig. 2 Variation of β^E with molar fraction of the metallic salt in EDTA-metal chelates in water-dioxane mixture

earlier paper[5]. Fig. 2 illustrates the variation of β^E with molar fraction. It can be seen from Fig. 2 that β^E has a peak value at 0.5 molar fraction, i.e. at 1:1 molar ratio in the first four mixtures.

As stated and explained in the earlier papers[5,6], the peak value of β^E obtained at 1:1 molar ratio is a measure of the maximum extent of chelation between EDTA and metal ion. The values of maximum extent of chelation in terms of compressibility are given for different mixtures in Table 1.

Table 1—Values of z/r, r/z and Maximum Extent of Chelation in EDTA-Metal Chelates

Metallic salt	Radius of metal ion (r) Å (Ref. 10)	Valency of metal ion	z/r	r/z Å	Maximum extent of chelation in terms of compressibility 10^{-12} cm²/dyn	
					In water	In water-dioxane mixture
$CrCl_3$	0.65	3	4.62	0.220	0.47	0.56
$ZnSO_4$	0.74	2	2.70	0.370	0.38	0.48
$CoCl_2$	0.82	2	2.44	0.410	0.37	0.45
$SrCl_2$	1.13	2	1.77	0.565	0.28	0.36
KNO_3	1.33	1	0.75	1.330		

Extent of chelation—The effects of r and z on the scope of association in general and EDTA-metal chelation in particular have been thoroughly discussed in the earlier papers[5,6]. To compare the effects of r and z on the extent of chelation in the present studies with those obtained when water was used as solvent, the variation of the maximum extent of chelation in terms of compressibility with z/r and r/z of the metallic cation are illustrated in Figs 3 and 4 respectively. It can be seen from Table 1 that in all mixtures, the maximum extent of chelation is reckonably more when water-dioxane is chosen as the solvent. These larger magnitudes are a reflection on the enhanced scope of association and should be attributed to the lower dielectric constant of the medium in the present studies.

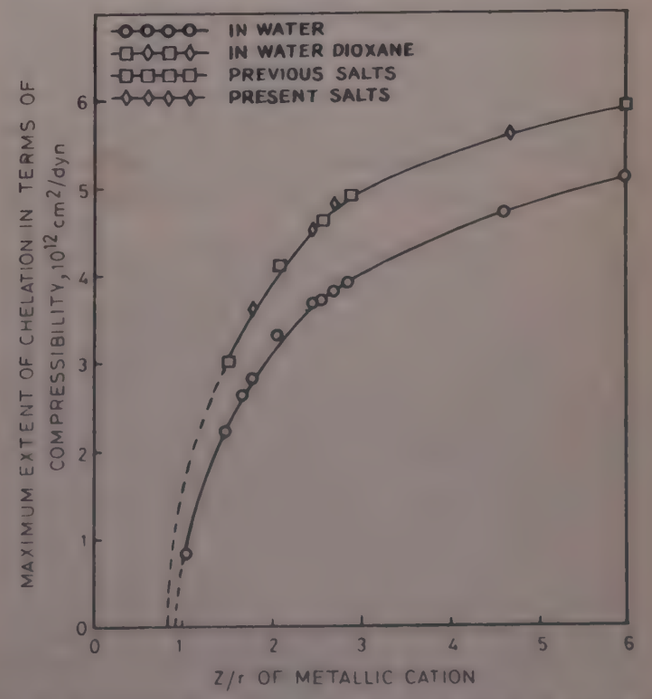

Fig. 3 Variation of maximum extent of chelation in terms of compressibility with z/r of metal ions in water-dioxane mixture and water

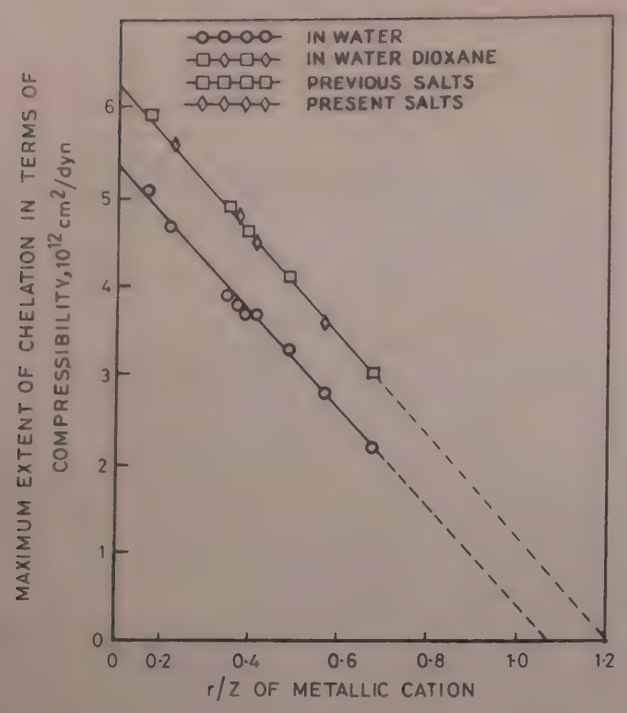

Fig. 4—Variation of maximum extent of chelation in terms of compressibility with r/z of metal ions in water-dioxane mixture and water

Scope of chelation—The variation of maximum extent of chelation with z/r of metal ion is the same as that obtained with the salts studied previously[8] (Fig. 3). This curve, when extrapolated downwards, cuts the z/r axis at 0.83. This is the minimum value of z/r for any metal ion to form a chelate with EDTA. Similarly, the straight line plot in Fig. 4, representing the variation of maximum extent of chelation with r/z, coincided with that obtained with the previous salts (Fig. 4). This straight line, when extrapolated downwards, cuts the r/z axis at 1.2 Å. This is the maximum value of r/z for any metal ion to form a chelate with EDTA. As the extrapolation of a curve in general involves inaccuracies, the optimum value of r/z has been used for the discussion of the results from now onwards.

The optimum value of r/z in the case of water as solvent, as reported in the earlier papers[5,6] is 1.08 Å, whereas it is 1.2 Å in the present studies with water-dioxane mixture as solvent. These optimum values of r/z reveal that (1) metal ions having r/z value greater than 1.08 Å have no chance for chelation with EDTA if water is used as a solvent; (2) if the r/z values of the same metal ions are greater than 1.08 Å, they can have the chance for chelation with EDTA if water-dioxane mixture is used as solvent. In the case of EDTA + KNO_3 mixture, the value of r/z for metal ion, viz. 1.33 Å, is greater than 1.08 as also 1.2 Å. That is why no chelation has been observed in either of the dielectric media. The cause for the higher optimum value of r/z and the resulting wider scope of chelation in the present studies may be attributed to the lower dielectric constant of the medium.

It can therefore be concluded that the two possible aspects with reference to which the dielectric constant can influence chelation unequivocally point out to the fact that the chelation increases as the dielectric constant of the medium decreases.

The above conclusion or deduction from the experimental observations can also be explained theoretically on the basis of Bjerrum's theory of ion association. Bjerrum's expression[11] for the minimum distance of approach (q) for the ions to be called as associated, namely

$$q = e^2 \frac{|z_1 z_2|}{2 \varepsilon k T}$$

(where the letters have their usual significance) tells that when z_1, z_2, k and T are constants, lower dielectric constant (ε) increases the value of q which in its turn gives more scope for ions to associate. It means that the scope of association or chelation is inversely related with dielectric constant of the medium. The dielectric constants[12] of 90%-10% water-dioxane and that of water at 30 C are 76.73 and 67.98 respectively.

The optimum values of r/z which are measures of scopes of chelation when water and water-dioxane are used as solvents are 1.08 Å and 1.20 Å respectively. The product of the optimum value of r/z in water and dielectric constant of water is $1.08 \times 76.73 = 82.87$. In the case of water-dioxane mixture, the product is $1.2 \times 67.98 = 81.58$. The product in the two cases is approximately the same. So, these experimental results are in accordance with the theoretical deductions based on Bjerrum's theory of ion association, both qualitatively and quantitatively.

The author expresses his thanks to Prof. Bh. Krishna Murthy for his valuable suggestions and to the authorities of the University Grants Commission, New Delhi, for financial help.

References

1 Laxmi S, Som Prakash & Satya Prakash, *Z Phys Chem NF (Germany)*, **61** (1968), 247.
2 Laxmi S & Som Prakash, *Z Phys Chem NF (Germany)*, **55** (1967), 259.
3 Prakash S & Laxmi S, *Z Phys Chem (Germany)*, **236** (1967), 59.
4 Prakash S & Som Prakash, *J Phys Chem (USA)*, **79** (1966), 3325.
5 Sastry G L N & Murthy J S R, *J Pure & Appl Ultrasonics (India)*, **3** (1981), 29.
6 Sastry G L N & Murthy J S R, *Indian J Pure & Appl Phys*, **19** (1981), 544.
7 Sastry G L N, *Indian J Pure & Appl Phys*, **20** (1982), 33.
8 Sastry G L N, *J Pure & Appl Ultrasonics (India)*, in press.
9 Job P, *Ann Chim (France)*, **6** (1963), 59.
10 Pauling J, *J Am Chem Soc (USA)*, **49** (1927), 765.
11 Bjerrum N, *Kgl Danske Videnskab (Sweden)*, **7** (1926), 9.
12 Conway B E, *Electrochemical data* (Elsevier, London), 1952, 42.

INSTRUCTIONS TO AUTHORS

SCOPE

The journal welcomes, for publication, full papers and short notes, reporting significant new results of research, in all areas of physics except space physics. The applied fields covered are electronics, electrical engineering, instrumentation and applied mathematics. However, papers in applied mathematics with emphasis on only derivation and proofs and having no direct physical significance, will not be considered. Review articles are not published normally.

SUBMISSION OF MANUSCRIPT

Manuscripts for consideration should be submitted, *in duplicate*, to Editor, Indian Journal of Pure & Applied Physics, Publications & Information Directorate, Hillside Road, New Delhi 110012. They should neither have been already published nor be under consideration elsewhere.

Manuscripts should be in English and typewritten on only one side of good quality paper, in double space, with adequate margin on all four sides. One original and one carbon or photo-copy, each complete in all respects including abstract, illustrations, appendixes, etc. are to be submitted.

PREPARATION OF MANUSCRIPT

Authors may consult recent issues of the Journal to familiarize themselves with the general style and practices adopted in regard to the various elements of a paper.

General

Manuscript should be presented in as concise a form as possible. Good attention should be given to spelling and grammar. In giving names of chemical compounds and structures, abbreviations of units of measurements, symbols and notations, the style and practices recommended by the IUPAP and IUPAC, should be followed.

Frequently repeating combinations of words, e.g. electric field gradient (EFG), junction field effect transistor (JFET), stimulated Raman emission (SRE), should be abbreviated subsequently, indicating the abbreviated form in parenthesis, as shown, at the place of their first occurrence.

Pages should be numbered consecutively and arranged in the following order: Title, authors' names with their institutional affiliations and abstract, along with relevant footnotes whenever necessary (on a separate sheet); introduction; experimental details/theory/method/analysis; results; discussion; conclusion(s); acknowledgement; references and appendixes. Tables, captions for figures (with legends) and appendixes should be typed *on separate sheets* and attached at the end of the manuscript.

Title

The title should be neither too brief/general nor unnecessarily long. It should reflect the content of the paper so as to derive the maximum advantage in indexing. If a paper forms part of a general series, a specific subtitle, indicating the particular aspect of the work covered in the paper, should be provided.

A short running title for the paper, the broad subject heading under which it should be classified in the contents page (authors may consult recent numbers of the journal for this purpose), and the author (indicated by an asterisk on the relevant author's name) and address for correspondence, should also be provided on the title page.

Abstract

The abstract, usually not exceeding 200 words, should indicate the scope and significant content of the paper, highlighting the principal findings and conclusions. It should be in such a form that abstracting periodicals can use it without modification.

Introduction

Long and elaborate introduction should be avoided. It should be brief and state the exact scope of the study in relation to the present status of knowledge in the field. Literature review should be limited strictly to what is necessary to indicate the essential background and the justification for undertaking the study.

Materials, methods, apparatus, etc.

The sources of materials and their purity, methods of preparation, procedure for measurements and their accuracies, etc. should be clearly stated to enable any other worker to repeat the work if necessary. New methods, techniques, theories, etc. should be described in adequate detail; but if they are well known, a mere literature reference to them will do; differences from standard ones, improvements or innovations should, however, be clearly mentioned.

Results

Only such primary data as are essential for understanding the discussion and main conclusions emerging from the study should be included. All secondary data as are of interest to a specific category of readership *should not be included* in the paper. Such data should be retained by the authors for supply, on request, to any interested research worker. A footnote to this effect may be inserted at the relevant place in the paper.

The results must be presented in a coherent sequence in a unified logical structure, avoiding repetition or confusion. Limitations of the results should be clearly stated.

The same data should not be presented in both tabular and graphic forms. Only such tables and figures as are essential should be included. Simple linear plots that can easily be discussed in the text, should not be included. Infrared, ultraviolet, NMR and other spectra, DTA curves, etc. should be included only if they pertain to new compounds and/or are essential to the discussion; otherwise only significant numerical data should be given in the text or in a table.

Discussion

Long rambling discussion should be avoided. The discussion should deal with the interpretation of results without repeating information already presented under results. It should relate new findings to the known and include logical deductions. A separate section on 'conclusions' can be given only when they are well established and of outstanding significance. Mere observation of qualitative trends of results should be distinguished from firm conclusions. Also, limitations, if any, to the conclusions should be clearly pointed out.

Mathematical portions

Special attention should be given to the mathematical portions of the paper. Equations must be well separated from the text and written clearly with good separation between the successive lines. The usual norms of breaking long mathematical expressions should be adhered to. Equations should be numbered consecutively in Arabic numerals with the number in parenthesis near the right hand margin. Superscripts and subscripts should be clearly indicated in pencil by V and Λ sign respectively. Capital and small letters,

particularly of the same letter when both occur, as well as letters or *symbols likely to be confused* one for the other, *should be* clearly *distinguished*. Special characters (e.g. Greek, script, vector, tensor, etc.) required must be indicated by marginal notes. Letters and symbols which should appear in bold face must be clearly indicated. To simplify typesetting: (i) long and complicated mathematical expressions which are frequently repeated should be replaced with single letter/symbol, *without clashing with the others used* in the paper; (ii) the "exp" form of complex exponential functions should be used; and (iii) to simplify fractions, the solidus (/) is to be used and fractional exponents are to be used instead of root signs, e.g.

write $\exp\{-i\omega_0(t_1-t_2)/2\}$ and *not* $e^{-i\omega_0(t_1-t_2)/2}$

write $(4\omega_{pl}K_{3\lambda}^2/\tilde{\omega}K_D^2)^{1/2}$ and *not* $\sqrt{\dfrac{4\omega_{pl}K_{3\lambda}^2}{\tilde{\omega}K_D^2}}$

Tables

Tables should be numbered consecutively in Arabic numerals and *should bear brief titles. Column headings should be brief*. Units of measurement should be abbreviated and placed below the headings. Nil results should be indicated and distinguished clearly from absence of data. Inclusion of structural formulae inside the tables should be avoided as far as possible. Tables should be referred to in the text by numbers and not by terms like 'above', 'below', 'preceding' or 'following'. Results should not be presented to a greater accuracy than that of the method employed.

Illustrations

The number of illustrations should be kept to the minimum. Wherever possible, e.g. a number of individual analogous figures referring to different variables, substances, molecules, etc. may be combined into one composite figure. All illustrations should be numbered consecutively in Arabic numerals. *Captions and legends* to the figures should be *self-explanatory*. Line drawings should be made with Indian ink on white drawing paper/cellophane sheet/tracing cloth, and drawn to approximately twice the printed size.

The lettering should be uniform, preferably in stencil, so as to be *not less than 1.5 mm after reduction* widthwise to full page size (165 mm) or column size (80 mm). The size of geometrical shapes (used to distinguish different graphs), dots, lines, etc. should be sufficiently *large to permit* the necessary *reduction without loss of detail*. In the case of photographs, *prints must be on glossy paper and contrasty*. If an illustration is taken from another publication, reference to the source should be given and prior permission secured. Illustrations should be referred to in the text by numbers and not by terms like 'above', 'following' etc.

Acknowledgement

Acknowledgements should not be exuberant and must be made only to real assistance rendered in connection with the work reported in the paper.

References

References cited should be limited to the absolute minimum (particularly in the case of short notes) based on their essential relevance. In the text, references to literature should be *numbered consecutively, in the order of their first occurrence*, and should be indicated by superscript Arabic numbers at the relevant places; as far as possible the placement of references on numerals or other symbols should be avoided; in such cases the reference may be given in parenthesis in running text, e.g. "this yielded for n a value of 2.3 (Ref. 5)". Full bibliographic details for all the references mentioned in the text should be listed in serial order at the end of the paper.

In citing references to research papers, names and initials of authors should be followed, in order, by the title of the periodical in the abbreviated form (underlined), the volume number (two lines underneath), the year within circular brackets and the page number [e.g. Chandra B P & Shrivastava K K, *J Phys & Chem Solids (GB)*, 39 (1978) 939]. For names of periodicals, the abbreviations followed by the *Physics Abstracts* should be used. For periodicals not covered by *Physics Abstracts*, the title abbreviations should be according to the *Bibliographic Guide for Editors and Authors*, 1974, published by the American Chemical Society, Washington DC, USA; additionally the country from which the journal is published should be given in parenthesis immediately after the title abbreviation. If a paper has been accepted for publication, the names of the authors and the journal (with volume number and year, if known) should be given followed by the words "in press" [e.g. Wahi P K & Patel N D, *Can J Spectrosc (Canada)*, in press.].

In references containing *up to four authors*, the *names of all* the *authors* with their respective initials should *be given*. The abbreviations *et al.*, idem and ibid should be avoided. When there are more than four authors, *only* the names of the *first three authors* with their respective initials should *be given*, followed by the words *'et al.'*

Reference to a book should include details in the following order: name and initials of authors, the title of the book (underlined), name of publisher and place of publication within circular brackets and year and page (s) [e.g. Clayton G B, *Operational amplifiers* (Newnes-Butterworths, London), 4th Edn, 1977, 26]. If the reference is to the work of an author published in a book by a different person, the fact that it is cited from the source book should be clearly indicated [e.g. Turnhout Van J, 'Thermally stimulated discharge of electrets' in *Topics in applied physics*: Vol. 33—*Electrets*, edited by C M Sessler (Springer Verlag, Berlin), 1980, 130].

Proceedings of conferences and symposia should be treated in the same manner as books. Reference to a paper presented at a conference, the proceedings of which are not published, should include, in the following order, names and initials of authors, title of the paper (underlined), name of the conference, and where and when it was held (e.g. Herczeg P, *Symmetry-violating kaon decays*, paper presented to the International Conference on High Energy Physics and Nuclear Structure, Vancouver, Canada, 13-17 August 1979).

Reference to a thesis should include the name of the author, title of the thesis (underlined), university or institution to which it was submitted and year of submission (e.g. Mehrotra S N, *Many-body techniques and their applications to interacting bosons*, Ph D thesis, Ranchi University, 1976).

Reference to a patent should include names of patentees, country of origin (underlined) and patent number, the organization to which the patent has been assigned (within circular brackets), date of acceptance of the patent and reference to an abstracting periodical where available [e.g. Labes M M, *US Pat.* 4,066,567 (to Temple University), 3 January 1978; *Chem. Abstr.*, **88** (No. 20) (1978), 138350 n].

PROOFS & REPRINTS

Authors will receive galley proofs and a reprint order form. The galley proofs, indicating the essential corrections, should be returned to the Editor without delay, enclosing the reprint order form. Authors are given 25 *free reprints* for each paper. *Extra* reprints can be had *at cost. If the reprint order is not received with the corrected proofs, it will be presumed that the author needs no extra reprints.* Later requests for *more* reprints cannot be complied with. Covers for reprints cannot be provided.

THE WEALTH OF INDIA

An Encyclopaedia of Indian Raw Materials and Industrial Products, published in two series: **(i) Raw Materials**, and **(ii) Industrial Products**.

RAW MATERIALS

The articles deal with Animal Products, Dyes & Tans, Essential Oils, Fats & Oils, Fibres & Pulps, Foods & Fodders, Drugs, Minerals, Spices & Flavourings, and Timbers and other Forest products. Names in Indian languages, and trade names are provided.

For important crops, their origin, distribution, evolution of cultivated types, and methods of cultivation, harvesting and storage are mentioned in detail. Data regarding area and yield and import and export are provided. Regarding minerals, their occurrence and distribution in the country and modes of exploitation and utilization are given. The articles are well illustrated. Adequate literature references are provided.

Eleven volumes of the series covering letters A – Z have been published.

Vol. I(A-B) Rs. 80.00; Vol. II (C) Rs. 95.00; Vol. III (D-E) Rs. 40.00; Vol. IV (F-G) Rs. 65.00; Vol. IV: Suppl. Fish & Fisheries Rs. 40.00; Vol. V (H-K) Rs. 75.00; Vol. VI (L-M) Rs. 90.00; Vol. VI: Suppl. Livestock Rs. 60.00; Vol. VII (N-Pc) Rs. 30.00; Vol. VIII (Ph-Re) Rs. 86.00; Vol. IX (Rh-So) Rs. 104.00; Vol. X (Sp-W) Rs. 152.00; Vol. XI (X-Z) Rs. 102.00.

INDUSTRIAL PRODUCTS

Includes articles giving a comprehensive account of various large, medium and small scale industries. Some of the major industries included are: Acids, Carriages, Diesel Engines, Fertilizers, Insecticides & Pesticides, Iron & Steel, Paints & Varnishes, Petroleum Refining, Pharmaceuticals, Plastics, Ship & Boat-building, Rubber, Silk, etc.

The articles include an account of the raw materials and their availability, manufacturing processes, and uses of products, and industrial potentialities. Specifications of raw materials as well as finished products and statistical data regarding production, demand, exports, imports, prices, etc., are provided. The articles are suitably illustrated. References to the sources of information are provided.

Nine volumes of the series covering letters A – Z have been published.

Part I (A-B) Rs. 54.00; Part II (C) Rs. 64.00; Part III (D-E) Rs. 25.00; Part IV (F-H) Rs. 25.00; Part V (I-L) Rs. 30.00; Part VI (M-Pi) Rs. 28.00; Part VII (Pl-Sh) Rs. 60.00; Part VIII (Si-Ti) Rs. 66.00; Part IX (To-Z) Rs. 80.00.

HINDI EDITION: BHARAT KI SAMPADA—PRAKRITIK PADARTH

Vols. I to VI and two supplements of Wealth of India—Raw Materials series in Hindi already published.

Published Volumes:

Vol. I (अ-औ) Rs. 38; Vol. II (क) Rs. 36; Vol. III (ख-न) Rs. 36; Vol. IV (प) Rs. 83; Vol. V (फ-मेरे) Rs. 60; Vol. VI (मेल-रू) Rs. 80.

Supplements:

Fish & Fisheries (Matsya & Matsyaki) Rs. 49; Liverstock (*Pashudhan aur Kukkut Palan*) Rs. 34.

Vols. VII to XI under publication.

Please contact:

Manager (Sales & Advertisement)

PUBLICATIONS & INFORMATION DIRECTORATE, CSIR

Hillside Road, New Delhi 110012

RN 7092/63

CSIR PUBLICATIONS

WEALTH OF INDIA

An encyclopaedia of the economic products and industrial resources of India issued in two series

RAW MATERIALS SERIES—contains articles on plant, animal and mineral resources

	Rs	$	£
Vol. I (A-B)	80.00	30.00	13.00
Vol. II (C)	95.00	33.00	17.00
Vol. III (D-E)	105.00	32.00	20.00
Vol. IV (F-G)	65.00	27.00	12.00
Supplement (Fish & Fisheries)	40.00	16.00	7.00
Vol. V (H-K)	75.00	28.00	12.50
Vol. VI (L-M)	90.00	34.00	15.00
Supplement (Livestock)	60.00	18.00	6.00
Vol. VII (N-Pe)	30.00	9.00	3.00
Vol. VIII (Ph-Re)	86.00	32.00	14.00
Vol. IX (Rh-So)	104.00	35.00	19.00
Vol. X (Sp-W)	152.00	65.00	23.00
Vol. XI (X-Z)	102.00	42.00	20.00

INDUSTRIAL PRODUCTS SERIES—deals with major, small-scale and cottage industries

Part I (A-B)	54.00	20.00	9.00
Part II (C)	64.00	24.00	11.00
Part III (D-E)	25.00	7.50	2.50
Part IV (F-H)	25.00	7.50	2.50
Part V (I-L)	30.00	9.00	3.00
Part VI (M-Pi)	28.00	8.00	2.80
Part VII (Pl-Sh)	60.00	18.00	6.00
Part VIII (Si-Ti)	66.00	27.00	10.00
Part IX (To-Z)	80.00	34.00	12.00

BHARAT KI SAMPADA (Hindi Edition of Wealth of India, Raw Materials)

Vol. I	(अ-औ)	38.00	16.00	6.50
Vol. II	(क)	36.00	15.00	6.00
Vol. III	(ख-न)	36.00	15.00	6.00
Vol. IV	(प)	83.00	34.00	16.00
Vol. V	(फ-मेरे)	60.00	22.00	10.00
Vol VI	(मेल-ह)	80.00	27.00	13.00
Livestock (Kukkut Palan)		34.00	15.00	6.00
Fish & Fisheries (Matsya aur Matsyaki)		49.00	21.00	8.00
A Dictionary of Generic & Specific Names of Plants and Animals Useful to Man with their English and Latin pronunciation in Devanagari.		30.00	11.00	5.00

OTHER PUBLICATIONS

	Rs	$	£
Proceedings: seminar on primary communications in Science & Technology in India by Sh. R.N. Sharma & S. Seetharama	52.00	17.50	9.00
Flora of Delhi by J.K. Maheshwari	28.00	8.00	2.80
Indian Fossil Pteridophytes by K.R. Surange	23.00	8.00	2.30
Indian Thysanoptera by T.N. Ananthakrishnan	26.00	8.00	2.60
The Millipede Thyropygus by G. Krishnan	12.00	3.50	1.20
Drug Addiction with special reference to India by R.N. Chopra & I.C. Chopra	12.00	3.50	1.20
Glossary of Indian Medicinal Plants by R.N. Chopra & I.C. Chopra	35.00	13.00	6.00
Fluidization & Related Processes	12.00	4.00	1.20
Evolution of Life by M.S. Randhawa, A.K. Dey, Jagjit Singh & Vishnu Mitre	22.50	7.00	2.25
Collected Scientific Papers of Meghnad Saha	30.00	9.00	3.00
Proteaceae by C. Venkata Rao	34.00	11.00	3.40
Pinus by P. Maheshwari & R.N. Konar	30.00	11.00	5.00
Cellulose Research I	3.00	0.90	0.30
Cellulose Research II	6.00	1.75	0.60
Chemical Process Design	9.00	2.50	0.90
Low Temperature Carbonization of Non-coking Coals & Lignites & Briquetting Coal Fines:			
Vol. I	17.50	5.50	1.75
Vol. II	17.50	5.50	1.75
Nucleic Acids	10.00	3.00	1.00
IGY Symposium: Vol. I	9.00	2.50	0.90
IGY Symposium: Vol. II	9.00	2.50	0.90
CNS Drugs	16.50	5.00	1.65
Kinetics of Electrode Processes & Null Points of Metals	2.50	0.75	0.25
Indian Sardines by R.V. Nair	22.00	7.00	2.20
Termite Problems in India	9.00	3.00	0.90
Loranthaceae by B.M. Johri & S.P. Bhatnagar	32.00	11.00	3.20
Abies and Picea by K.A. Chowdhury	14.00	6.00	2.10
Gnetum by P. Maheshwari and Vimla Vasil	20.00	6.00	2.00
Aquatic Angiosperms by K. Subramanyam	20.00	6.00	2.00
Supplement to Glossary of Indian Medicinal Plants by R.N. Chopra, I.C. Chopra & B.S. Varma	18.00	7.00	3.00
Herbaceous Flora of Dehra Dun by C.R. Babu	144.00	60.00	22.00
Diosgenin and Other Steroid Drug Precursors by Y.R. Chadha & Miss L.V. Asolkar	36.00	13.00	6.00
Research & Development Management by Inder Dev	25.00	10.00	—
Rural Development and Technology—A Status Report-cum-Bibliography by P.R. Bose & V.N. Vashist	100.00	38.00	17.00

Packing and Postage extra

Please contact:

Manager (Sales & Advertisement)
PUBLICATIONS & INFORMATION DIRECTORATE, CSIR
Hillside Road, New Delhi 110012

Printed & Published by D.S. Sastry, Editor, Publications & Information Directorate (PID)
Hillside Road, New Delhi 110012, at PID Photocomposition Unit

D(C)540